

# Laser-Beam Transport And Burn Analysis in Inertial Confinement Fusion

*A Thesis  
submitted for the degree of*

**Doctor of Philosophy**  
*in Physics*

*submitted by*

**Oriza Kamboj**  
**11814131**

*under the guidance of*

**Prof. Niti Kant, Lovely Professional University, Punjab, India**  
**Dr. John Pasley, University of York, UK**



Department of Physics  
Lovely Professional University, Punjab, India  
September 2021

## DECLARATION

I declare that the thesis entitled, LASER BEAM TRANSPORT AND BURN ANALYSIS IN INERTIAL CONFINEMENT FUSION, has been prepared by me under the guidance of Prof. Niti Kant, Professor of Physics, Lovely Professional University, Punjab, India and under the co-supervision of Dr. John Pasley, Senior Lecturer, York Plasma Institute, University of York, UK. No part of the thesis has formed the basis for the award of any degree or fellowship previously.

**Oriza Kamboj**

11814131

Dept. of Physics

Lovely Professional University,

144411

Place: Phagwara, Punjab

Date: 1<sup>st</sup> September 2021

# THESIS CERTIFICATE

This is to certify that the thesis titled **Laser-Beam Transport And Burn Analysis in Inertial Confinement Fusion**, submitted by **Oriza Kamboj (11814131)**, to the Lovely Professional University, Punjab, for the award of the degree of **Doctor of Philosophy**, is a bona fide record of the research work done by her under my supervision. The contents of this thesis, in full or in parts, have not been submitted to any other Institute or University for the award of any degree or diploma.

**Prof. Niti Kant**

Professor

Department of Physics

Lovely Professional University,

144411

Place: Phagwara, Punjab



**Dr. John Pasley**

Sr. Lec.

York Plasma Institute

University of York, UK.

Place: York, UK

Date: 7<sup>th</sup> September 2021

## ACKNOWLEDGEMENTS

*I want to extend sincere thanks to my supervisor, Prof. Niti Kant, for guiding me throughout my research journey, shaping my research, building a researcher in me, and providing an environment in which I could grow. Apart from research, the kind of wisdom, positivity, and life and research ethics that I've learned from him will always be in my life's foundation. Thank you, Sir.*

*I sincerely thank my co-supervisor, Dr. John Pasley, for accepting me as his student, improving me at every step of research, and giving me the support I needed in my career. Because of his constant supervision, I tackled so many struggles that had come during my Ph.D. journey and I genuinely feel that I have come out as a better researcher. Thank you, Sir.*

*I want to thank Dr. Dieter H.H. Hoffmann for supporting me throughout my research journey and boosting my confidence in whatever work I did and Ms. Jyoti Wadhwa for taking out time and sharing her work experience with me. I would also like to thank Dr. D. N. Gupta for sharing his knowledge, for making me understand the importance of the foundation of research, and for his constant guidance whenever I needed it. I thank each member of our laser-plasma group in Lovely Professional University, Dr. Vishal Thakur, Dr. Jyoti Rajput, Dr. Alka Mehta and all the faculty members of the Department of Physics, Lovely Professional University, specially Prof. Kailash Juglan, Dr. A. K. Shrivastava, Dr. Naveen Gupta and Dr. Sanjay Mishra for providing me with the help I needed in my Ph.D. journey. The positivity and happiness I felt in this university will be unforgettable.*

*I also want to show my gratitude to my undergraduate college, St. Xavier's College, Mumbai, and my School, Navy Children School, Mumbai, in inculcating the basic knowledge, values, and valuable experiences which helped me in walking this path. I thank all my teachers, from my school and undergraduate college, colleagues, and friends who helped in shaping me.*

*I would like to give a special mention to the two amazing friends in my life, Sakshi and Ashish, who heard me and stood by me in my failures and achievements in my struggles and in my success. Thank you so much.*

*The journey of my education started and kept growing only because of the supportive family I have. I thank my family for just being there, because words will not express the emotions I feel for them and how grateful I am for having them in my life and I thank god for blessing me with a life that I have.*

*Thank you...*

# ABSTRACT

The community worldwide has been pursuing the aim of controlled fusion energy for decades. The bulk of inertial confinement fusion research, one area of fusion research in general, has concentrated on central hot spot ignition. Alternative methods, such as rapid ignition, provide the possibility of more extensive benefits with lower symmetry requirements, making them suitable for fusion energy generation. This thesis focuses on proposing solutions to significant challenges in ICF linked to instabilities and advanced fuels in ICF from an environmental standpoint.

One important component of the fast ignition scheme is the formation of pre-plasma in a cone-guided ICF scheme. When employing the conventional optical components of a chirped-pulse-amplified (CPA) laser-beam chain in a big laser system, the spot sizes generated are frequently much larger than would be ideal for fast ignition. This thesis aims to lower the focus spot size in the interior of the re-entrant cone's tip to the minimum size necessary for effective coupling to the densely imploded fuel core. The existence of pre-plasma in the cone is used in the method outlined. Due to the difficulties of reducing laser pre-pulse to below the threshold for plasma formation, such pre-plasma filling is difficult to eliminate completely when illuminating a cone with a high-energy CPA laser system. Paraxial theory in a WKB approximation was employed to derive the differential equation that regulates the progress of the laser beam-width with propagation distance. A simulation is run assuming strong self-focusing in line with the laser parameters and plasma density profile specified.

One of the processes limiting the power scaling in inertial confinement fusion is stimulated Raman scattering (SRS) (ICF). This thesis shows that the combined effects of static density fluctuations and an azimuthal magnetic field may effectively suppress SRS in this paper. A gaussian laser beam imparted on a density rippled magnetized plasma experiences stimulated forward Raman scattering (SFRS), resulting in two radially localized electromagnetic sideband waves and a lower-hybrid wave. Ion density variations saturate absolute and growing modes, which reduce instability growth through mode coupling. After saturation, the modes modulated by the azimuthal magnetic field are effectively damped. As a result, the total pace of instability increases slows. We examined the development of the SFRS and estimated it for ICF key factors using nonlocal theory.

Another approach is considered to suppress SRS. A five-wave theory is developed, connecting stimulated Raman backscattering and decay instability produced in plasma with static magnetic field containing hot drifting electrons. A downward shifting electro-magnetic wave (EMW) and a forward-moving plasma wave are created by a Gaussian laser beam propagat-

ing in a static magnetic field. The plasma wave degrades into an ion acoustic wave (IAW) and a backward propagating secondary Langmuir wave with a larger wavelength. This energy diversion and linear Landau dampening of Langmuir wave by hot electrons suppresses SRS process. The plasma wave and the sideband EMW amplitudes fluctuate with time. The EPW amplitude has a similar effect.

Finally, our last objective looks at the burn-up of non-equimolar DT under inertial confinement fusion conditions (ICF). Deuterium: Tritium burn-up calculations analytical tests are carried out on the ratios of 60:40 DT, 70:30 DT, 80:20 DT, and 90:10 DT, as well as the 50:50 DT case. The analytical work is then compared to 1-D hydrodynamic simulations. Based on this research, we can calculate the proportion of available fuel that will be used vs. the fuel's areal density in each instance. Non-equimolar DT has the potential to be used in ICF fuel capsules that achieve equimolar DT ignition and then propagate the burn into tritium sparse fuel to reduce the demands on the tritium breeding cycle.

# Contents

<b>ACKNOWLEDGEMENTS</b>	<b>1</b>
<b>ABSTRACT</b>	<b>2</b>
<b>LIST OF TABLES</b>	<b>7</b>
<b>LIST OF FIGURES</b>	<b>9</b>
<b>ABBREVIATIONS</b>	<b>10</b>
<b>NOTATION</b>	<b>11</b>
<b>1 INTRODUCTION</b>	<b>1</b>
1.1 Introduction to Inertial Confinement Fusion . . . . .	1
1.1.1 Nuclear Fusion . . . . .	1
1.1.2 Inertial Confinement Fusion . . . . .	3
1.1.3 Fast Ignition . . . . .	5
1.2 Objectives of the Proposed Work . . . . .	6
1.3 Thesis Outline . . . . .	6
<b>2 Research Methodology</b>	<b>13</b>
2.1 Description of work . . . . .	13
2.2 Fluid Model . . . . .	13
2.2.1 Introduction . . . . .	13
2.2.2 Fluid Equation of Motion . . . . .	14
2.3 Laser-Plasma Interaction . . . . .	15

---

2.3.1	The Plasma Frequency . . . . .	16
2.3.2	Paraxial Ray Approximation . . . . .	17
2.3.3	Ponderomotive Force . . . . .	18
2.3.4	Self-Focusing of Laser Beam . . . . .	18
2.3.5	Plasma Density Ramp . . . . .	19
2.3.6	Parametric Instabilities in ICF . . . . .	19
2.4	Magnetic Field in Plasma . . . . .	23
<b>3</b>	<b>Enhanced self-focusing of laser in the cone-guided scheme for inertial confinement fusion.</b>	<b>27</b>
3.1	Introduction . . . . .	27
3.2	Theoretical Considerations . . . . .	30
3.3	Relativistic Self-focusing . . . . .	31
3.4	Results . . . . .	34
3.5	Conclusions . . . . .	38
<b>4</b>	<b>SRS of a laser in a magnetized plasma with density ripple</b>	<b>42</b>
4.1	Introduction . . . . .	42
4.2	Instability Analysis . . . . .	43
4.3	Results and Discussion . . . . .	46
4.4	Conclusion . . . . .	48
<b>5</b>	<b>Ignition and Burn calculations for advanced fuels in ICF</b>	<b>52</b>
5.1	Introduction . . . . .	52
5.2	Hydrodynamic simulation results . . . . .	54
5.3	Target Design . . . . .	57
5.4	Conclusion . . . . .	59
<b>6</b>	<b>SRS coupling with decay instability in a magnetized plasma.</b>	<b>61</b>



6.1	Introduction . . . . .	61
6.2	Theoretical Considerations . . . . .	62
6.3	Instability Analysis . . . . .	63
6.4	Instability Coupling . . . . .	65
6.5	Results and Discussions . . . . .	67
6.6	Conclusion . . . . .	71
<b>7</b>	<b>Summary and Conclusion</b>	<b>74</b>

## List of Tables

5.1	Overall burn fraction equivalent to $f_{bt} = 0.3$ . . . . .	54
5.2	Density-Radius product and mass of fuel for different radius of sphere . . .	54

# List of Figures

1.1	The maximum in the graph for $^{62}\text{Ni}$ is binding energy per nucleon against atomic mass number. Among the light nuclei, the $^4\text{He}$ nucleus has an unusually high binding energy. The difference in binding energy per nucleon between fusion reactions of light nuclides with $^4\text{He}$ as one of the reaction products (5 MeV/nucleon) and $^{235}\text{U}$ fission (0.9 MeV/nucleon) is approximated [5] . . . . .	2
1.2	In an inertial-confinement capsule, there are four steps to a fusion reaction: (a) The outer layer is heated with a laser. (b) Ablation of the capsule's outer layer compresses the capsule. (c) The density and temperature of the core are sufficient for ignition. (d) Through the compressed fuel, the burn wave spreads quickly [23] . . . . .	4
2.1	Upward Plasma Density Ramp . . . . .	20
2.2	Feedback mechanism of SRS . . . . .	22
3.1	Schematic representation of the cone-guided fast ignition scheme . . . . .	28
3.2	In this figure (a) Variation of beam width parameter with normalised propagation distance and (b)Phase space plot for self-focused Gaussian laser beam, for $\omega r_0/c = 40, 50$ and $60$ at $\omega_{p0}/\omega = 0.3, d=8$ is shown . . . . .	35
3.3	In this figure (a) Variation of beam width parameter with normalised propagation distance and (b) Phase space plot for self-focused Gaussian laser beam, for $d = 8, 10$ and $12$ at $\omega r_0/c= 40$ and $\omega_{p0}/\omega = 0.3$ is shown. . . . .	36
3.4	In this figure (a) Variation of beam width parameter with normalised propagation distance and (b) Phase space plot for self-focused Gaussian laser beam, for different values of $\omega_{p0}/\omega = 0.3, 0.4$ and $0.5$ at $\omega r_0/c= 40$ and $d=8$ is shown. . . . .	37
4.1	Variation of normalized growth rate in the presence of magnetic field at various Eigen values . . . . .	47
4.2	Variation of growth rate with magnetic field in the presence and absence of density ripple . . . . .	47
4.3	Variation of growth rate with the spot size of laser beam at various Eigen values . . . . .	49

5.1	Maximum energy released in DT fusion reactions . . . . .	55
5.2	Variation of tritium burn fraction ( $f_b$ ) with density-radius product ( $\rho r$ ) for 10%T . . . . .	56
5.3	Variation of tritium burn fraction ( $f_b$ ) with density-radius product ( $\rho r$ ) for 20%T . . . . .	56
5.4	Variation of tritium burn fraction ( $f_b$ ) with density-radius product ( $\rho r$ ) for 30%T . . . . .	57
5.5	Variation of tritium burn fraction ( $f_b$ ) with density-radius product ( $\rho r$ ) for 40%T . . . . .	58
5.6	Layered schematic diagram . . . . .	58
6.1	Schematic diagram representing the SRS coupled to decay instability . . . . .	64
6.2	Normalized amplitudes of pump wave ( $a_o$ ) with normalized time (t) in hot electron plasma. The parameters used are as follows; $\lambda = 0.035\mu m$ , $r_o = 10\mu m$ , $\omega_p/\omega_o = 0.022$ , $T_e = 400eV$ . . . . .	67
6.3	Normalized amplitudes of back-scattered electromagnetic wave ( $a_1$ ) with normalized time (t) in hot electron plasma. The parameters used are as follows; $\lambda = 0.035\mu m$ , $r_o = 10\mu m$ , $\omega_p/\omega_o = 0.022$ , $T_e = 400eV$ . . . . .	68
6.4	Normalized amplitudes of $E_{pw1}$ ( $a_W$ ) with normalized time (t) in hot electron plasma. The parameters used are as follows; $\lambda = 0.035\mu m$ , $r_o = 10\mu m$ , $\omega_p/\omega_o = 0.022$ , $T_e = 400eV$ . . . . .	68
6.5	Normalized amplitudes of $E_{pw1}$ ( $a_W$ ) with normalized time (t) in hot electron plasma with varying in magnetic field. The parameters used are as follows; $\lambda = 0.035\mu m$ , $r_o = 10\mu m$ , $\omega_p/\omega_o = 0.022$ , $T_e = 400eV$ . . . . .	69
6.6	Normalized amplitudes of $E_{pw1}$ ( $a_W$ ) with normalized time (t) in the presence and absence of hot electron plasma with constant magnetic field ( $\omega_c/\omega_o = 0.03$ ). The parameters used are as follows; $\lambda = 0.035\mu m$ , $r_o = 10\mu m$ , $\omega_p/\omega_o = 0.022$ , $T_e = 400eV$ . . . . .	69
6.7	Normalized amplitudes of $E_{pw2}$ ( $a_D$ ) with normalized time(t) in hot electron plasma. The parameters used are as follows; $\lambda = 0.035\mu m$ , $r_o = 10\mu m$ , $\omega_p/\omega_o = 0.022$ , $T_e = 400eV$ . . . . .	70
6.8	Normalized amplitudes of $E_{pw2}$ ( $a_D$ ) with normalized time (t) in hot electron plasma with varying in magnetic field. The parameters used are as follows; $\lambda = 0.035\mu m$ , $r_o = 10\mu m$ , $\omega_p/\omega_o = 0.022$ , $T_e = 400eV$ . . . . .	70

## ABBREVIATIONS

<b>ICF</b>	Inertial Confinement Fusion
<b>PRA</b>	Paraxial Ray Approximation
$\mu m$	Micrometer
<b>ps</b>	Picoseconds
<b>SRS</b>	Stimulated Raman Scattering
<b>SFRS</b>	Stimulated Forward Raman Scattering
<b>SBRS</b>	Stimulated Backward Raman Scattering
<b>TPD</b>	Two plasmon decay
<b>EMW</b>	Electromagnetic wave
<b>SBW</b>	Side-band wave
<b>IAW</b>	Ion Acoustic wave
<b>NIF</b>	National ignition facility
<b>UHW</b>	Upper Hybrid Wave

## NOTATION

$e$	Charge on electrons
$m$	Mass of the electron
$m_i$	Mass of the ion
$m_{pi}$	Mass of the ions in plasma
$n_{cr}$	Critical Density
$n_o$	Equilibrium plasma density
$\omega_p$	Plasma frequency
$F_p$	Ponderomotive force
$\rho$	Density
$r$	Radius
$r_o$	Spot-size
$v_{th}$	Thermal Velocity
$B$	Magnetic Field

# Chapter 1

## INTRODUCTION

According to the World Energy Council, an UN-accredited global energy agency, the world population will grow by almost 2.5 billion people by 2050 [1], and despite the decreasing pace of development, India's population will continue to rise since it is primarily young. According to predictions over the following 80 years, India's population would peak at 1.65 billion in 2060 before declining. From the reports of the United Nations Millennium Development Goals (MDG) program [2], 8 million Indians (out of 1.2 billion) lived in poverty in 2018–19 which accounts for about 6.7 percent of the country's population living in poverty. The impoverished have limited access to essential utilities such as electricity and water. Despite significant advances in renewable energy technologies, the Council warns that fossil fuels will primarily supply this demand and that global CO<sub>2</sub> emission objectives would be difficult to meet without more stringent global agreements and perhaps intolerable carbon pricing.

The aim from Nuclear fusion is to search for environmental friendly, long-term energy and to provide carbon-free electricity with considerably less radioactive waste than today's fission power plants-while also removing the threat of a reactor meltdown. This is accomplished by employing a hydrogen isotope as a fuel. Since the mid-twentieth century, however, obtaining this era-defining technology has remained out of reach. Today's research is divided into magnetic confinement fusion (MCF) and inertial confinement fusion (ICF). In this thesis, the author has worked on laser-plasma interactions and burn analysis related to inertial confinement fusion. This chapter explains the concept of ICF, as well as motivating and outlining the research given in the rest of the thesis.

## 1.1 Introduction to Inertial Confinement Fusion

### 1.1.1 Nuclear Fusion

When the mass of the reactants surpasses the mass of the products in a nuclear reaction, According to Einstein's equation, energy is released,  $E = \Delta mc^2$  where, the speed of light is  $c$  and  $\Delta m$  the mass difference between the reactants and products. This can also be explained in terms of binding energy of nucleons. The binding energy is defined as the mass difference between the sum of nucleon masses and the mass of the nucleus as a whole and is given by,

$$B = (Zm_p + (A - Z)m_n - m)c^2 \quad (1.1)$$

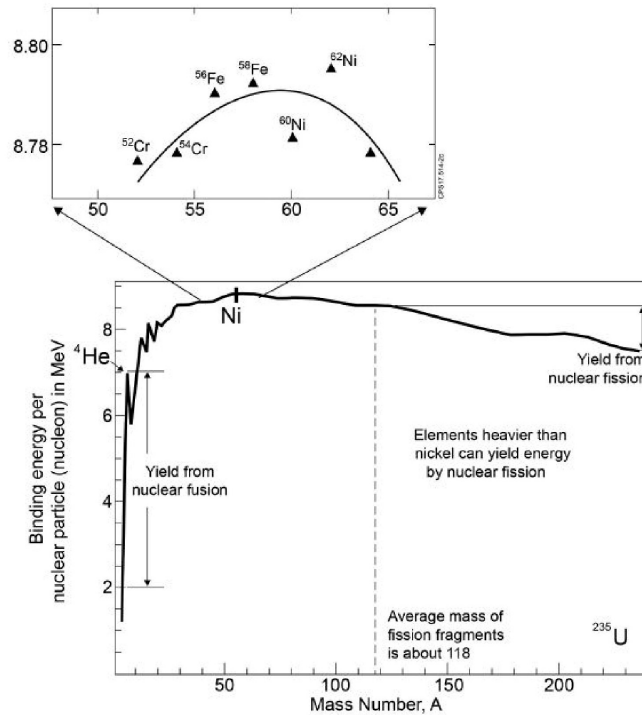


Figure 1.1: The maximum in the graph for  $^{62}\text{Ni}$  is binding energy per nucleon against atomic mass number. Among the light nuclei, the  $^4\text{He}$  nucleus has an unusually high binding energy. The difference in binding energy per nucleon between fusion reactions of light nuclides with  $^4\text{He}$  as one of the reaction products (5 MeV/nucleon) and  $^{235}\text{U}$  fission (0.9 MeV/nucleon) is approximated [5]

Here,  $m_p$  is the mass of proton,  $m_n$  is the mass of neutron,  $m$  is the atomic mass,  $B$  is the binding energy and  $A$  the atomic mass number. Examining the binding energy per nucleon for various isotopes, as displayed in Figure 1.1, is informative. The binding energy per nucleon peaks at iron,  $A = 56$ , before dropping again, as seen in this diagram. The mass of the nucleons will be larger than the atom's mass, resulting in lighter products than reactants. This disparity converts into energy. Splitting elements with masses substantially higher than iron follows the same logic. Hence, despite appearing to be opposed processes, both fusion and fission may produce energy. The neutrons and the protons that make up the nucleus of an atom are held together by a strong nuclear force. However, this nuclear force is short-ranged and decreases considerably faster than the Coulomb force, which repels nuclear protons. There is a point when a proton will be in an unstable equilibrium due to the balance between these attractive and repulsive forces. The Coulomb barrier is the potential energy at this point - when the potential at infinity is set to zero. When two particles collide with enough energy to break the Coulomb barrier, the electromagnetic repulsion is broken, enabling the nuclear force to take hold and form a new atom.

Heating a plasma increases the average kinetic energy of the particles, resulting in high collision velocities. Temperatures of over  $10^7$  K are necessary for fusion to occur in the laboratory. Furthermore, the plasma in a fusion reactor must be either highly dense or



restricted for long periods in order for the bulk of the fuel to collide and fuse. ICF focuses on high-density methods, whereas MCF focuses on considerably longer confinement duration at lower densities. Lawson [3, 4] formalized these needs by balancing the energy generated by these reactions with the system's energy losses owing to different processes such as diffusive and bremsstrahlung losses. As a result, the Lawson criteria became widely used in fusion research,

$$nT\tau_e > 10^{15} (keV cm^{-3} s) \quad (1.2)$$

Here,  $E$  is the confinement time, which is the period after which diffusive losses have matched the energy content of the plasma, and  $n$  and  $T$  are the density and temperature of the fuel, respectively.

### 1.1.2 Inertial Confinement Fusion

The goal of ICF is to ignite a target holding compressed fuel for fusion, deuterium (D) and tritium (T), to the point that the target burns (reacts) considerably before blowing itself up. The energy needed to begin the burn should be considerably less in comparison the energy generated in fusion processes if this is to be used for energy generation. In addition, the energy released by the target must be tiny enough to be contained and transformed into useable power. Deuterium and tritium (DT) undergo a thermonuclear reaction that produces helium (an alpha particle) and a neutron. In a subsequent process, the neutron is utilized to "breed" tritium from lithium. The amount of energy given out is enormous: only 12 mg of a 50-50 DT mixture produces 4.2 GJ of energy. Random collisions of D and T create more energy via the fusion process in a DT plasma at temperatures above 50 million degrees than is reflected away by photons [22]. This is the predicted fusion burn starting temperature—the plasma typically heats up to about 200 million degrees during the burn. Temperature and density affect the rate of reaction per particle. The reaction rate per particle at 200 million degrees is  $5.2 \cdot 10^7 \rho s^{-1}$ , where  $\rho$  is the mass density of the DT mixture in grams per cubic centimeter. An isothermal sphere's disassembly time is about  $R/(3 Cs)$ , where radius is  $R$  and  $Cs$  is sound speed, roughly  $10^8$  cm/s<sup>2</sup> at 200 million degrees. Thus, in order to obtain a substantial fraction of the nuclei to react in the disassembly time, we need an areal density,  $\rho R$ , of  $>3\text{-}7\text{g/cm}^2$ . At DT liquid density, this would necessitate a sphere with a radius of 10-30 cm and a massive energy release. A tiny sphere (weighing a few milligrams) must be utilized to keep the energy required to ignite fusion minimal and the energy produced manageable. Compression is required for this. During compression, the areal density grows (at fixed mass  $R$  image  $R-2$ ) until it reaches a significant percentage of fusion-relevant levels (of order  $3\text{-}7\text{g/cm}^2$ ). For 3 mg of solid/liquid DT, a density increase on the order of a thousand is required. In this thesis the burn calculations for advance fuels is studied.

Over the years, researchers have made significant development in method of fusion. Ex-

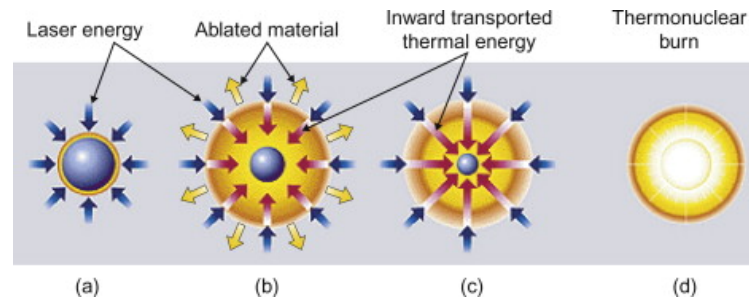


Figure 1.2: In an inertial-confinement capsule, there are four steps to a fusion reaction: (a) The outer layer is heated with a laser. (b) Ablation of the capsule's outer layer compresses the capsule. (c) The density and temperature of the core are sufficient for ignition. (d) Through the compressed fuel, the burn wave spreads quickly [23]

periments at the Lawrence Livermore National Laboratory's National Ignition Facility in California, USA, recently revealed the alpha-heating regime – where the implosion created more energy than was incident onto the target [16]. However, due to inefficiencies in the delivery mechanism, such as hohlraum losses, the total input required to transfer that energy was still considerably larger. It is challenging to go beyond this phase and into the burning plasma regime. High implosion velocities are necessary to create the central hot-spot. Thin shells, which are prone to hydrodynamic instabilities, are required. These instabilities frequently cause the shell to break apart and the shell material to mix with the fuel [18, 19, 20]. This interferes with the fusion process, limiting the improvements made so far with central hot spot ignition [21, 22]. Figure 1.4 gives the summarized steps of Inertial confinement fusion.

Many non-linear LPI's can occur in the region of the plasma corona below the critical density called underdense plasma. The TPD instability, occurs near the quarter-critical density and in which the incident EMW excites two EPW's (plasmons), and the SRS instability, which occurs below the quarter-critical density and excites a scattered EMW of lower frequency and a plasmon, are the two most notable. Because the electric fields associated with plasmons have the potential to accelerate electrons to high energies, these instabilities are cause for concern. Another significant process is SBS, which is similar to SRS but replaces the plasmon with an IAW. This instability can occur anywhere below the critical density, causing energy to be lost. Cross-beam energy transfer (CBET) is a form of SBS in which laser energy is lost when it is scattered from one laser beam's receiving rays into another's departing rays. As laser power increases, the impact of these instabilities intensifies, limiting laser pulse-shape design. The research of SRS and decay instability is the subject of this thesis.

### 1.1.3 Fast Ignition

Max Tabak et al. suggested an alternate method for ignition in ICF in 1994, in which the compression and ignition phases are divided [24]. The DT fuel capsule is compressed isochorically rather than isobarically. Because the driving pulses do not need to ignite the capsule, the compression requirements are far less stringent than traditional central hot spot ignition. Allowing lower shell velocities to be utilized enables considerably more stable and efficient implosions [25, 26]. Because of the lower implosion velocities, smaller in-flight-aspect-ratios (the ratio of shell radius to thickness) may be used to prevent shell breakup, allowing more target mass to be imploded with the same driver energy [27]. Ignition is then initiated by a short-duration petawatt laser pulse that creates a diverging stream of fast electrons when it hits the critical isosurface of the surrounding plasma. The fast electrons then go to the dense core, where they deposit their energy through collisions. For ignition to occur, around 20 kJ of energy must be deposited in the compressed target in roughly 20 ps across a radius of about 20  $\mu\text{m}$  [28, 29]. To be stopped collisionally in the compressed core, the electron beam's divergence must be kept to a minimum, and the electrons must have energy in the 1-3 MeV range [30]. The initial rapid ignition technique suggested the notion of channeling to minimize electron beam divergence and offer better control over the electron spectrum [24]. Another high-intensity beam propagates through the plasma before the ignition pulse is put in, reaching as near to the compressed core as possible. This provides a low-density channel that, if built appropriately, can stretch beyond the initial critical surface, preventing the plasma from significantly changing the ignition pulse's characteristics and giving additional control over the fast electron spectrum while limiting overall divergence. This notion was based in part on early experimental work in 1990s [31, 32, 33] that demonstrated the ejection of plasma from the path of a laser pulse. With two-dimensional particle-in-cell codes, the energy needs for the channeling beam to reach the critical surface of a plasma with a 430 $\mu\text{m}$  scale length is predicted to range between roughly 1.7 kJ to 20.4 kJ for channeling intensities of  $10^{18} \text{ W cm}^{-2}$  and  $10^{21} \text{ W cm}^{-2}$ , respectively [34]. While significant, this energy is marginal in contrast to the mega-joule implosions utilized at the National Ignition Facility. The two beams can also be adjusted for their respective functions by separating these pulses. Since the introduction of this approach, several experimental campaigns have been conducted to study various facets of fast ignition. These studies have ranged from scaled-down proof of concept experiments that successfully showed high-gain fusion [35] to topic-specific studies of the coupling of the laser pulse to fast electrons [36, 37] and the transport of these electrons through the plasma [38, 39, 39, 40, 41]. Research into channeling has been performed using both long-duration, low-intensity pulses [42, 43] and short ( $\leq 1 \text{ ps}$ ), high-intensity ( $\sim 10^{18} - 10^{19} \text{ Wcm}^2$ ) pulses [44, 45, 46]. Still, several challenges continue to exist today, and due to the predicted increased energy requirements. In this thesis the author has worked on the concept of self-focusing in cone-guided fast ignition scheme.

## 1.2 Objectives of the Proposed Work

Based on the challenges faced in ICF, the following are the objectives for the work done in this thesis.

- 1) Enhanced self-focusing of laser in the cone-guided scheme for inertial confinement fusion.
- 2) SRS coupling with decay instability in a magnetized plasma.
- 3) SRS of a laser in a magnetized plasma with density ripple.
- 4) Ignition and Burn calculations for advanced fuels in ICF.

## 1.3 Thesis Outline

The author's study on the laser-plasma interaction and burn analysis in context to inertial confinement fusion is the subject of this thesis. This research was split into analytical, numerical and simulations based investigations. The work is organized as follows:

Chapter 2 introduces the underlying theory required to investigate the events presented in this thesis. This provides a brief overview of the relevant plasma physics, such as laser-plasma interaction and burn analysis.

Chapter 3 presents the results of self-focusing in a cone guided scheme in a density rippled plasma. This includes analytically working on wave equation with WKB approximation and then using paraxial ray approximation for obtaining beam width parameter equation. Then final simulations are done. Work related to this study has been published in European Physical Journal-Plus, 2021. The author has given an invited talk at APPS-DPP 2021 conference on this paper. The author has also given an oral presentation on this work in Kudowa Summer School-2020 and poster related to this work in International Conferences, PMP 2019 and ICPSA 2019 and in Indian Science Congress 2019.

Chapter 4 shows the effect on the growth rate of SRS in presence of a density rippled magnetized plasma. This includes solving continuity equation analytically and doing the instability analysis to achieve the growth rate equation of SRS. Simulations are done further. The author was awarded with "The outstanding talk" in International Summer School on Physics of Plasma-Surface interactions, Moscow, for giving an oral presentation related to this work. The author has also presented work related to this study in the international conference, RAFAS 2021. This chapter forms the basis of a manuscript which is being drafted for submission to Physics of Plasmas.

Chapter 5 gives the advanced fuel calculations for DT. Previous analysis that has been performed for 50-50 D-T is replicated for advanced fuels. This analysis particularly focuses upon the burn-up of these advanced fuels. This aims to determine the fraction of the available fuel that would be utilized in an inertially confined fuel mass of a given size. Whilst it is not thought that a design based upon ignition in an advanced fuel is realizable with

current technology, there are some schemes that consider ignition in 50-50 DT and then burn spread into another markedly different region of fuel. Such schemes may offer a path to ignition in advanced fuels. In support of the analytical work performed, 1-D radiation hydrodynamics simulations are also performed. A part of this work has been presented in GSI-FAIR workshop, Germany 2021 as a poster and in ICPSA 2021 as an oral presentation. This chapter forms the basis of a manuscript which is being drafted for submission to Plasma Physics and Controlled Fusion.

Chapter 6 presents the results of the growth rate of SRS when coupled with decay instability in presence of magnetized plasma. This includes solving continuity equation analytically and doing the instability analysis for all the coupled equations to achieve the growth rate of SRS. Simulations are done further.

Finally, Chapter 7 summarises the work provided in this thesis, as well as the implications that may be taken from it and future research intentions on the subject.

## Bibliography

- [1] P. Scherrer, C. Frei, R. Whitney, H. W. Schiffer, K. Rose, D. A. Rieser, A. Al-Qahtani, and P. Thomas, *World Energy Scenarios: Composing energy futures to 2050*, (World Energy Council, 2013).
- [2] Puja Mehra *8% GDP growth helped reduce poverty: UN report*, (The Hindu, 16 August 2017).
- [3] J. D. Lawson, Proceedings of the physical society. Section B, **70**, (1957) 6.
- [4] S. Atzeni and J. Meyer-ter-Vehn, *The physics of inertial fusion: beam plasma interaction, hydrodynamics, hot dense matter*, OUP Oxford, **125**, (2004).
- [5] J. Ongena, *Fusion: A true challenge for an enormous reward*, EPJ Web of Conferences, **98**, (2015) 05004.
- [6] H. Takabe, K. Mima, L. Montierth, R. L. Morse, The Physics of fluids, **28**, (1985) 3676–3682.
- [7] S. P. Regan, D. K. Bradley, A. V. Chirokikh, R. S. Craxton, D. D. Meyerhofer, W. Seka, R. W. Short, A. Simon, R. P. J. Town, B. Yaakobi, J. J. Carroll, and R. P. Drake, Physics of Plasmas, **6**, (1999) 2072–2080.
- [8] I. V. Igumenshchev, A. B. Zylstra, C. K. Li, P. M. Nilson, V. N. Goncharov, and R. D. Petrasso, Physics of Plasmas, **21**, (2014) 062707.
- [9] R. L. McCrory, D. D. Meyerhofer, R. Betti, R. S. Craxton, J. A. Delettrez, D. H. Edgell, V. Y. Glebov, V. N. Goncharov, D. R. Harding, D. W. Jacobs-Perkins, J. P. Knauer, F. J. Marshall, P. W. McKenty, P. B. Radha, S. P. Regan, T. C. Sangster, W. Seka, R. W. Short, S. Skupsky, V. A. Smalyuk, J. M. Soures, C. Stoeckl, B. Yaakobi, D. Shvarts, J. A. Frenje, C. K. Li, R. D. Petrasso, and F. H. Seguin, Physics of Plasmas, **15**, (2008) 055503.
- [10] R. S. Craxton, K. S. Anderson, T. R. Boehly, V. N. Goncharov, D. R. Harding, J. P. Knauer, R. L. McCrory, P. W. McKenty, D. D. Meyerhofer, J. F. Myatt, A. J. Schmitt, J. D. Sethian, R. W. Short, S. Skupsky, W. Theobald, W. L. Kruer, K. A. Tanaka, R. Betti, T. J. B. Collins, J. A. Delettrez, S. X. Hu, J. A. Marozas, A. V. Maximov, D. T. Michel, P. B. Radha, S. P. Regan, T. C. Sangster, W. Seka, A. A. Solodov, J. M. Soures, C. Stoeckl, and J. D. Zuegel, Physics of Plasmas, **22**, (2015) 110501.

- [11] R. Betti and O. A. Hurricane, *Nature Physics*, **12**, (2016) 435–448.
- [12] L. Ceurvorst, *Relativistic channeling with applications to inertial confinement fusion Electronic Thesis or Dissertation, University of Oxford* (2017).
- [13] R. Kulsrud, E. Valeo, and S. Cowley, *Nuclear fusion*, **26** (1986) 1443.
- [14] R. E. Brown, N. Jarmie, and R. A. Hardekopf, *IEEE Transactions on Nuclear Science*, **30** (1983) 1164–1168.
- [15] National Research Council, *Interim Report—“ Status of the Study” An Assessment of the Prospects for Inertial Fusion Energy*, National Academies Press (2012).
- [16] O. A. Hurricane, D. A. Callahan, D. T. Casey, P. M. Celliers, C. J. Cerjan, E. L. Dewald, T. R. Dittrich, T. Döppner, D. E. Hinkel, L. F. B. Hopkins, J. L. Kline, S. Le Pape, T. Ma, A. G. MacPhee, J. L. Milovich, A. Pak, H.-S. Park, P. K. Patel, B. A. Remington, J. D. Salmonson, P. T. Springer and R. Tommasini, *Nature*, **506** (2017) 343–348.
- [17] S. P. Regan, R. Epstein, B. A. Hammel, L. J. Suter, H. A. Scott, M. A. Barrios, D. K. Bradley, D. A. Callahan, C. Cerjan, G. W. Collins, S. N. Dixit, T. Döppner, M. J. Edwards, D. R. Farley, K. B. Fournier, S. Glenn, S. H. Glenzer, I. E. Golovkin, S. W. Haan, A. Hamza, D. G. Hicks, N. Izumi, O. S. Jones, J. D. Kilkenny, J. L. Kline, G. A. Kyrala, O. L. Landen, T. Ma, J. J. MacFarlane, A. J. MacKinnon, R. C. Mancini, R. L. McCrory, N. B. Meezan, D. D. Meyerhofer, A. Nikroo, H.-S. Park, J. Ralph, B. A. Remington, T. C. Sangster, V. A. Smalyuk, P. T. Springer, and R. P. J. Town, *Physical review letters*, **111** (2013) 045001.
- [18] S. P. Regan, R. Epstein, B. A. Hammel, L. J. Suter, H. A. Scott, M. A. Barrios, D. K. Bradley, D. A. Callahan, C. Cerjan, G. W. Collins, S. N. Dixit, T. Döppner, M. J. Edwards, D. R. Farley, K. B. Fournier, S. Glenn, S. H. Glenzer, I. E. Golovkin, S. W. Haan, A. Hamza, D. G. Hicks, N. Izumi, O. S. Jones, J. D. Kilkenny, J. L. Kline, G. A. Kyrala, O. L. Landen, T. Ma, J. J. MacFarlane, A. J. MacKinnon, R. C. Mancini, R. L. McCrory, N. B. Meezan, D. D. Meyerhofer, A. Nikroo, H.-S. Park, J. Ralph, B. A. Remington, T. C. Sangster, V. A. Smalyuk, P. T. Springer, and R. P. J. Town, *Physical review letters*, **111** (2013) 045001.
- [19] D. Kang, S. Zhu, W. Pei, S. Zou, W. Zheng, J. Gu, and Z. Dai, *arXiv preprint arXiv:1702.05587*, **111** (2017).
- [20] T. Ma, P. K. Patel, N. Izumi, P. T. Springer, M. H. Key, L. J. Atherton, M. A. Barrios, L. R. Benedetti, R. Bionta, E. Bond, D. K. Bradley, J. Caggiano, D. A. Callahan, D. T. Casey, P. M. Celliers, C. J. Cerjan, J. A. Church, D. S. Clark, E. L. Dewald, T. R. Dittrich, S. N. Dixit, T. Döppner, R. Dylla-Spears, D. H. Edgell, R. Epstein, J. Field, D. N. Fittinghoff, J. A. Frenje, M. Gatu Johnson, S. Glenn, S. H. Glenzer, G. Grim, N.

- Guler, S. W. Haan, B. A. Hammel, R. Hatarik, H. W. Herrmann, D. Hicks, D. E. Hinkel, L. F. Berzak Hopkins, W. W. Hsing, O. A. Hurricane, O. S. Jones, R. Kauffman, S. F. Khan, J. D. Kilkenny, J. L. Kline, B. Koziowski, A. Kritcher, G. A. Kyrala, O. L. Landen, J. D. Lindl, S. Le Pape, B. J. MacGowan, A. J. Mackinnon, A. G. MacPhee, N. B. Meezan, F. E. Merrill, J. D. Moody, E. I. Moses, S. R. Nagel, A. Nikroo, A. Pak, T. Parham, H.-S. Park, J. E. Ralph, S. P. Regan, B. A. Remington, H. F. Robey, M. D. Rosen, J. R. Rygg, J. S. Ross, J. D. Salmonson, J. Sater, D. Sayre, M. B. Schneider, D. Shaughnessy, H. Sio, B. K. Spears, V. Smalyuk, L. J. Suter, R. Tommasini, R. P. J. Town, P. L. Volegov, A. Wan, S. V. Weber, K. Widmann, C. H. Wilde, C. Yeaman, and M. J. Edwards, *Physics of Plasmas*, **24** (2017) 056311.
- [21] T. Ma, P. K. Patel, N. Izumi, P. T. Springer, M. H. Key, L. J. Atherton, L. R. Benedetti, D. K. Bradley, D. A. Callahan, P. M. Celliers, C. J. Cerjan, D. S. Clark, E. L. Dewald, S. N. Dixit, T. Döppner, D. H. Edgell, R. Epstein, S. Glenn, G. P. Grim, S. W. Haan, B. A. Hammel, D. Hicks, W. W. Hsing, O. S. Jones, S. F. Khan, J. D. Kilkenny, J. L. Kline, G. A. Kyrala, O. L. Landen, S. Le Pape, B. J. MacGowan, A. J. Mackinnon, A. G. MacPhee, N. B. Meezan, J. D. Moody, A. Pak, T. Parham, H.-S. Park, J. E. Ralph, S. P. Regan, B. A. Remington, H. F. Robey, J. S. Ross, B. K. Spears, V. A. Smalyuk, L. J. Suter, R. Tommasini, R. P. Town, S. V. Weber, J. D. Lindl, M. J. Edwards, S. H. Glenzer, and E. I. Moses, *Physics of Plasmas*, **111** (2013) 085004.
- [22] H.-S. Park, O. A. Hurricane, D. A. Callahan, D. T. Casey, E. L. Dewald, T. R. Dittrich, T. Döppner, D. E. Hinkel, L. F. Berzak Hopkins, S. Le Pape, T. Ma, P. K. Patel, B. A. Remington, H. F. Robey, J. D. Salmonson, and J. L. Kline, *Physical Review Letters*, **112** (2014) 055001.
- [23] G. McCracken and P. Stott, *Inertial-Confinement Fusion*, Fusion (Second Edition) (2013).
- [24] M. Tabak, J. Hammer, M. E. Glinsky, W. L. Kruer, S. C. Wilks, J. Woodworth, E. M. Campbell, M. D. Perry, and R. J. Mason, *Physics of Plasmas*, **1** (1994) 1626–1634.
- [25] R. Betti, K. S. Anderson, J. P. Knauer, T. J. B. Collins, R. L. McCrory, P. W. McKenty, and S. Skupsky, *Physics of Plasmas*, **12** (2005) 042703.
- [26] S. E. Bodner, A. J. Schmitt, and J. D. Sethian, *Physics of Plasmas*, **1** (2013) 2–10.
- [27] R. Betti and C. Zhou, *Physics of Plasmas*, **12** (2005) 110702.
- [28] R. Betti and C. Zhou, *High Power Laser Science and Engineering*, **2** (2014) e6.
- [29] R. Kodama, P. A. Norreys, K. Mima, A. E. Dangor, R. G. Evans, H. Fujita, Y. Kitagawa, K. M. Krushelnick, T. Miyakoshi, N. Miyanaga, T. Norimatsu, S. J. Rose, T. Shozaki, K. Shigemori, A. Sunahara, M. Tambo, K. A. Tanaka, Y. Toyama, T. Yamanaka, and M. Zepf, *Nature*, **412** (2001) 798–802.



- [30] A. J. Kemp, F. Fiuza, A. Debayle, T. Johzaki, W. B. Mori, P. K. Patel, Y. Sentoku, and L. O. Silva, *Nuclear Fusion*, **54** (2014) 054002.
- [31] X. Liu and D. Umstadter, *Physical review letters*, **69** (1992) 1935.
- [32] A. B. Borisov, A. V. Borovskiy, V. Korobkin, A. M. Prokhorov, O. B. Shiryaev, X. M. Shi, T. S. Luk, A. McPherson, J. C. Solem, K. Boyer, and C. K. Rhodes, *Physical review letters*, **68** (1992) 2309.
- [33] C. G. Durfee and H. M. Milchberg, *Physical review letters*, **71** (1993) 2409.
- [34] G. Li, R. Yan, C. Ren, T.-L. Wang, J. Tonge, and W. B. Mori, *Physical review letters*, **100** (2008) 125002.
- [35] R. Kodama, H. Shiraga, K. Shigemori, Y. Toyama, S. Fujioka, H. Azechi, H. Fujita, H. Habara, T. Hall, Y. Izawa, T. Jitsuno, Y. Kitagawa, K. M. Krushelnick, K. L. Lancaster, K. Mima, K. Nagai, M. Nakai, H. Nishimura, T. Norimatsu, P. A. Norreys, S. Sakabe, K. A. Tanaka, A. Youssef, M. Zepf, and T. Yamanaka, *Nature*, **418** (2002) 933–934.
- [36] N. Booth, R. J. Clarke, D. Doria, L. A. Gizzi, G. Gregori, P. Hakel, P. Koester, L. Labate, T. Levato, B. Li, M. Makita, R. Mancini, J. Pasley, P. Rajeev, D. Riley, A. P. L. Robinson, E. Wagenaars, J. Waugh, and N. C. Woolsey, *Nuclear Instruments and Methods in Physics Research Section A: Accelerators, Spectrometers, Detectors and Associated Equipment*, **653** (2011) 137–139.
- [37] J. S. Green, V. M. Ovchinnikov, R. G. Evans, K. U. Akli, H. Azechi, F. N. Beg, C. Bellei, R. R. Freeman, H. Habara, R. Heathcote, M. H. Key, J. A. King, K. L. Lancaster, N. Lopes, T. Ma, A. J. MacKinnon, K. Markey, A. McPhee, Z. Najmudin, P. M. Nilson, R. Onofrei, R. B. Stephens, K. Takeda, K. A. Tanaka, W. Theobald, T. Tanimoto, J. Waugh, L. D. Van Woerkom, N. C. Woolsey, M. Zepf, J. R. Davies, and P. A. Norreys, *Physical review letters*, **100** (2008) 015003.
- [38] R. Kodama, Y. Sentoku, Z. L. Chen, G. R. Kumar, S. P. Hatchett, Y. Toyama, T. E. Cowan, R. R. Freeman, J. Fuchs, Y. Izawa, M. H. Key, Y. Kitagawa, K. Kondo, T. Matsuoka, H. Nakamura, M. Nakatsutsumi, P. A. Norreys, T. Norimatsu, R. A. Snavely, R. B. Stephens, M. Tampo, K. A. Tanaka, and T. Yabuuchi, *Nature*, **432** (2004) 1005–1008.
- [39] L. Labate, E. Förster, A. Giulietti, D. Giulietti, S. Höfer, T. Kämpfer, P. Köster, M. Kozlova, T. Levato, R. Löttsch, A. Lübcke, T. Mocek, J. Polan, B. Rus, I. Uschmann, F. Zamponi, and L. A. Gizzi, *Laser and Particle Beams*, **27** (2009) 643–649.
- [40] R. H. H. Scott, F. Perez, J. J. Santos, C. P. Ridgers, J. R. Davies, K. L. Lancaster, S. D. Baton, P. Nicolai, R. M. G. M. Trines, A. R. Bell, S. Hulin, M. Tzoufras, S. J. Rose, and P. A. Norreys, *Physics of Plasmas*, **19** (2012) 053104.

- 
- [41] L. Volpe, J.-L. Feugeas, P. Nicolai, J. J. Santos, M. Touati, J. Breil, D. Batani, and V. T. Tikhonchuk, *Physics of Plasmas*, **90** (2014) 063108.
- [42] P. E. Young, M. E. Foord, J. H. Hammer, W. L. Kruer, M. Tabak, and S. C. Wilks, *Physical review letters*, **75** (1995) 1082.
- [43] K. A. Tanaka, H. Hashimoto, R. Kodama, K. Mima, Y. Sentoku, and K. Takahashi, *Physical review letters*, **60** (1999) 3283.
- [44] M. Borghesi, A. J. MacKinnon, L. Barringer, R. Gaillard, L. A. Gizzi, C. Meyer, O. Willi, A. Pukhov, and J. Meyer-ter Vehn, *Physical review letters*, **78** (1997) 879.
- [45] J. Fuchs, J. C. Adam, F. Amiranoff, S. D. Baton, P. Gallant, L. Gremillet, A. Héron, J. C. Kieffer, G. Laval, G. Malka, J. L. Miquel, P. Mora, H. Pépin, and C. Rousseaux, *Physical review letters*, **80** (1998) 2326.
- [46] Z. Najmudin, K. M. Krushelnick, M. Tatarakis, E. L. Clark, C. N. Danson, V. Malka, D. Neely, M. I. K. Santala, and A. E. Dangor, *Physics of Plasmas*, **10** (2003) 438–442.
- [47] W. L. Kruer, *The Physics of Laser Plasma Interactions* (Addison-Wesley, Redwood City, CA,) 1988.
- [48] J. F. Myatt, J. Zhang, R. W. Short, A. V. Maximov, W. Seka, D. H. Froula, D. H. Edgell, D. T. Michel, I. V. Igumenshchev, D. E. Hinkel and P. Michel, *Physics of Plasmas*, **21** (2014) 055501.

# Chapter 2

## Research Methodology

### 2.1 Description of work

The work described in this thesis spans a wide range of physics topics, including Plasma Physics Fundamentals, Fluid Theory, Kinetic Theory, Paraxial Ray Approximation (PRA), WKB approximation, Polarisation of laser beam, Self-focusing, Parametric Instabilities, Density Rippled, Applied Magnetic Fields in Plasma and Inertial Confinement Fusion (ICF). It is impossible to do justice to any of these topics here because each might be the book's subject. As a result, only the most critical aspects from each topic are provided, and the reader will be referred to great resources for additional study instead of a more extensive dissertation. The next section of this chapter gives an overview of these theories, which allow for the modeling of situations with a wide dynamic range.

### 2.2 Fluid Model

#### 2.2.1 Introduction

In the fluid approximation, the plasma is considered to be made up of two or many interlayer fluids, one for each type. When there are just one ion species, we will require two equations of motion, for the positively and the the negatively charged ion and electron fluid repectively. The equation is also required for the fluid of neutral atoms in a partly ionized gas. Collisions are the only way for the neutral fluid to interact with the ions and electrons. Because the E and B fields are created, the ion and electron flows will interact with each other even if there are no collisions.

## 2.2.2 Fluid Equation of Motion

### Collisions and thermal motion are ignored

Consider a particle with velocity  $\vec{v}$ . Equation of motion is given by

$$m \frac{d\vec{v}}{dt} = q(\vec{E} + \vec{v} \times \vec{B}) \quad (2.1)$$

Because collisions and thermal impacts are ignored, all parts of a fluid element will flow at the same average velocity. We can also use  $\vec{u} = \vec{v}$ , and the equation of motion for a fluid element with a density of  $n$  particles is;

$$nm \frac{d\vec{u}}{dt} = nq(\vec{E} + \vec{u} \times \vec{B}) \quad (2.2)$$

### Variables that move with the fluid element (fixed frame)

Consider any property of a fluid in one-dimensional  $x$  space as  $V(x, t)$  to make the transformation to variables in a fixed frame. The sum of two terms determines the change in  $x'$  with time in a frame moving with the fluid:

$$\frac{dx'}{dt} = \frac{\partial x'}{\partial t} + u_x \frac{\partial x'}{\partial x} \quad (2.3)$$

The first term on the right represents the change in  $x'$  at a fixed location in space, and the change in  $x'$  when the observer travels with the fluid into a region where  $x$  is different is represented by the second term on the right. In three dimensions;

$$\frac{d\vec{x}'}{dt} = \frac{\partial \vec{x}'}{\partial t} + (\vec{u} \cdot \nabla) \vec{x}' \quad (2.4)$$

This is called the convective derivative. In the case of a plasma, we take  $\vec{x}'$  to be the fluid velocity  $\vec{u}$ ,

$$nm \left( \frac{\partial \vec{u}}{\partial t} \right) + (\vec{u} \cdot \nabla) \vec{u} = nq(\vec{E} + \vec{u} \times \vec{B}) \quad (2.5)$$

### Including Thermal Effects

When considering thermal movements, a pressure force must be applied. The random mobility of particles in and out of a fluid element gave rise to this force, which does not exist in the equation for a single particle. A collective effect describes the random mobility of the particles in the fluid element. This is the standard force of a pressure gradient. We get

the fluid equation by adding the electromagnetic forces and generalising to three dimensions:

$$nm \left( \frac{\partial \vec{u}}{\partial t} \right) + (u \cdot \nabla) \vec{u} = nq(\vec{E} + \vec{u} \times \vec{B}) - \vec{\nabla} p \quad (2.6)$$

### Collisions Included

If a neutral gas is present, collisions between the charged fluid and the neutral gas can interchange momentum. The amount of momentum lost each impact is proportional to the relative velocity  $\vec{u} - \vec{u}_o$ , where  $u_o$  is the neutral fluid's velocity. The resultant force term may be generally expressed as  $mn(\vec{u} - \vec{u}_o)/\tau$  if  $\tau$ , the mean free time between collisions, is essentially constant. Then, incorporating neutral collisions and thermal impacts, the fluid equation of motion is:

$$nm \left( \frac{\partial \vec{u}}{\partial t} + (u \cdot \nabla) \vec{u} \right) = nq(\vec{E} + \vec{u} \times \vec{B}) - \vec{\nabla} \cdot p - \frac{mn(u - u_o)}{\tau} \quad (2.7)$$

## 2.3 Laser-Plasma Interaction

A plasma must exhibit what is known as "collective behavior." In a neutral gas, particles are unaffected by electromagnetic fields and respond only to collisions. As a result, fluid evolution within such gas is defined by local interactions. However, in a plasma, the particles have charges, which means that local concentrations and movements give rise to electric and magnetic fields, which affect distant particles. A sufficiently heated plasma can even be regarded collisionless, enabling collisions to be ignored altogether as the plasma evolves through long-range electromagnetic interactions. As a result of collective behavior, the mobility of plasma is determined not just by local circumstances but also by the plasma's overall state.

Furthermore, plasma must be "quasi-neutral." When a probe charge is introduced into a plasma, the electrons move quickly to protect the probe charge from the effects of the electric and magnetic fields. The field from the external charge is attenuated over a distance known as the Debye length due to this. If the plasma's dimensions are significantly higher than the Debye length, the plasma stays primarily neutral, and the ion charge density and electron charge density are almost similar. Even yet, there are minor density variations that allow for intriguing electromagnetic interactions. Furthermore, for shielding to be a statistically meaningful notion, the plasma must include enough particles to accomplish the shielding. As a result, a plasma must have a vast enough spatial extent compared to the Debye length and a high enough density to hold numerous particles within a Debye-length sphere.

Finally, rather than hydrodynamic forces, electromagnetic forces must dominate the develop-

ment of the plasma. Plasma particles spontaneously oscillate. This activity has a significant impact on plasma macro-behavior. This process is inhibited if charged particles hit with neutral atoms faster than they usually oscillate, and the gas tends to hydrodynamic evolution. As a result, the frequency of typical oscillations must be greater than the frequency of charge-neutral collisions. The rest of this chapter covers the laser-plasma interaction theory needed to comprehend plasma evolution, which is done to acquire a better knowledge of the phenomena and analyses discussed in the following chapters of this thesis.

### 2.3.1 The Plasma Frequency

Because there are two overlapping, oppositely charged fluids in the plasma, if there is any charge separation, the fluids will adapt to shield out the electrostatic forces. Because electrons are hundreds of times lighter than ions, the electron species will account for the vast bulk of movement. Indeed, many of the phenomena observed in plasmas employing picosecond-duration laser pulses may be explained if the ions are stationary in space. Only the equations regulating the electron fluid and the Poisson equation, which read respectively as;

$$m_e n_e \left( \frac{\partial \vec{v}}{\partial t} + (\vec{v}_e \cdot \nabla) \vec{v}_e \right) = -n_e e (\vec{E} + \vec{V}_e \times \vec{B}) - \nabla \vec{P}_e + m_e n_e v_{ei} (\vec{v}_e - \vec{v}_i) \quad (2.8)$$

must be considered in this instance. The above equation is the electron fluid equation.

$$\frac{\partial n_e}{\partial t} + \vec{\nabla} \cdot n_e \vec{v}_e = 0 \quad (2.9)$$

The above equation is the electron continuity equation.

$$\vec{\nabla} \cdot \vec{E} = \frac{e}{\varepsilon_o} (Z n_i - n_e) \quad (2.10)$$

Each denotations' mass, density, velocity, and pressure are represented as  $m$ ,  $n$ ,  $v$ , and  $P$ , with  $e$  subscripts indicating electron species and  $i$  subscripts suggesting ion species. The electron-ion collision rate is  $v_{ei}$ , the charge state is  $Z$ , and the units of time, elementary charge, electric field, magnetic field, and free space permittivity are  $t$ ,  $e$ ,  $\vec{E}$ ,  $\vec{B}$  and  $\varepsilon_o$  correspondingly. The reader is referred to Chen [1] for a more thorough treatment.

Consider a cold ( $Pe = 0$ ), collisionless ( $v_{ei} = 0$ ), homogeneous, and neutral plasma that is at rest with no external fields. In order to reestablish charge neutrality, any charge separation would drive electrons to migrate towards the ions. They would, however, overshoot the ions and begin to bounce about them due to their inertia. Given the period of electron oscillations, the plasma is expected to be homogeneous and at rest with no externally imposed fields, and the ions are considered to be immobile. Therefore,

$$\nabla n_o = n_{i1} = v_o = B_o = E_o = 0 \quad (2.11)$$

$$\frac{\partial n_o}{\partial t} = \frac{\partial v_o}{\partial t} = \frac{\partial E_o}{\partial t} = \frac{\partial B_o}{\partial t} = 0 \quad (2.12)$$

Expanding Equations 2.8-2.10 and keeping only the first order terms gives:

$$m_e n_{eo} \frac{\partial v_{e1}}{\partial t} = -n_{eo} e \vec{E}_1 \quad (2.13)$$

$$\frac{\partial n_{e1}}{\partial t} + n_{eo} \vec{\nabla} \cdot \vec{v}_{e1} = 0 \quad (2.14)$$

$$\vec{\nabla} \cdot \vec{E}_1 = -\frac{e}{\varepsilon_o} n_{e1} \quad (2.15)$$

Combining the above equations and eliminating the perturbed quantities we get,

$$m_e \varepsilon_o \omega^2 = n_{eo} e^2 \quad (2.16)$$

let  $\omega = \omega_p$ . Therefore, we get

$$\omega_p = \sqrt{\frac{ne^2}{m_e \varepsilon_o}} \quad (2.17)$$

This is one of the essential characteristics of a plasma, and it depicts the natural oscillations of electron species around ion species. Because  $m_e$  is so tiny, the plasma frequency in inertial confinement fusion is generally relatively high. This thesis is majorly concerned with plasmas of densities ranging from  $10^{19} \text{cm}^{-3}$  to  $10^{22} \text{cm}^{-3}$ , with plasma frequencies ranging from  $10^{13} \text{Hz}$  to  $10^{15} \text{Hz}$ .

### 2.3.2 Paraxial Ray Approximation

Paraxial Ray Approximation (PRA), Variational Method, and Moment Theory are some of the approaches used to analyze the nonlinear processes during laser-plasma contact. According to the literature review, the Paraxial Ray Approximation (near axis) technique proposed by Akhmanov et al. [2] in 1968 is the simplest and qualitatively corresponds with experimental data. Only the behavior of rays near the axis will be considered using this method (or paraxial). Sodha et al. investigated the propagation of electromagnetic waves in semiconductors, dielectrics, and gaseous plasmas. Sodha et al. [3] used the PRA method to investigate electromagnetic wave propagation in semiconductors, dielectrics, and gaseous plasmas. An introductory book and a review article were also produced in 1974 and 1976 to discuss the phenomenon of self-focusing using the PRA method [3, 4]. As a result, we have used the PRA method in a chapter of this thesis.

### 2.3.3 Ponderomotive Force

In an inhomogeneous oscillating electromagnetic field, a charged particle feels a ponderomotive force, a nonlinear force. Instead of oscillating about an initial point as in a homogeneous field, it leads the particle to migrate towards the weaker field strength area. This happens because the particle experiences a larger magnitude of force during the half of the oscillation period when it is in the stronger field region. The net force in the weaker area in the second half of the oscillation does not cancel out the net force in the first half, causing the particle to migrate towards the weaker area throughout the cycle. It is expressed as,

$$F_p = \frac{-e^2}{4m\omega^2} \nabla E^2 \quad (2.18)$$

It is measured in newtons (in SI units), with  $e$  equaling the particle's electrical charge,  $m$  equaling its mass,  $\omega$  equaling the field's angular frequency of oscillation, and  $E$  equaling the electric field's amplitude. The magnetic field exerts very little force at low enough amplitudes. In an in-homogeneous oscillating field, a charged particle oscillates at the field's frequency and is also propelled toward the weak field direction by  $F_p$ .

### 2.3.4 Self-Focusing of Laser Beam

Over the last few decades, the phenomenon of laser beams self-focusing in plasma has been a matter of significant research [5]. The wave-front of the laser acquires a curvature as a result of the generated refractive index changes and therefore tends to concentrate. This is known as self-focusing. Self-focusing occurs as a result of the many processes that generate refractive index changes.

The self-focusing phenomenon is fascinating and important in a variety of applications, including laser-driven fusion, plasma-based charged accelerators, x-ray lasers, harmonic production, electron acceleration in wake-field, and inertial confinement fusion, among others. It is unsuitable for situations where fuel pellet compression can be avoided, but it does give a way of achieving high flux densities, which are required to research laser plasma interactions [8]. It also limits the amount of power that can be transferred over an optical medium, and it frequently causes damage to optical materials [7]. If the laser power is above the critical power, the laser propagates in a periodic concentrated fashion, and if it is below the critical power, the laser diverges [6]. Relativistic mass change causes the relativistic self-focusing effect. If the frequency of electron oscillations in plasma exceeds the natural frequency, the electrons will be pushed to migrate away from the beam field. The concentrated beam then imposes a radial ponderomotive force on electrons, causing them to migrate away from the beam, resulting in a lower density area and radiation focusing [7]. There are four types of self-focusing; Plasma self-focusing, Thermal self-focusing, Relativistic self-focusing, and



ponderomotive self-focusing. In this thesis we work on relativistic self-focusing.

### Relativistic self-focusing

This is the nonlinear mechanism that causes the refractive index of plasma to change. The mass increase of electrons causes relativistic self-focusing, which changes the refractive index to  $\eta_{rel}$  as  $\eta_{rel} = (1 - \omega_p^2/\omega^2)^{1/2}$ , where  $\omega_p$  is the relativistic plasma frequency.

### 2.3.5 Plasma Density Ramp

The plasma density ramp, also known as the density transition in plasma, plays an essential and fascinating function in laser-plasma interactions because it is exploited to counteract laser beam defocusing [9]. Due to the relativistic effect, a powerful laser beam passing through underdense plasma obtains a minimal spot size, resulting in frequent and repetitive self-focusing or defocusing of the beam. The density ramp is thought to make the self-focusing effect a little greater [10, 11, 12]. Because the laser beam detects a narrower channel in the density ramp area, the oscillation amplitude contracts in this environment as the frequency of the laser beam increases. As the laser beam penetrates further into the plasma, the dielectric constant of the plasma falls fast due to the rising electron density as a function of propagation distance. As a result, the laser beam becomes more focused, enhancing the self-focusing effect [15]. In an underdense plasma, the duration of the density ramp should be extended to prevent the laser from defocusing and to observe a better and maximum focusing nature [9]. As a result, the plasma density ramp plays a fascinating function in enhancing the self-focusing effect. Such a plasma density ramp has been seen in gas jet plasma studies. In combination with a density ramp, magnetic fields have been shown to improve beam focusing capacity [13, 14]. Because the laser beam is concentrated and propagates over a considerable distance without diverging, this method may be utilized for a variety of laser-driven applications.

### 2.3.6 Parametric Instabilities in ICF

In the plasma, parametric instabilities are a nonlinear phenomena in which a high amplitude wave triggers two decay waves. It may be thought of as the decay of a photon (or Plasmon) with energy  $h\omega_o$  and momentum  $hk_o$  into photons/plasmons with energy and momentum  $(h\omega, h\vec{k})$  ( $h\omega_1, h\vec{k}_1$ ). Because momentum and energy are preserved, the phase matching requirements are  $k_o = k_1 + k_2$ ,  $\omega_o = \omega_1 + \omega_2$ . Only when one of the decay waves is an electrostatic wave are these requirements met. An electrostatic or electromagnetic wave

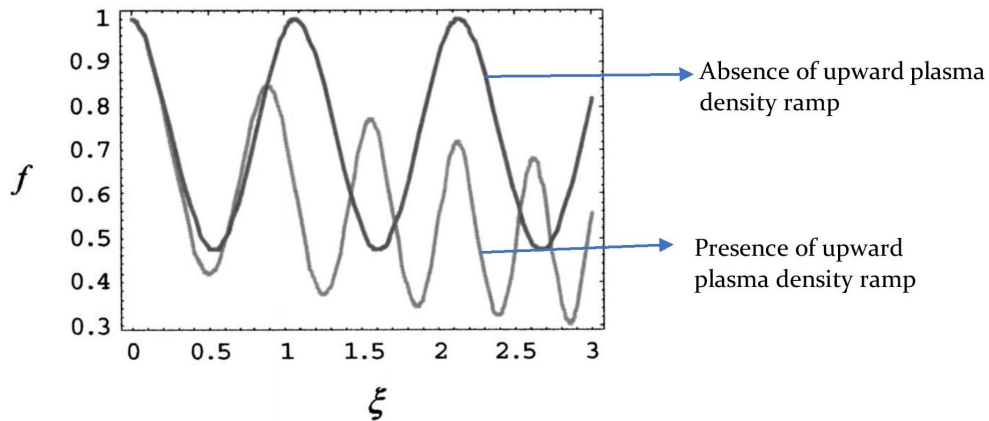


Figure 2.1: Upward Plasma Density Ramp

might be the other decay wave. The parametric process follows the following dynamics: The plasma electrons are given an oscillating velocity by the huge amplitude pump wave. The density perturbation associated with one of the decay waves combines with the oscillatory velocity caused by the pump wave to generate a nonlinear current, which is the source of the second decay wave. The laser beats with the pump to impose a ponderomotive force on the electrons to generate the initial decay wave. As a result, both the decaying wave and the pump energy grow. In many laser-driven ICF experiments, parametric instabilities have been found [16]. Kaw, Kruer, Liu, and Nishikawa [17] and Liu and Tripathi [21] provide comprehensive studies of parametric instabilities in magnetized and unmagnetized plasmas. The following parametric instabilities are particularly important in laser-produced plasmas:

- (1) Raman scattering with a stimulus (SRS)

- (2) Two Plasmon Decay (TPD)
- (3) Brillouin Scattering Stimulated (SBS)
- (4) Decay Instability

In this thesis the author consider the role of SRS and decay instability in ICF

### Stimulated Raman Scattering

In direct drive or indirect drive fusion, a laser ablates a spherical shell in ICF [4] to compress fusion fuel to thermonuclear temperatures and densities. In the coronal plasma, laser-plasma instabilities (LPI)[19, 20] may create supra-thermal (“hot”) electrons, which preheat the cold fuel, reduce compressibility, and therefore impede the ignition process. Therefore the study of SRS is considered very important. In this thesis the author considers various plasma profiles which could help in the suppression of SRS.

At plasma concentrations below quarter critical  $n_o^o = n_{cr}/4$ , the huge amplitude pump wave decays into a sideband electromagnetic wave and a Langmuir wave [21] (where  $n_{cr}$  is the critical density at which the plasma frequency becomes equal to the laser frequency). SRS has the following feedback mechanism: Plasma electrons are given oscillatory velocity by a pump wave with frequency  $\omega_o$  and wave vector  $\vec{k}_o$  at  $(\omega_o, \vec{k}_o)$ . The oscillatory velocity interacts with the density perturbation  $n_\omega$  (caused by the Langmuir wave at  $(\omega, \vec{k})$ ) to produce a nonlinear current density at  $(\omega_1, \vec{k}_1)$ , where  $\omega_1 = \omega_o + \omega$  and  $\vec{k}_1 = \vec{k}_o + \vec{k}$  are constants. The resonance criteria relate to energy conservation and momentum conservation, respectively. Nonlinear current, in turn, drives a resonant electromagnetic sideband wave at  $(\omega_1, \vec{k}_1)$ . The Langmuir wave is driven by a nonlinear ponderomotive force produced by the sideband electromagnetic wave  $(\omega_1, \vec{k}_1)$  and the pump wave  $(\omega_o, \vec{k}_o)$ . As a result of the feedback mechanism, both the Langmuir wave and the sideband electromagnetic wave expand at the price of pump wave energy. Figure 2.2 shows a schematic diagram of the Raman process (1.5). SRS can be further analysed in two parts; Stimulated Forward Raman scattering that has been stimulated in forward direction (SFRS) and Stimulated backward Raman scattering in the reverse direction (SBRS).

### Decay Instability

The pump wave decays into counter-propagating ion-acoustic and Langmuir waves throughout this process. When plasma density approaches the critical density, i.e.,  $n_o \approx n_{cr}$  [21], decay instability occurs. The pump plasma wave can resonantly trigger a pair of low-frequency ion acoustic wave (IAW) [23, 24, 25, 27] and side scattered plasma waves near the critical layer, resulting in decay instability. It causes low-frequency turbulence in the plasma, changing macroscopic characteristics such as particle movement, thermal conductivity, and plasma resistivity [28]. The following is the mechanism behind the parametric decay process. The pump wave beats with the sideband Langmuir wave, causing a low-frequency ponderomotive force on the plasma electrons, which drives the low-frequency IAW. Low-frequency IAW and sideband waves increase at the price of pump energy in this fashion. The local approximation was utilized in previous investigations of decay instability, which were limited to unbounded plasma. The resonant decay instability of a Langmuir wave in a plasma slab was explored by Jain et al.[29]. The rate of development of the instability was shown to rise with plasma slab width and approaches the value for infinite uniform plasma. The boundary effect stopped decay wave energy from diffusing and lowered the threshold for parametric instabilities to appear. The process's growth rate falls as the frequency of the pump and the number of decay waves in the azimuthal mode decrease.

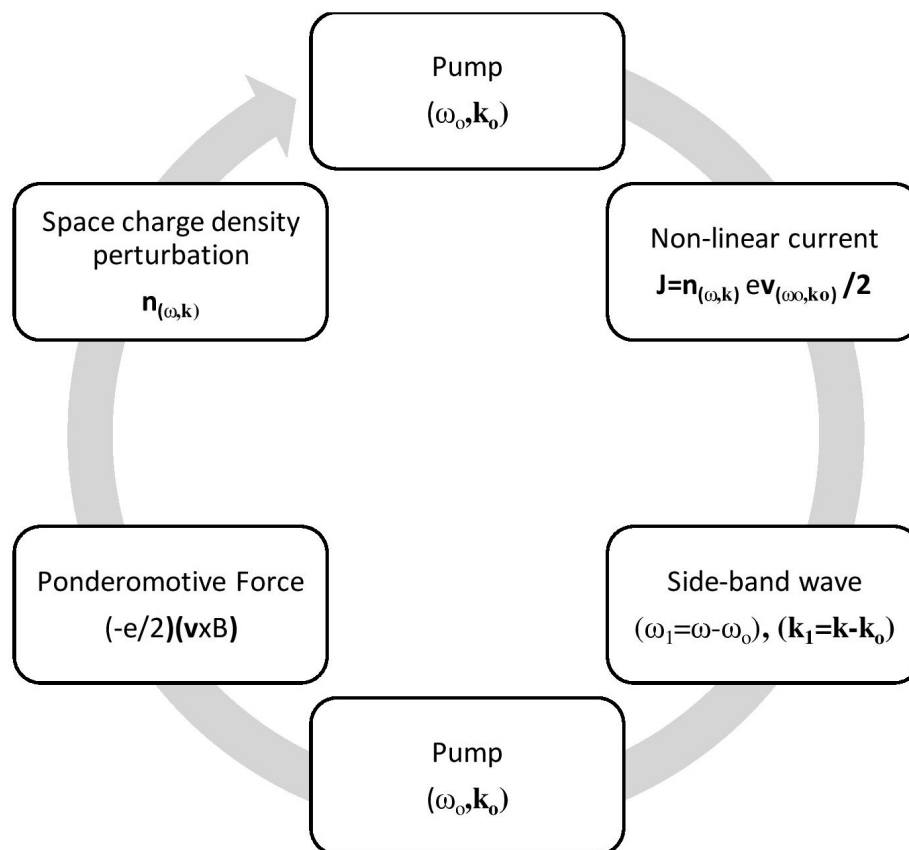


Figure 2.2: Feedback mechanism of SRS

## 2.4 Magnetic Field in Plasma

The production of high magnetic fields is the third significant phenomenon seen in laser-plasma interaction. Multi mega-Gauss magnetic fields in plasma in front of solid objects have been recorded [30, 31] and ascribed to the  $\nabla n \times \nabla T$  mechanism, which arises when the temperature gradient ( $= T$ ) and the plasma density gradient ( $nabla n$ ) are not collinear. Strong magnetic fields may significantly affect the direction and magnitude of heat fluxes in plasmas [32]; thus, they can be helpful in laser-plasma-based fusion systems such as direct and indirect drive ICF. Magnetic fields have been shown to restrict heat transfer in hohlraums, resulting in abnormally high electron temperatures [34]. In solid density plasmas, numerical simulations applicable to the rapid ignitor version of ICF have recently projected self-generated magnetic fields ranging from 30 to 1000 MG [34].

To explain magnetic-field production in solid density plasmas, Davies et al. [37] created a hybrid particle/fluid code. In his model, he injects a beam of strong electrons depicted as particles into a backdrop of warm electrons described as a fluid. Magnetic fields will arise inside the uniform density target, concentrating the fast electrons and allowing them to travel through many microns of dense plasma, according to this concept. Magnetic fields inside dense, uniform plasmas have also been anticipated using particle-in-cell (PIC) simulations, again in the presence of beams of fast electrons, but under conditions where collisional effects are less relevant.

Simulations reveal that more than 30% of the energy transferred from the laser to relativistic electrons is transmitted in the fast ignition method [38]. The azimuthal magnetic fields around the laser's axis are caused by relativistic electrons traveling with the light. The presence of strong self-generated magnetic fields in laser-produced plasmas alters the dynamics of parametric instabilities dramatically. The magnetic field has a tremendous impact on the plasma eigenmodes, resulting in many new modes and new parametric decay channels. Lower hybrid waves, for example, are supported by magnetized plasma. The inhomogeneous azimuthal magnetic field significantly impacts the frequency and mode structure of a lower hybrid mode. The azimuthal magnetic field would have a large signature if the laser was parametrically coupled with this mode.

## Bibliography

- [1] F. F. Chen, *Introduction to Plasma Physics and Controlled Fusion*, Springer US, Boston, MA, 2 edition (1984).
- [2] R. A. Akhmedzhanov, I. E. E. Ilyakov, V. A. Mironov, E. V. E. Suvorov, D. A. Fadeev and B.V Shishkin, JETP letters, **88**, (2008) 569–573.
- [3] M. S. Sodha, S. K. Mishra S K and S. Mishra, Journal of plasma physics, **75**, (2009) 731–748.
- [4] M. S. Sodha, A. K. Ghatak and V. K. Tripathi, *Self-focusing of Laser Beams in Dielectrics*, Plasmas and Semiconductors, Tata McGraw-Hill, New Delhi (1974).
- [5] R. Bharuthram, J. Parashar and V. K. Tripathi, Physics of Plasmas, **6**, (1999) 1611.
- [6] H. Hora, JOSA, **65**, (1975) 882-886.
- [7] H. Hora, Journal of plasma physics, **226**, (1969) 156–159.
- [8] M. R. Siegrist, Optics Communications, **16**, (1976) 402–407.
- [9] D. N. Gupta, M. S. Hur, I. Hwang, H. Suk, Hyyong and A. K. Sharma, JOSA B, **24**, (2007) 1155–1159.
- [10] N. Kant, S. Saralch and H. Singh, Nukleonika, **56**, (2007) 149–153.
- [11] V. Nanda and N. Kant, Physics of Plasmas, **21**, (2014) 042101.
- [12] M. Habibi and F. Ghamari, JOSA B, **32**, (2015) 1429–1434.
- [13] D. N. Gupta, M. N. Hur and H. Suk, Applied Physics Letters, **91**, (2007) 081505.
- [14] M. Wani, A. Manzoor and N. Kant, Optik, **127**, (2016) 6710–6714.
- [15] S. D. Patil and M. V. Takale, Physics of Plasmas, **20**, (2013) 083101.
- [16] C. Yamanaka, *Inertial confinement fusion: The quest for ignition and energy gain using indirect drive*, IOP Publishing (1999).
- [17] P. K. Kaw , W. L. Kruer, C. S. Liu, K. Nishikawa, Advances in plasma physics, **6** (1976).

- [18] S. Atzeni and J. Meyer-ter-Vehn, *The physics of inertial fusion: beam plasma interaction, hydrodynamics, hot dense matter*, OUP Oxford, **125**, (2004).
- [19] W. L. Kruer, *The Physics of Laser Plasma Interactions* (Addison-Wesley, Redwood City, CA,) 1988.
- [20] J. F. Myatt, J. Zhang, R. W. Short, A. V. Maximov, W. Seka, D. H. Froula, D. H. Edgell, D. T. Michel, I. V. Igumenshchev, D. E. Hinkel and P. Michel, *Physics of Plasmas*, **21** (2014) 055501.
- [21] C. S. Liu and V. K. Tripathi, *Interaction of electromagnetic waves with electron beams and plasmas*, World Scientific, (1994).
- [22] *Interim Report— " Status of the Study" An Assessment of the Prospects for Inertial Fusion Energy"*, National Research Council and others, National Academies Press (2012).
- [23] C. Nyack, P. Christiansen and G. Martelli, *Magnetospheric physics, Wave Particle Interaction—Some Laboratory Observations* **6** (1974) 215-230.
- [24] R. Franklin, S. Hamberger, G. Lampis and G. Smith, *Physical Review Letters*, **27** (1971) 1119.
- [25] E. J. Yadlowsky , and P. D. Goldan, *Physics of Fluids*, **17** (1974) 1443-1448.
- [26] A. Bakai , E. Kornilov and S. Krivoruchko , *Excitation op ion-acoustic waves by langmuir waves and stationary regimes in a beam-plasma system*, (1970).
- [27] A. Bakai , E. Kornilov and S. Krivoruchko , *Excitation op ion-acoustic waves by langmuir waves and stationary regimes in a beam-plasma system*, (1970).
- [28] C. E. Max, *Physics of the Coronal plasma in Laser Fusion target*, *Laser-Plasma Interaction*, in Les Houches Session XXXIV, 1980,, edited by R. Balian and J. C. Adam (North Holland, Amsterdam, (1982)
- [29] V. K. Jain , A. K. Sharma , V. K. Tripathi, *Journal of Applied Physics* **64** 2 (1988).
- [30] J. A. Stamper, K. Papadopoulos, R. N. Sudan, S. O. Dean, *Physical Review Letters*, **26** (1971) 1012-1015.
- [31] J. A. Stamper and B. H. Ripin, *Physical Review Letters*, **34**, (1975) 138-140,
- [32] S. I. Braginskii, edited by M. A. Leontovich (Consultants Bureau, New York, NY,), **1** (1965).
- [33] S. H. Glenzer, W. E. Alley, K. G. Estabrook, J. S. De Groot, M. G. Haines, J. H. Hammer, J. P. Jadaud, B. J. MacGowan, J. D. Moody, W. Rozmus, L. J. Suter, T. L. Weiland and E. A. Williams, *Physics of Plasmas*, **6**, (1999) 2117-2128.

- 
- [34] E. L. Clark, K. Krushelnick, J. R. Davies, M. Zepf, M. Tatarakis, F. N. Beg, A. Machacek, P. A. Norreys, M. I. Santala, I. Watts and A. E. Dangor, *Physical Review Letters*, **84**, (2000) 70-673.
- [35] P. A. Norreys, M. Santala, E. Clark, M. Zepf, I. Watts, F. N. Beg, K. Krushelnick, M. Tatarakis, A. E. Dangor, X. Fang, P. Graham, T. McCanny, R. P. Singhal, K. W. D. Ledingham, A. Creswell, D. C. W. Sanderson, J. Magill, A. Machacek, J. S. Wark, R. Allott, B. Kennedy and D. Neely, *Physics of Plasmas*, **6** (1999) 2150-2156.
- [36] M. G. Haines, *Canadian Journal of Physics*, **64**, (1986) 912.
- [37] J. R. Davies, A. R. Bell, M. G. Haines, S. M. Guerin, *Physical Review E*, **56**, (1997) 7193-7203.
- [38] K. B. Wharton, S. P. Hatchett, S. C. Wilks, M. H. Key, J. D. Moody, V. Yanovsky, A. A. Offenberger, B. A. Hammel, M. D. Perry, J. D. Perry, C. Joshi, *Physical Review Letters*, **81** (1998) 822-825.



## Chapter 3

# Enhanced self-focusing of laser in the cone-guided scheme for inertial confinement fusion.

### 3.1 Introduction

Much recent work on Fast Ignition (FI) [1] for Inertial Confinement Fusion (ICF) [2] has involved the use of capsules in which a re-entrant gold cone has been imbedded [3]. As in the original scheme described in Ref. 1 the re-entrant cone-guided FI scheme employs a laser pulse with power on the order of 10 PW and energy of around 100 kJ to heat a region of approximately  $1000 \times$  compressed equimolar deuterium-tritium (DT) fuel, that satisfies the  $\rho r$  criterion for ignition, to the multi-keV temperatures required for alpha particle bootstrapping and subsequent propagating burn. Here, the igniter laser pulse is incident on the interior of the gold cone, which is embedded in the capsule such that the cone tip is directed toward, and located within approximately  $100 \mu\text{m}$  of, the assembled dense fuel core. The object of this cone interface being to avoid the requirement that either the igniter pulse, or a less intense ‘hole boring’ pulse, first channel through some few millimeters of plasma such as would ordinarily surround the core formed from the uniform spherical implosion of a fuel shell.

The cone-guided fast ignition concept initially showed some promise [4] and these early promising results led to the commencement of the FIREX project in Japan [5], and also formed part of the rationale for adding high energy short pulse beams to Omega and NIF [6, 7]. However, over the past two decades physicists have become increasingly aware of a number of difficulties with the cone-guided fast ignition concept. These difficulties are all related to the challenge of efficiently coupling the energy of the high energy short-pulse laser to the dense imploded fuel core [8]. Essentially there are three main components to this problem: 1) poor collimation of the beam of hot particles (usually envisaged to be electrons) from their point of origin to the dense fuel, 2) the source of the hot particles being too distant from the dense fuel to enable adequate coupling given that the hot particle beam is divergent, and 3) the hot particles having too long a mean free path in the dense fuel. This final point is a problem because, in order for inertially confined fusion to offer the potential of achieving high gain, ignition must necessarily proceed from a compact hotspot which represents only a small fraction of the total fuel mass. The bulk of the fuel must be heated to ignition temperatures by the propagating thermonuclear burn wave. Heating a large fraction of

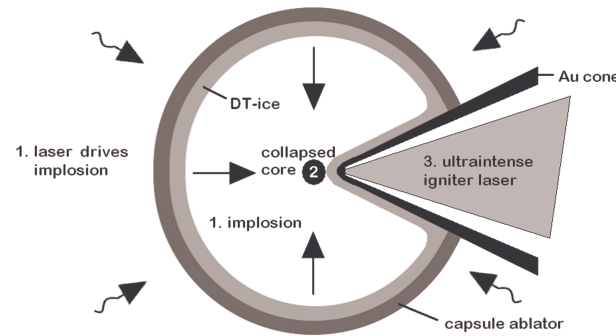


Figure 3.1: Schematic representation of the cone-guided fast ignition scheme

the compressed fuel up to ignition temperatures using the driver nullifies the possibility of achieving significant gain even if ignition is achieved. For electron fast ignition, this difficulty manifests itself in the form of the fast ignition "Catch 22", which may be stated as follows: allowing for other coupling inefficiencies, in order to deposit sufficient energy in the hotspot for it to ignite, prior to it hydrodynamically disassembling, the laser intensity has to be so high that the hot electron temperature ( $T_{hot}$ ) produced by the interaction of the igniter pulse with the plasma is too high to form a compact hotspot. If the hotspot is larger than is desirable, the energy requirements for ignition are increased, and so therefore the required intensity becomes even larger. This in turn increases  $T_{hot}$  even more, and so on and so forth until one ends up with an unfeasibly large short pulse laser heating up the entirety of the fuel; a situation which, as mentioned, can never result in high gain. Another issue posed by the cone-guided scheme is that of the disturbance of the symmetry of the implosion by the presence of the cone. This has recently caused a reconsideration of super-penetration schemes in which the route to the fuel is provided not by a cone but by a laser-produced plasma channel [9].

A further difficulty may also be added to the above list, which is more of a technological challenge on the laser side than a target-physics issue. The first generation of high-energy short-pulse lasers suffered from two difficulties: excessive prepulse and the challenge of producing a near diffraction-limited focal spot. The first of these issues has been quite effectively addressed over the past 15 years, with available laser contrasts increasing from around  $10^6$  to close on  $10^{10}$ , however the second is more challenging. Omega EP for instance, which is a large, state-of-the-art multi-beam high energy short-pulse laser system, constrains about 80 % of its energy within a 40-50  $\mu\text{m}$  diameter focal spot. Impressive though this is, it is far from optimal if one wishes to efficiently deposit energy in a hotspot of less than 10  $\mu\text{m}$  diameter. This difficulty is related to the scale of such lasers, which have beam-paths hundreds of metres in length. It should be noted also that Omega EP uses deformable mirrors and other advanced technologies to minimise the focal spot diameter [10]. From a fast ignition standpoint, what is critical is the fast electron beam width at the dense fuel. This may be minimized by reducing the source size and the divergence of the

electron beam from the interaction region to the dense fuel. Much work has been performed to attempt to minimise the divergence of the hot electron beam, for instance the use of a magnetic switchyard [11] or one of a range of double pulse approaches that use the magnetic field generated by a prior laser-plasma interaction to guide a subsequent high-intensity pulse [12, 13, 14]. Other studies have shown that using a particularly high-contrast laser pulse may enhance self-collimation [15, 16]. It is not clear as yet however which of these approaches will work effectively in a full-scale fast ignition target. Experiments to date have tended to use comparatively short pulse lengths and much lower energies, where both the hydrodynamic and magnetic field evolution during the main pulse is less pronounced than would be the case for the  $\sim 100$  kJ,  $\sim 10$ ps laser pulses required for fast ignition.

Here we consider whether target physics might assist in reducing the hot electron source size by further focusing down the incident beam within the re-entrant cone. It must be stressed however that in doing this the intensities produced must still be limited so as not to produce an excessively high  $T_{hot}$ . There are several routes that one might consider to achieving this in a general case (without worrying too much about the specific requirements of fast ignition). One might propose a target-level focusing scheme that is based on target geometry, such as that described in [17], or one might rely upon the tendency of a high-intensity laser to self-focus in a low-density plasma background. This latter approach is that which is considered here, i.e. the possibility of using an ambient plasma to self-focus a laser, which would otherwise have a focused intensity of around  $10^{18}$  to  $10^{19}$  W/cm<sup>2</sup>, up to intensities suitable for fast ignition ( $10^{19}$  W/cm<sup>2</sup> + ) whilst at the same time reducing the focal spot diameter so as to optimise coupling to a compact hotspot. Clearly self-focusing requires the presence of some ambient plasma medium in order to operate, however such a medium tends to be present in the case of cone-guided fast ignition anyway. Whilst, as noted, laser contrast levels have been greatly improved since the advent of high-energy short-pulse laser technology, it is still challenging to entirely avoid the formation of some pre-plasma within the cone. This scheme therefore also has the benefit of making use of this pre-plasma, indeed it may be argued that what is proposed here does not actually represent any kind of evolution of the existing cone-guided fast ignition target - it merely emphasizes the potential utility of what is often considered to be a problem (pre-plasma) in terms of it providing a possible solution for another issue (the over-large focal spots of high energy lasers). There also exist more substantial modifications to the established fast ignition schemes, such as the double-cone ignition scheme proposed by Zhang *et al.* [18] in which the use of a magnetic field generated by a nanosecond laser is evoked to guide the fast electrons toward their target and the compression geometry is also substantially modified.

The current work may be seen as an advancement upon a number of related analytical and simulation-based studies, using similar techniques, that have been published previously. Hafizi *et al.* [19] proposed a theoretical model for the propagation of an intense laser beam in a plasma, considering pondermotive and relativistic effects. Lui and Tripathi [20] presented

observations of the effects of a self-generated azimuthal magnetic field upon the relativistic self-focusing of an intense laser beam in a plasma. Gupta *et al.* [21] considered the case of an upward plasma-density ramp in underdense plasma, and concluded that introducing such an upward plasma-density ramp allows for the achievement of the minimum spot size via self-focusing. In the absence of a density ramp, diffraction tends to dominate and the laser beam becomes defocussed. Kant *et al.* [22] observed self-focusing of a Hermite Gaussian laser beam in the presence of an upward plasma density ramp which also led to stronger self-focusing. Saedajali *et al.* [23], studied the interaction of a self-focused laser beam with a plasma-loaded cone in the context of cone-guided fast ignition. Here we take the obvious further step of introducing an upward plasma density ramp into the cone in order to obtain stronger self-focusing. This is also of interest since an upward plasma density ramp is inevitably created by the interaction of the laser pre-pulse with the interior of the cone, though of course given that this is a largely analytical study, the density profile is idealised. Self-focusing has also been invoked in fast-ignition related experiments, often in the cone-less variant of the technique, as a phenomenon that may assist in conveying the energy of the igniter beam to the dense fuel [24, 25]. Another well-known component of high-intensity laser-plasma interactions, closely related to whole-beam self-focusing, is beam filamentation. It has been previously shown that in a collisional plasma with finite thermal conduction, the extent of filamentation is significantly less than that of self-focusing, hence it is not considered further here [26].”

It should be noted that with a reduced-physics model, such as that which is employed here, it is not possible to make any firm statements as to the overall effect of pre-plasma in a cone-guided fast ignition scenario. Indeed experimental studies have illustrated how the presence of preplasma can significantly inhibit coupling of laser energy to the cone tip [27] albeit at a greatly reduced energy scale. The present study serves only to illustrate one aspect of the physics of the interaction, and suggest a way in which it may be beneficial. Also, as stated, it is reasonable to expect that some preplasma may be present in a full-scale fast ignition experiment, and so it is important to examine the many different ways in which its presence may affect the interaction. With the model employed here, only one aspect of the interaction can be interrogated, and this should be borne in mind when considering the results presented.

## 3.2 Theoretical Considerations

Let us consider a Gaussian laser beam propagating along the z-axis in a plasma. In the presence of a collisionless plasma, the propagation of a Gaussian laser beam is characterized by

$$\varepsilon = \varepsilon_0 + \phi(\langle EE^* \rangle), \quad (3.1)$$

with  $\omega_p^2 = 4\pi n(\xi)e^2/m$ ,  $\varepsilon_0 = 1 - \omega_p^2/\omega^2$ . Here, the frequency of laser used is given by  $\omega$ , the linear and non-linear parts of dielectric constants are represented by  $\varepsilon_0$  and  $\phi$  respectively,  $\omega_p^2$  is the plasma frequency, electron charge is given by  $e$  and electron mass is given by  $m$ . The upward plasma density ramp density ramp profile is modulated as

$$n(\xi) = n_0 \tan\left(\frac{\xi}{d}\right), \quad (3.2)$$

where the equilibrium electron density is denoted as  $n_0$ ,  $\xi = z/R_d$  is the normalized propagation distance and  $d$  is a dimensionless adjustable parameter which specifies the gradient of the slope. The extent of the plasma that will be employed here ( $\sim 100$  microns) is in keeping with that to be expected based upon previous studies and the expected speed of sound and time duration relevant to the prepulse interaction in a fast ignition target. The non-linearity in the dielectric constant is mainly due to the pondermotive force and the non-linear part of the dielectric constant is given by

$$\phi(EE^*) = \frac{\omega_p^2}{\omega^2} \left[ 1 - \exp\left(-\frac{3m\alpha EE^*}{4M}\right) \right], \quad (3.3)$$

with  $\alpha = e^2 M / 6m^2 \omega^2 k_b T_0$ , where  $M$  is the mass of the scatterer in the plasma,  $k_b$  is the Boltzmann constant and  $T_0$  is the equilibrium plasma temperature.

### 3.3 Relativistic Self-focusing

Consider a high intensity laser beam propagating in plasma with an upward density ramp through a cone. The wave equation governing the propagation of a laser beam in the plasma is:

$$\nabla^2 E + \frac{\omega^2}{c^2} \varepsilon E = 0. \quad (3.4)$$

The above equation is solved by using the WKB approximation. The solution of the wave equation is,

$$E = A(x, y, z) \exp[i(\omega t - kz)], \quad (3.5)$$

where

$$k = \sqrt{1 - \frac{\omega_p^2}{\gamma \omega^2} \tan\left(\frac{\xi}{d}\right)} \left(\frac{\omega}{c}\right) \quad (3.6)$$

and the plasma frequency  $\omega_p^2$  is given by,

$$\omega_p^2 = \frac{\omega_{p0}^2}{\gamma} \tan\left(\frac{\xi}{d}\right). \quad (3.7)$$

Differentiating equation (3.4) twice with respect to  $r$  and  $z$  we get,

$$\frac{\partial E}{\partial r} = \exp[i(\omega t - kz)] \frac{\partial}{\partial r} A(r, z), \quad (3.8)$$

$$\frac{\partial^2 E}{\partial r^2} = \frac{\partial^2}{\partial r^2} (A(r, z) \exp[i(\omega t - kz)]), \quad (3.9)$$

$$\frac{\partial E}{\partial z} = \frac{\partial}{\partial z} (A(r, z) \exp[i(\omega t - kz)]). \quad (3.10)$$

Substituting  $\tan\left(\frac{\xi}{d}\right) = \tan\left(\frac{z}{dR_d}\right)$  where,  $R_d$  denotes the diffraction length, into equation (3.9) we get,

$$\begin{aligned} \frac{\partial E}{\partial z} &= \exp[i(\omega t - kz)] \left[ \frac{\partial A}{\partial z} \right] + \\ &\frac{Ai\omega}{c} \sqrt{1 - \frac{\omega_{p0}^2}{\gamma\omega^2} \tan\left(\frac{z}{dR_d}\right)} + \\ &\frac{i\omega z}{2cdR_d} \frac{\omega_{p0}^2}{\gamma\omega^2} z A \sec^2\left(\frac{z}{dR_d}\right) \\ &\frac{1}{\sqrt{1 - \frac{\omega_{p0}^2}{\gamma\omega^2} \tan\left(\frac{z}{dR_d}\right)}}. \end{aligned} \quad (3.11)$$

Similarly,

$$\begin{aligned} \frac{\partial^2 E}{\partial z^2} &= -\frac{\omega^2 A}{c^2} \exp[i(\omega t - kz)] \\ &\left[ \frac{\omega_{p0}^4 z^2 \sec^4\left(\frac{z}{dR_d}\right)}{\gamma^2 \omega^4 d^2 R_d^2 \left[1 - \frac{\omega_{p0}^2}{\omega^2} \tan\left(\frac{z}{dR_d}\right)\right]} \right] + \\ &\left[ 1 - \frac{\omega_{p0}^2}{\gamma\omega^2} \tan\left(\frac{z}{dR_d}\right) \right]. \end{aligned} \quad (3.12)$$

Writing the wave equation in cylindrical coordinates and substituting in equations (3.8), (3.9), (3.10) and (3.11) we get,

$$\begin{aligned}
& \frac{i\omega}{c} \left[ 2 \sqrt{1 - \frac{\omega_{p0}^2}{\gamma\omega^2} \tan\left(\frac{z}{dR_d}\right)} \right. \\
& \left. - \frac{\frac{\omega_{p0}^2}{\gamma\omega^2} z \sec^2\left(\frac{z}{dR_d}\right)}{dR_d \sqrt{1 - \frac{\omega_{p0}^2}{\gamma\omega^2} \tan\left(\frac{z}{dR_d}\right)}} \right] \frac{\partial A}{\partial z} \\
& - \frac{\frac{\omega_{p0}^2}{\gamma\omega^2} A \sec^2\left(\frac{z}{dR_d}\right)}{dR_d \sqrt{1 - \frac{\omega_{p0}^2}{\gamma\omega^2} \tan\left(\frac{z}{dR_d}\right)}} \left[ 1 + \frac{A}{dR_d} \left( \tan\left(\frac{z}{dR_d}\right) \right. \right. \\
& \left. \left. + \frac{\frac{\omega_{p0}^2}{\gamma\omega^2} Az \sec^2\left(\frac{z}{dR_d}\right)}{4 \left(1 - \frac{\omega_{p0}^2}{\gamma\omega^2} \tan\left(\frac{z}{dR_d}\right)\right)} \right) \right] \tag{3.13}
\end{aligned}$$

Now,

$$A(r, z) = A_0(r, z) \exp[-ikS(r, z)]. \tag{3.14}$$

In order to solve equation (3.12), we differentiate equation (3.13) and substitute in equation (3.12). Considering only the real part of the obtained solution,

$$\begin{aligned}
& \frac{c^2}{\omega^2 A_0} \left( \frac{\partial^2 A_0}{\partial r^2} + \frac{1}{r} \frac{\partial A_0}{\partial r} \right) + \phi(A_0^2) \\
& = \left[ \left( 2 \left( 1 - \frac{\omega_{p0}^2}{\gamma\omega^2} \tan\left(\frac{z}{dR_d}\right) \right) \right) - \frac{\omega_{p0}^2}{\gamma\omega^2} \frac{z \sec^2\left(\frac{z}{dR_d}\right)}{dR_d} \right] \frac{\partial S}{\partial z} \\
& + \left[ 1 - \frac{\omega_{p0}^2}{\gamma\omega^2} \tan\left(\frac{z}{dR_d}\right) \right] \left( \frac{\partial S}{\partial r} \right)^2 \\
& - \frac{\omega_{p0}^2}{dR_d \gamma\omega^2} \sec^2\left(\frac{z}{dR_d}\right) \\
& \times \left[ S + z - \frac{\omega_{p0}^2}{\gamma\omega^2} \frac{z}{2dR_d} \sec^2\left(\frac{z}{dR_d}\right) \frac{z}{dR_d} \frac{(S-z)/2}{1 - \frac{\omega_{p0}^2}{\gamma\omega^2} \tan\left(\frac{z}{dR_d}\right)} \right] \tag{3.15}
\end{aligned}$$

In a paraxial approximation, the relation between amplitude,  $A_0$  and  $S$ , and the curvature

of the wavefront of the beam are given as:

$$S(r, z) = \frac{r^2}{2} \frac{1}{f(z)} \frac{\partial f(z)}{\partial z} + \phi_0(z), \quad (3.16)$$

$$A_0(r, z) = \frac{A_{00}}{f(z)} \exp\left(\frac{-r^2}{f^2(z)r_0^2}\right). \quad (3.17)$$

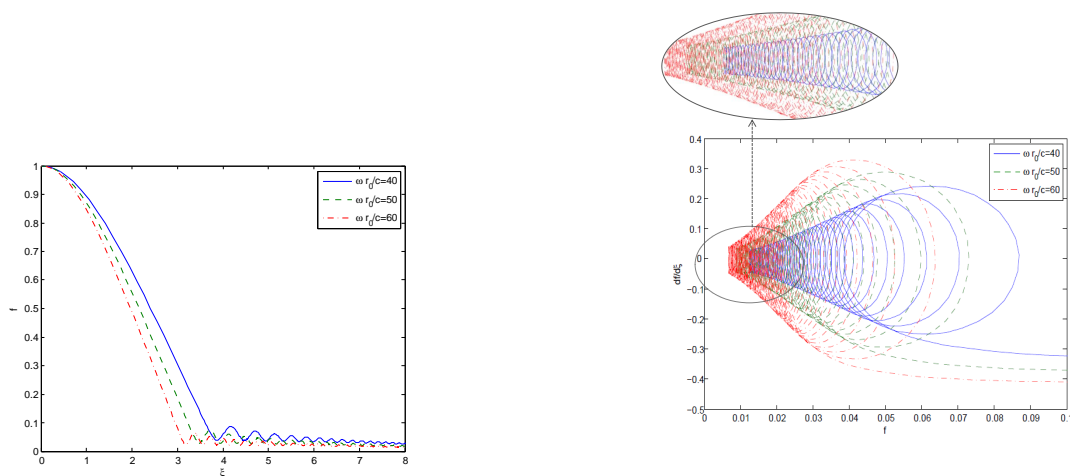
where  $A_{00}$  is the initial magnitude of laser beam at  $z = 0$ ,  $f$  is the dimensionless beam-width parameter and  $r_0$  is the initial beam-width radius. Substituting equation (3.15) and (3.16) into (3.14) and taking coefficients of  $r^2$  using the paraxial approximation, and using the dimensionless parameters,  $\alpha = \omega_{p0}^2/\omega$  and  $\beta = \omega r_0/c$  and  $x = \alpha A_{00}^2$ , the following equation for the beam-width parameter is deduced,

$$\begin{aligned} \frac{d^2 f}{d\xi^2} = & \left[ \frac{1}{\frac{\alpha^2 \xi}{2d} \sec^2\left(\frac{\xi}{d}\right) + (1 - \alpha^2 \tan\left(\frac{\xi}{d}\right))} \right] \\ & \left[ \frac{1}{f(\xi)} \left[ 2 \left( 1 - \alpha^2 \tan\left(\frac{\xi}{d}\right) \right) + \alpha^2 \xi \right] \left( \frac{df}{d\xi} \right)^2 + \right. \\ & \left. \left( 1 - \alpha^2 \tan\left(\frac{\xi}{d}\right) \right)^{\frac{1}{2}} \right. \\ & \left. \left( \frac{1}{\beta^2 f^3(\xi)} - \frac{x \alpha^2 \beta \tan\left(\frac{\xi}{d}\right)}{2f(\xi)} \right) \left( 1 + \frac{x}{2f^2(\xi)} \right)^{\frac{-3}{2}} - \right. \\ & \left. \left( \frac{\alpha^2 \beta}{2d} \sec^2\left(\frac{\xi}{d}\right) \right) \left( 1 - \frac{\alpha^2 \xi}{2d} \sec^2\left(\frac{\xi}{d}\right) \frac{1}{1 - \alpha^2 \tan\left(\frac{\xi}{d}\right)} \right) \right. \\ & \left. \left( 1 - \alpha^2 \tan\left(\frac{\xi}{d}\right) \right)^{\frac{1}{2}} \right]. \end{aligned} \quad (3.18)$$

### 3.4 Results

In order to solve the equation of the beam width parameter numerically, we have performed simulations for the following parameters,  $\omega = 1.778 \times 10^{14}$  rad/sec and  $r_0 = 253 \mu m$ . The initial laser intensity  $I_0 = 10^{19} W/cm^2$  and the initial temperature  $T_0 = 10^5 K$ . Figure 3.2(a) shows variation of beam width parameter with propagation distance for values of  $\omega r_0/c = 40, 50$  and  $60$ , keeping  $\omega_{p0}/\omega = 0.3$  and  $d = 8$ . It is found that initially its beam width parameter decreases sequentially and maintains a small spot size as it propagates. Due to the Gaussian intensity side view of the laser beam, the relativistic mass of the plasma electrons is highest at the center of the wave front and is lowest in its wings. Hence, the central portion of the wave front experiences a higher refractive index than that which is off-axis. This results in bending of the wave-front and self-focusing of the laser. As the beam





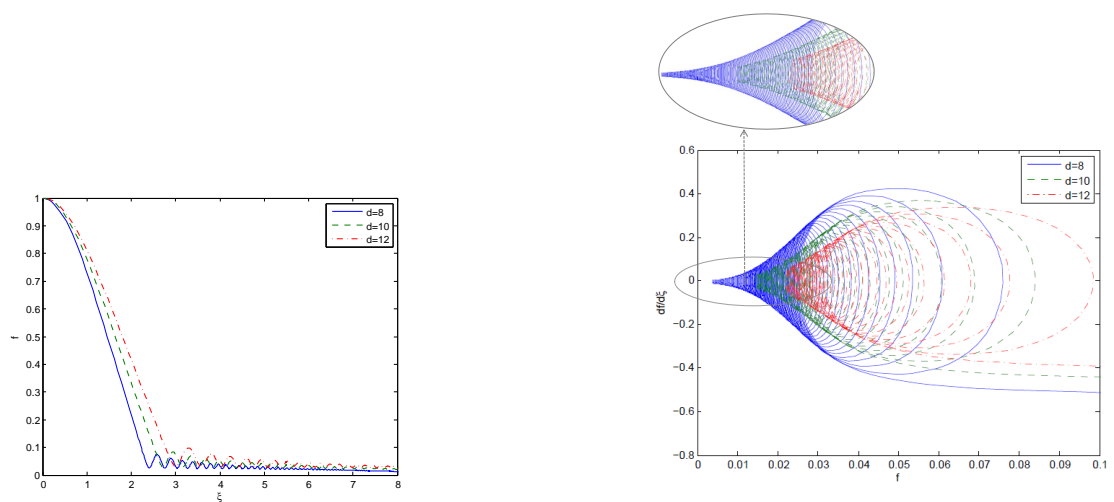
(a)

(b)

Figure 3.2: In this figure (a) Variation of beam width parameter with normalised propagation distance and (b) Phase space plot for self-focused Gaussian laser beam, for  $\omega r_0/c = 40, 50$  and  $60$  at  $\omega_{p0}/\omega = 0.3$ ,  $d=8$  is shown

propagates through the plasma, it maintains its reduced spot size up to several Rayleigh lengths. It is also observed that after every focal spot the maxima and minima of the spot size of the laser beam shift downwards. This observation is in agreement with 3D PIC simulation results described by Pukhov and Meyer-ter Vehn in [28]. Similarly, figure 3(a) shows the variation of beam-width parameter with propagation distance for values of  $d = 8, 10$  and  $12$  with  $\omega_{p0}/\omega = 0.3$  and  $\omega r_0/c = 40$  and figure 4(a) shows the variation of the beam-width parameter with propagation distance for values  $\omega_{p0}/\omega = 0.3, 0.4, 0.5$ , with  $\omega r_0/c = 40$  and  $d = 8$ . It is clear that as the laser spot size increases, the repetition of the oscillations grows faster and hence self-focusing becomes stronger and occurs at earlier values of  $f$ . The beam is also observed to remain converged for a greater propagation distance.

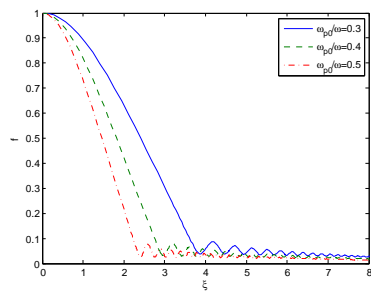
Figures 3.2(b), 3.3(b) and 3.4(b) are the phase-space plots demonstrating the propagation dynamics of the laser beam. The trajectories obtained are spirally phased which indicates the internal oscillations of the laser beam. These oscillations are rich in different frequencies. In these figures, it can be clearly seen that for smaller values of  $f$ , these spiral lines becomes denser, leading to stronger self-focusing. In figure 3.2(b) self-focusing occurs faster for a larger beam-width parameter. In figure 3.3(b) at  $d = 8$ , a significant increase in the strength of the self-focusing is apparent, and also this self-focusing has occurred faster. Figure 3.4(b)



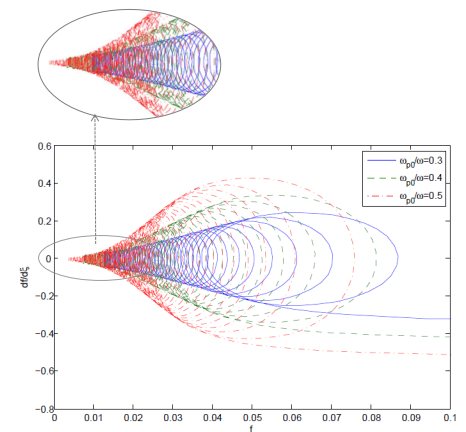
(a)

(b)

Figure 3.3: In this figure (a) Variation of beam width parameter with normalised propagation distance and (b) Phase space plot for self-focused Gaussian laser beam, for  $d = 8, 10$  and  $12$  at  $\omega r_0/c = 40$  and  $\omega_{p0}/\omega = 0.3$  is shown.



(a)



(b)

Figure 3.4: In this figure (a) Variation of beam width parameter with normalised propagation distance and (b) Phase space plot for self-focused Gaussian laser beam, for different values of  $\omega_{p0}/\omega = 0.3, 0.4$  and  $0.5$  at  $\omega r_0/c = 40$  and  $d=8$  is shown.

---

shows the presence of denser plasma leads to stronger self-focusing.

## 3.5 Conclusions

This study presents an investigation into strong self-focusing of a Gaussian laser beam in the presence of an upward plasma density ramp in a plasma-loaded cone which may be considered in the context of cone-guided fast ignition or other applications where it is advantageous to reduce focal spot size and/or increase laser intensity (for instance in imaging applications, such as those discussed in reference 11). The field distribution of the laser beam is expressed in terms of the beam-width parameter. This setup reduces the defocusing of the laser beam. Hence, the laser beam remains focused to a small spot size up to several Rayleigh lengths which is essential for consistent performance in an extended plasma formed by the interaction of a laser prepulse. The simulation results show that the plasma frequency increases and the self-focusing occurs faster in such a scenario than in a uniform density plasma. Clearly these are the results of a reduced model of laser-plasma interaction, and as such substantial further investigation would be required to clearly establish the importance and utility of this behaviour to cone-guided fast ignition. The heating beam in fast ignition is necessarily rather long,  $\sim 10$  ps, and on such a time-scale a model which properly accounts for the evolution and hydrodynamic motion of the plasma within the cone is called for. Furthermore, the reader is reminded that the presence of preplasma has been shown to have a negative influence on coupling in experimental studies at reduced scale, and that here we consider only one aspect of the laser-plasma interaction.

## Bibliography

- [1] M. Tabak, J. Hammer, M. E. Glinsky, W. L. Kruer, S. C. Wilks, J. Woodworth, W. M. Campbell, M. D. Perry, and R. J. Mason, *Physics of Plasmas*, **1**, (1994) 1626.
- [2] J. Nuckolls, L. Wood, A. Thiessen, and G. Zimmerman, *Nature*, **239**, (1972) 139.
- [3] M. Tabak, J. H. Hammer, E. M. Campbell *et al.*, Lawrence Livermore National Laboratory patent disclosure, IL8826B, 1997, Lawrence Livermore National Laboratory, Livermore, CA; S. Hatchett and M. Tabak, “Cone focus geometry for Fast Ignition,” presentation given at 30th Annual Anomalous Absorption Conference, Ocean City, MD (April 2000); S. Hatchett, M. Herrmann, M. Tabak *et al.*, *Bull. Am. Phys. Soc.* **46**, 47.
- [4] R. Kodama, P. A. Norreys, K. Mima, A. E. Dangor, R. G. Evans, H. Fujita, Y. Kitagawa, K. Krushelnick, T. Miyakoshi, N. Miyanaga, T. Norimatsu, S. J. Rose, T. Shozaki, K. Shigemori, A. Sunahara, M. Tampo, K. A. Tanaka, Y. Toyama, T. Yamanaka, and M. Zepf, *Nature*, **412**, (2001) 798.
- [5] Mayuko Koga, Y. Arikawa, H. Azechi, Y. Fujimoto, S. Fujioka, H. Habara, Y. Hironaka, H. Homma, H. Hosoda, T. Jitsuno, T. Johzaki, J. Kawanaka, R. Kodama, K. Mima, N. Miyanaga, M. Murakami, H. Nagatomo, M. Nakai, Y. Nakata, H. Nakamura, H. Nishimura, T. Norimatsu, Y. Sakawa, N. Sarukura, K. Shigemori, H. Shiraga, T. Shimizu, H. Takabe, M. Tanabe, K. A. Tanaka, T. Tanimoto, T. Tsubakimoto, T. Watari, A. Sunahara, M. Isobe, A. Iwamoto, T. Mito, O. Motojima, T. Ozaki, H. Sakagami, T. Taguchi, Y. Nakao, H. Cai, M. Key, P. Norreys, J. Pasley, *Nuclear Instruments and Methods in Physics Research Section A: Accelerators, Spectrometers, Detectors and Associated Equipment*, **653**, (2011) 84.
- [6] D N Maywar, J H Kelly, L J Waxer, S F B Morse, I A Begishev, J Bromage, C Dorrer, J L Edwards, L Folsbee, M J Guardalben, S D Jacobs, R Jungquist, T J Kessler, R W Kidder, B E Kruschwitz, S J Loucks, J R Marciante, R L McCrory, D D Meyerhofer, A V Okishev, J B Oliver, G Pien, J Qiao, J Puth, A L Rigatti, A W Schmid, M J Shoup III, C Stoeckl, K A Thorp and J D Zuegel, *Journal of Physics: Conference Series*, **112**, (2008) 032007.
- [7] J K Crane, G Tietbohl, P Arnold, E S Bliss, C Boley, G Britten, G Brunton, W Clark, J W Dawson, S Fochs, R Hackel, C Haefner, J Halpin, J Heebner, M Henesian, M Hermann, J Hernandez, V Kanz, B McHale, J B McLeod, H Nguyen, H Phan, M Rushford, B Shaw, M Shverdin, R Sigurdsson, R Speck, C Stolz, D Trummer, J Wolfe, J N Wong, G C Siders and C P J Barty, *Journal of Physics: Conference Series*, **244**, (2010) 032003.

- [8] P.A. Norreys, R.H.H. Scott, K.L. Lancaster, J.S. Green, A.P.L. Robinson, M. Sherlock, R.G. Evans, M.G. Haines, S. Kar, M. Zepf, M.H. Key, J. King, T. Ma, T. Yabuuchi, M.S. Wei, F.N. Beg, P. Nilson, W. Theobald, R.B. Stephens, J. Valente, J.R. Davies, K. Takeda, H. Azechi, M. Nakatsutsumi, T. Tanimoto, R. Kodama and K.A. Tanaka, *Nuclear Fusion*, **49**, (2009) 10.
- [9] T. Gong, H. Habara, K. Sumioka, M. Yoshimoto, Y. Hayashi, S. Kawazu, T. Otsuki, T. Matsumoto, T. Minami, K. Abe, K. Aizawa, Y. Enmei, Y. Fujita, A. Ikegami, H. Makiyama, K. Okazaki, K. Okida, T. Tsukamoto, Y. Arikawa, S. Fujioka, Y. Iwasa, S. Lee, H. Nagatomo, H. Shiraga, K. Yamanoi, M. S. Wei and K.A. Tanaka, *Nature Communications*, **10**, (2019) 1.
- [10] J. Bromage, S.-W. Bahk, D. Irwin, J. Kwiatkowski, A. Pruyne, M. Millecchia, M. Moore, and J. D. Zuegel, *Optics Express*, **16**, (2008) 1656.
- [11] A. P. L. Robinson, M. H. Key and M. Tabak, *Physical Review Letters* **108**, (2012) 125004.
- [12] R.H.H. Scott, S.J. Rose, P.A. Norreys, K. Markey, K. Lancaster, C.M. Brenner, I.O. Musgrave, A.P.L. Robinson, M. M. Notley, D. Neely, C. Beaucourt, J.J. Santos, J.-L. Feugeas, P. Nicolai, G. Malka, V.T. Tikhonchuk, H.-P. Schlenvoigt, S. Baton, C. P. Ridgers, R. J. Gray, P. McKenna, J. Pasley, K. Li and J. R. Davies, *Physical Review Letters* **109**, (2012) 015001.
- [13] M. Bailly-Grandvaux, J.J. Santos, C. Bellei, P. Forestier-Colleoni, S. Fujioka, L. Giuffrida, J.J. Honrubia, D. Batani, R. Bouillaud, M. Chevrot, J.E. Cross, R. Crowston, S. Dorard, J.-L. Dubois, M. Ehret, G. Gregori, S. Hulin, S. Kojima, E. Loyez, J.-R. Marquès, A. Morace, Ph. Nicolai, M. Roth, S. Sakata, G. Schaumann, F. Serres, J. Serval, V.T. Tikhonchuk, N. Woolsey and Z. Zhang, *Nature Communications* **9**, (2018) 102.
- [14] Sophia Malko, Xavier Vaisseau, Frederic Perez, Dimitri Batani, Alessandro Curcio, Michael Ehret, Javier Honrubia, Katarzyna Jakubowska, Alessio Morace, João Jorge Santos and Luca Volpe1, *Scientific Reports*, **9**, (2019) 1.
- [15] J. Rassuchine, E. d’Humières, S. D. Baton, P. Guillou, M. Koenig, M. Chahid, F. Perez, J. Fuchs, P. Audebert, R. Kodama, M. Nakatsutsumi, N. Ozaki, D. Batani, A. Morace, R. Redaelli, L. Gremillet, C. Rousseaux, F. Dorchies, C. Fourment, J. J. Santos, J. Adams, G. Korgan, S. Malekos, S. B. Hansen, R. Shepherd, K. Flippo, S. Gaillard, Y. Sentoku, and T. E. Cowan, *Physical Review E*, **79**, (2009) 036408.
- [16] X. Vaisseau, A. Morace, M. Touati, M. Nakatsutsumi, S. Baton, S. Hulin, Ph. Nicolai, R. Nuter, D. Batani, F.N. Beg, J. Breil, R. Fedosejevs, J.-L. Feugeas, P. Forestier-Colleoni, C. Fourment, S. Fujioka, L. Giuffrida, S. Kerr, H.S. McLean, H. Sawada, V.T. Tikhonchuk, and J.J. Santos, *Physical Review Letters*, **118**, (2017) 205001.

- [17] Andrew G. MacPhee, David Alessi, Hui Chen, Ginevra Cochran, Mark R. Hermann, Daniel H. Kalantar, Andreas J. Kemp, Shaun M. Kerr, Anthony J. Link, Tammy Ma, Andrew J. Mackinnon, Derek A. Mariscal, David Schlossberg, Riccardo Tommasini, Scott Vonhof, Clifford C. Widmayer, Scott C. Wilks, G. Jackson Williams, Wade H. Williams, and Kelly Youngblood, *Optica*, **7**, (2020) 129.
- [18] J. Zhang, W. M.Wang, X. H.Yang, D. Wu, Y. Y. Ma, J. L. Jiao, Z. Zhang, F. Y. Wu, X. H. Yuan, Y. T. Li and J. Q. Zhu, *Philosophical Transactions of the Royal Society*, **378**, (2020) 2184.
- [19] B. Hafizi, A. Ting, P. Sprangle and R. Hubbard, *Physical Review E*, **62**, (2000) 4120.
- [20] C. Liu and V. Tripathi, *Physics of Plasmas*, **3**, (1996) 3410.
- [21] D. Gupta, M.S. Hur and H. Suk, *Applied Physics Letters*, **91**, (2007) 081505.
- [22] N. Kant, M.A. Wani, A. Kumar, *Optics Communication*, **285**, (2012) 4483.
- [23] N. Saedjalil, M. Mehrangiz, S. Jafari, A. Ghasemizad, *The European Physical Journal Plus*, **131**, (2016) 188.
- [24] K.A.Tanaka, R.Kodama, N.Izumi, K.Takahashi, M.Heya, H.Fujita, Y.Kato, Y.Kitagawa, K.Mima, N.Miyanaga, T.Norimatsu, Y.Sentoku, A.Sunahara, H.Takabe, T.Yamanaka, T.Koase, T.Iwatani, F.Ohtani, T.Miyakoshi, H.Habara, M.Tanpo, S.Tohyama, F.A.Weber, T.W.Barbee Jr. and L.B.Dasilva, *Comptes Rendus de l'Académie des Sciences-Series IV-Physics*, **1**, (2000) 737.
- [25] B. T. Spiers, M. P. Hill, C. Brown, L. Ceurvorst, N. Ratan, A. F. Savin, P. Allan, E. Floyd, J. Fyrth, L. Hobbs, S. James, J. Luis, M. Ramsay, N. Sircombe, J. Skidmore, R. Aboushelbaya, M.W. Mayr, R. Paddock, R. H. W. Wang and P. A. Norreys, *Philosophical Transactions of the Royal Society A*, **371**, (2020) 2189.
- [26] Ghanshyam and V.K. Tripathi, *Journal of Plasma Physics*, **49** , (1993) 243.
- [27] S. D. Baton, M. Koenig, J. Fuchs, A. Benuzzi-Mounaix, P. Guillou, B. Loupiau, T. Vinci, L. Gremillet, C. Rousseaux, M. Drouin, E. Lefebvre, F. Dorchie, C. Fourment, J. J. Santos, D. Batani, A. Morace, R. Redaelli, M. Nakatsutsumi, R. Kodama, A. Nishida, N. Ozaki, T. Norimatsu, Y. Aglitskiy, S. Atzeni, and A. Schiavi, *Physics of Plasmas*, **15**, (2008) 4.
- [28] A. Pukhov, J. Meyer-ter Vehn, *Physical Review Letters*, **76**, (1996) 3975.

## Chapter 4

# SRS of a laser in a magnetized plasma with density ripple

### 4.1 Introduction

LPI play a crucial role in both schemes as they can contribute to implosion output degradation by reducing laser coupling to the target, drive asymmetries, and preheat the fuel via the production and deposition of suprathermal electrons. Laser plasma instabilities, such as SRS [4], SBS, and CBET, obstruct the creation of the required time-dependent drive-symmetry in ICF.

One of the most important suprathermal-electron-producing processes is SRS. [5, 6, 7, 12, 13, 28]. SRS was not initially believed to be an issue for direct drive, which was more commonly impacted by two-plasmon decay (TPD) in subscale studies [8, 9, 10]. Recently, a study performed at the NIF examined the SRS process in direct-drive ignition-scale plasmas [11], SRS intensity thresholds and SRS scaling with laser intensity for various laser beam angles of incidence were investigated.

Introduction of magnetic field in plasma might help in reducing the issues of preheating of fuel. Creating a magnetic field several tens of Tesla [14] and using the alternating polarization method [15] show significant reduction in the growth of SRS. Beyond its application in studies relating to laser-plasma instabilities, the imposition of a magnetic field on an ICF target has also been suggested as a way of enabling ignition via the effect of the magnetic field on thermonuclear  $\alpha$ -particle motion and electron conductive hotspot cooling. The presence of such a field can thereby help confine charged particles within the hotspot, thereby shifting the boundary for ignition to lower hotspot  $\rho r$  or lower temperature (or both). It has also been suggested that imposing a magnetic field might allow for the achievement of ignition at the NIF, or at least higher fusion yields [16]. In the OMEGA Laser Facility, a 5 T externally supplied magnetic field has been compressed by the implosion to a strength of more than 3000 T [17]. In a computational study employing a 3-D magnetohydrodynamics code, the effect of thermal conduction suppression, the Lorentz force, and  $\alpha$ -particle magnetization was observed on spatially deformed hot-spots [20]. Magnetization improved target performance and was also found to affect the hotspot spatial evolution. Studies observing the effect of magnetic fields on SRS have also found significant suppression of the instability's development [19, 21, 22].



Considering the variation in plasma density profile, for example, using rippled plasma density decreased the growth of the SRS instability. This decrease may help in a consequent reduction in the electron preheating that impeded ignition. [25, 23, 26]. The viability of a given plasma wave is a function of the density of the plasma in which it is propagating and therefore the presence of density ripples can significantly affect the SRS mechanism, which in turn can potentially mitigate some of its undesirable consequences.

The effect of an magnetic-field (azimuthal) on induced SFRS in laser-produced density rippled plasma is investigated in this article. A lower hybrid wave and two side-band waves are excited by the laser. The density perturbation caused by the lower hybrid wave combines with the electrons' oscillatory velocity caused by the pump to provide a nonlinear current that drives the electromagnetic SBW. The electrons driving the LHW extract ponderomotive energy from the pump and sideband waves. We investigate SFRS in a density rippled plasma in Sec. 2. by solving the coupled mode equations for both sideband waves, we get a nonlinear dispersion relation. The growth determines the transverse extent of the lower-hybrid mode, while the electromagnetic SBW are well developed. In Section 3, the results are presented and discussed. Conclusion and acknowledgement are given in Section 4 and 5 respectively.

## 4.2 Instability Analysis

Consider a laser of electric field  $\vec{E}_o = \vec{E}_o(r)e^{-i(\omega_o t - k_o z)}$ , propagating through a plasma with equilibrium plasma density  $n_o^o$  and a pre-existing density ripple  $n_e^q \sim n_{q_o} e^{iq_o z}$  in the presence of azimuthal magnetic field  $B_\theta = (B_o/r_o)(y\hat{x} - x\hat{y})$ . Here,  $n_{q_o}$  is the initial ripple density and  $q_o$  is density ripple wave number. This imparts oscillatory velocity  $\vec{v}_o^v$  to electrons,  $\vec{v}_o^v = \left(\frac{eE_o}{m_i\omega_o}\right)$ . Here,  $e$  and  $m$  are charge and mass of the electrons respectively. Assuming  $v_o^2/2c^2 \ll 1$ , the nonlinear plasma dielectric constant is given by  $\epsilon_o = \epsilon_{oo} + \epsilon_{o2}|E|^2$ . Here,  $\epsilon_{oo} = 1 - \omega_p^2/\omega_o^2$ , is the linear dielectric constant and  $\epsilon_{o2} = (\omega_p^2/\omega_o^2)(e^2/4\pi m\omega_o^2 c^2)$ , is the non-linear dielectric constant responsible for self-focusing and plasma frequency is given by  $\omega_p = \sqrt{4\pi n_o e^2/m}$ . Because of the nonlinear refraction and diffraction, the beam converges and diverges respectively. It converges to a length of  $Z' = r_o(\epsilon_{oo}/\epsilon_{o2}A_o^2)^{1/2}$  and diverges over a Rayleigh length  $R_d = k_o r_o^2 = (\omega_o/c)\epsilon_{oo}^{1/2} r_o^2$  where,  $r_o$  is the initial spot size of laser beam, and  $R_d$  is responsible for defocusing. In the underdense plasma,  $Z' = R_d$  satisfies the condition of laser beam, i.e.,  $r_o\omega_p/c \approx 2c/v_o(0)$ .

The pump wave leads to parametric excitation of two electromagnetic SBW  $\vec{E}_{1,2}$  and lower hybrid wave of electric field of potential  $\Phi$ ,

$$\phi = \Phi(r)e^{-i(\omega t - k_z z)}, \quad (4.1)$$

$$\vec{E}_{1,2} = E_{1,2} e^{-i(\omega_{1,2}t - k_{1,2}z)}, \quad (4.2)$$

Here,  $\omega_{1,2} = \omega \mp \omega_o$  and  $\vec{k}_{1,2} = \vec{k}_z \mp \vec{k}_o$  and  $k_z$  is the lower hybrid wave number.

The sideband imparts electron oscillatory velocity,  $\vec{v}_{1,2} = e\vec{E}_{1,2}/mi\omega_{1,2}$ . Due to the coupling of these sideband waves with the pump wave, electrons exert ponderomotive force  $\vec{F}_p = e\nabla\Phi_p$  at  $(\omega, \vec{k}_z)$ . Here, ponderomotive potential,  $\Phi_p = -(m/2e)(\vec{v}_o \cdot \vec{v}_1 + \vec{v}_o^* \cdot \vec{v}_1)$ . Due to the presence of electrostatic potential and ponderomotive potential, the electron density perturbation is obtained by solving the continuity equation,

$$\begin{aligned} n = & \left( \frac{-2(n_o^o + n_{qo}e^{iq_oz})e^2B_o}{m^2i\omega^3r_oF'} + \frac{(n_o^o + n_{qo}e^{iq_oz})ek_z}{mi\omega^2F'} - \frac{-2(n_o^o + n_{qo}e^{iq_oz})e^4B_o^3r^2}{m^4i\omega^5r_o^3F'^2} \right) \frac{-\partial\Phi_p}{\partial r} \\ & \left( \frac{-2(n_o^o + n_{qo}e^{iq_oz})e}{m\omega^2} + \frac{(n_o^o + n_{qo}e^{iq_oz})e^3B_o^2r^2}{m^3\omega^4r_o^2F'} \right) \frac{-\partial^2\phi}{\partial^2r} - \\ & \left( \frac{-2(n_o^o + n_{qo}e^{iq_oz})e}{m\omega^2r} + \frac{4(n_o^o + n_{qo}e^{iq_oz})e^3B_o^2r}{m^3\omega^4r_o^2F'} \right) \\ & + \frac{-2(n_o^o + n_{qo}e^{iq_oz})e^5B_o^4r^3}{m^5\omega^6r_o^4F'^2} - \frac{e^2k_zB_or(n_o^o + n_{qo}e^{iq_oz})}{m^2\omega^3r_oF'} \frac{-\partial\phi}{\partial r} \end{aligned} \quad (4.3)$$

where,  $F' = 1 - (e^2B_o^2r^2/m^2\omega^2r_o^2)$ . In the Poisson equation  $\nabla^2\Phi = en/\epsilon_o$ , substituting this value of density perturbation we get,

$$\frac{\partial^2\Phi}{\partial\xi'^2} + \frac{1}{\xi'} \frac{\partial\Phi}{\partial\xi'} + (\alpha'^2 - \xi'^2)\Phi = \left( \frac{k_z^2r_o \left( \frac{\omega_p^2}{\omega^2} + \frac{\omega_{pq}^2}{\omega^2} \right) - 2k_z \frac{\omega_p\omega_c}{\omega^3}}{\frac{r_o}{R_o} 2 \left( \frac{\omega_p^2}{\omega^2} + \frac{\omega_{pq}^2}{\omega^2} - 1 \right)} \right) \Phi_p. \quad (4.4)$$

Here,  $R_o'^2 = 2\omega^2r_o[(\omega_p^2/\omega^2 + \omega_{pq}^2/\omega^2) - 1]/\omega_p\omega_c k_z$ ,  $\alpha'^2 = k_z^2R_o'^2/2(\omega_p^2/\omega^2 + \omega_{pq}^2/\omega^2) - 1$ ,  $\omega_{pq} = n_{qo}e^2/m\epsilon_o$ ,  $\xi' = r/R_o'$ . Ignoring the non-linear coupling term we get associated Laguerre polynomial solution from equation (4.4),

$$\Phi = A\Psi(\xi'), \quad (4.5)$$

where,  $\Psi(\xi') = (1/\sqrt{\alpha_p})e^{-\xi'^2/2}L_p^o(\xi'^2)$  and integer p gives eigenvalues 0,1,2... for  $\alpha_p^2 = 2p+1$  For  $(\omega_p, \omega_c) > \omega > \omega_{pi}$  lower hybrid modes exist at  $\xi'$ . The dispersion relation for radial eigen mode is given by  $\omega = \sqrt{\omega_p\omega_c/k_zr_o}$ .

The pump wave's oscillatory velocity combines with the density perturbation of electron, n at  $(\omega, \vec{k}_z)$  to create current densities that are nonlinear,  $\vec{J}_1 = -n_o e\vec{v}_1 - \frac{1}{2}ne\vec{v}_o$  (linear current density) and  $\vec{J}_2 = -n_o e\vec{v}_2 - \frac{1}{2}ne\vec{v}_o$  (non-linear current density) at  $(\omega_{1,2}, \vec{k}_{1,2})$ . Substituting

the values of linear and non-linear current densities in wave equation, we get

$$\frac{d^2 \vec{E}_{1,2}}{d\xi'^2} + \frac{1}{\xi'} \frac{d\vec{E}_{1,2}}{d\xi'} + \alpha'_{1,2}{}^2 \vec{E}_{1,2} = \frac{i\omega_{1,2}}{2c^2} \nabla^2 \Phi \vec{v}_{oj} \quad (4.6)$$

Here,  $j = 0, 1$ ,  $\vec{v}_{o1} = \vec{v}_o^*$ ,  $\vec{v}_{o2} = \vec{v}_o$  and  $\alpha'_{1,2}{}^2 = [(\omega_{1,2}^2 - \omega_p^2)/c - k_z^2] R_o^2$ . Ignoring the non-linear coupling in Eq.(4.6) and reducing it to Bessel form,

$$E_{1,2} = A_{1,2} \Psi_{1,2}(\xi') \quad (4.7)$$

Where,  $\Psi(\xi') = J_o(\alpha_{1,2}\xi')$ .

Now, substitute Eq.(4.7) in Eq.(4.4) and multiply the result by  $\Psi(\xi')$ . Integrating the resultant equation from 0 to  $\infty$  over  $\xi' d\xi'$ , we get

$$(\alpha^2 - \alpha_p^2)A = \frac{\beta'_1}{I'} \frac{v_o}{2i\omega_1} A_1 + \frac{\beta'_2}{I'} \frac{v_{*o}}{2i\omega_2} A_2 \quad (4.8)$$

Here,  $I' = \int_0^\infty \Psi(\xi') \Psi(\xi') d\xi'$  and

$$\beta'_{1,2} = - \int_0^\infty \frac{k_z^2 r_o (\frac{\omega_p^2}{\omega^2} + \frac{\omega_{pq}^2}{\omega^2}) - 2k_z \frac{\omega_c \omega_p^2}{\omega^3}}{\frac{r_o}{R_o^2} (2[\frac{\omega_p^2}{\omega^2} + \frac{\omega_{pq}^2}{\omega^2} - 1])} d\xi'.$$

Similarly, From Eq.(4.5) and (4.6) we get,

$$(\alpha_{1,2}^2 - \alpha_{r1,r2}^2) A_{1,2} = \frac{\beta'_{3,4} i\omega_{1,2} \vec{v}_{oj}}{I'_{1,2} 2c^2} A R_o \quad (4.9)$$

Here,  $I'_{1,2} = \int_0^\infty \Psi_{1,2}(\xi') \Psi_{1,2}(\xi') d\xi'$ ,  $\beta_{3,4} = \int_0^\infty \Psi_{1,2}(\xi') \nabla^2 \Psi(\xi') d\xi'$  and  $c$  is the speed of light. Combining Equations (4.8) and (4.9), we get

$$(\alpha^2 - \alpha_p^2) = \frac{\beta'_1 \beta'_3 v_o^2}{II_2 4c^2} \frac{1}{\alpha_1^2 - \alpha_{r1}^2} - \frac{\beta'_2 \beta'_4 v_o^2}{II_1 4c^2} \frac{1}{\alpha_2^2 - \alpha_{r2}^2} \quad (4.10)$$

Substitute  $(\alpha^2 - \alpha_p^2) = r_o k_z (\omega^2 - \omega_r^2) / \omega_p \omega_c$ ,  $\alpha_1^2 - \alpha_{r1}^2 = (\omega_1^2 - \omega_{r2}^2) R_o^2 / c^2$  and  $\alpha_2^2 - \alpha_{r2}^2 = (\omega_2^2 - \omega_{r2}^2) R_o^2 / c^2$  in Eq.(10).

$$(\omega^2 - \omega_r^2) \frac{r_o k_z}{\omega_p \omega_c} = \frac{\beta'_1 \beta'_3 v_o^2}{II_3 4c^2} \frac{1}{(\omega_1^2 - \omega_{r1}^2)} - \frac{\beta'_2 \beta'_4 v_o^2}{II_2 4c^2} \frac{1}{(\omega_2^2 - \omega_{r2}^2)} \quad (4.11)$$

Here,  $\omega_r$  is the real part of the frequency and,  $\omega_{r1}$  and  $\omega_{r2}$  are the real parts of scattered waves at  $\omega_1$  and  $\omega_2$  respectively. Substituting above  $\omega_1 = \omega - \omega_o$ ,  $\vec{k}_1 = \vec{k}_3 - \vec{k}_o$  and  $\omega = \omega_r + i\Gamma$

for lower side-band, we get

$$\omega_1^2 - \omega_{r1}^2 = (\Delta - i\Gamma)2(\omega_o - \omega_r) \quad (4.12)$$

Here,  $\Delta$  is the small frequency shift as a result of pondermotive force given by  $\Delta = -\frac{\omega_r^2 \omega_o^2}{2\omega_o^3} \left(1 + \frac{5.76c^2}{\omega_o^2 r_o^2}\right)$  and  $\Gamma$  is the growth rate of SRS.

Similarly, for upper side-band we get,

$$\omega_2^2 - \omega_{r2}^2 = (\Delta - i\Gamma)2(\omega_o + \omega_r) \quad (4.13)$$

Substituting Eq.(4.12) and (4.13) in Eq.(4.11) we get non-linear growth rate of Raman Scattering,

$$\Gamma^3 + \Delta^2\Gamma = -i \frac{\beta'_1 \beta'_3}{II_1} \frac{\Delta v_o^2}{4\omega_o R_o'^2} \sqrt{\frac{\omega_p \omega_c}{(2p+1)r_o k_z}} \quad (4.14)$$

### 4.3 Results and Discussion

We have solved Eq.(4.14) numerically for laser of wavelength  $\lambda = 0.35\mu m$ , electron density considered is  $10^{21} cm^{-3}$ , initial spot-size  $r_o = 10\mu m$ , normalized spot-size and wave number considered are  $r_o \omega_o / c = 5000$  and  $k_z r_o = 473$  respectively. The critical density obtained is  $9 \times 10^{21} cm^{-3}$ . These values satisfies the SRS condition, i e.,  $n_o^o \leq n_{cr}/4$ .

We then plot the normalized growth rate ( $\Gamma/\omega_o$ ) against normalized cyclotron frequency in the presence and the absence of density ripple for different eigen values;  $p = 1, 2$  and  $3$ .

Figure 4.1 shows variation of the normalized growth rate with cyclotron frequencies at  $p= 1, 2$  and  $3$ . The growth rate of SFRS is reduced with the increase in cyclotron frequency. Many of the decay waves in this mechanism travel along with the pulse, resulting in a long contact duration and a high growth rate for the Raman process, therefore we see maximisation of growth rate. The interaction is localised by the nonuniformity of the azimuthal magnetic field present in the density rippled plasma, and the growth of SFRS rises with ( $r_o$ ). For greater  $r_o$ , electrons will undergo less magnetic fields at a given  $r$ . The localization effect of a magnetic field with a greater  $r_o$  would be weak. The Raman process will evolve at a faster pace as a result of this. The growth rate rises with  $\omega_c/\omega_o$ , reaches a peak, and then declines. The integral of the decay wave's overlapping wave-function determines the SFRS growth rate, and the maximum rate of growth is achieved at maximum-overlapping. As plasma density grows, so does the rate of increase. Plasma frequency rises as electron plasma density rises, resulting in a faster growth rate.

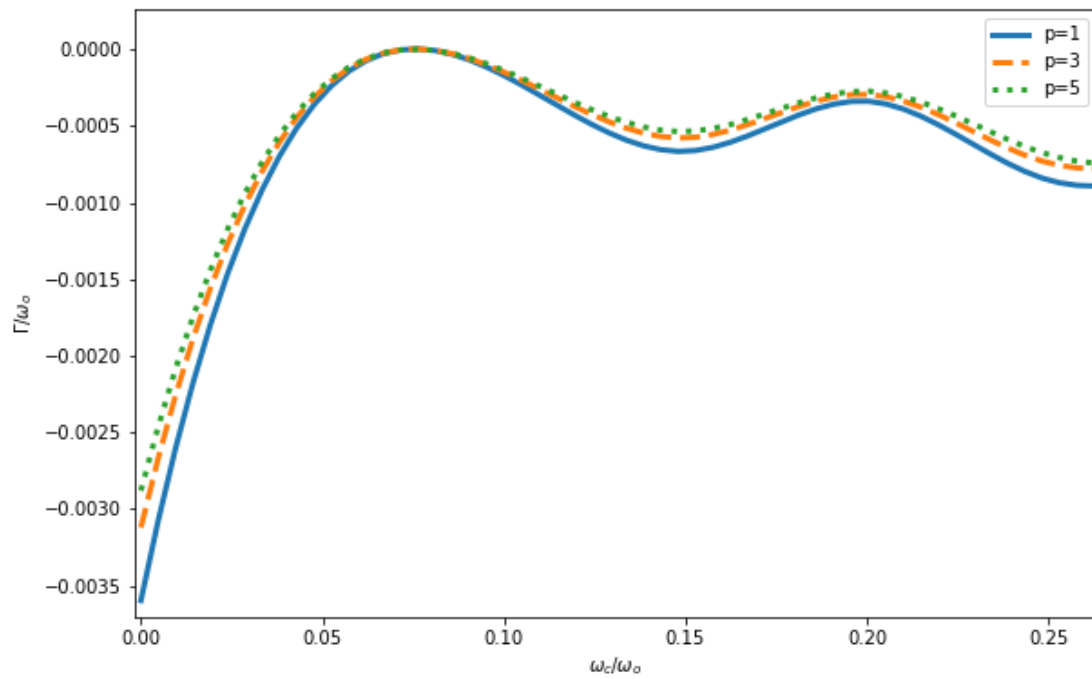


Figure 4.1: Variation of normalized growth rate in the presence of magnetic field at various Eigen values

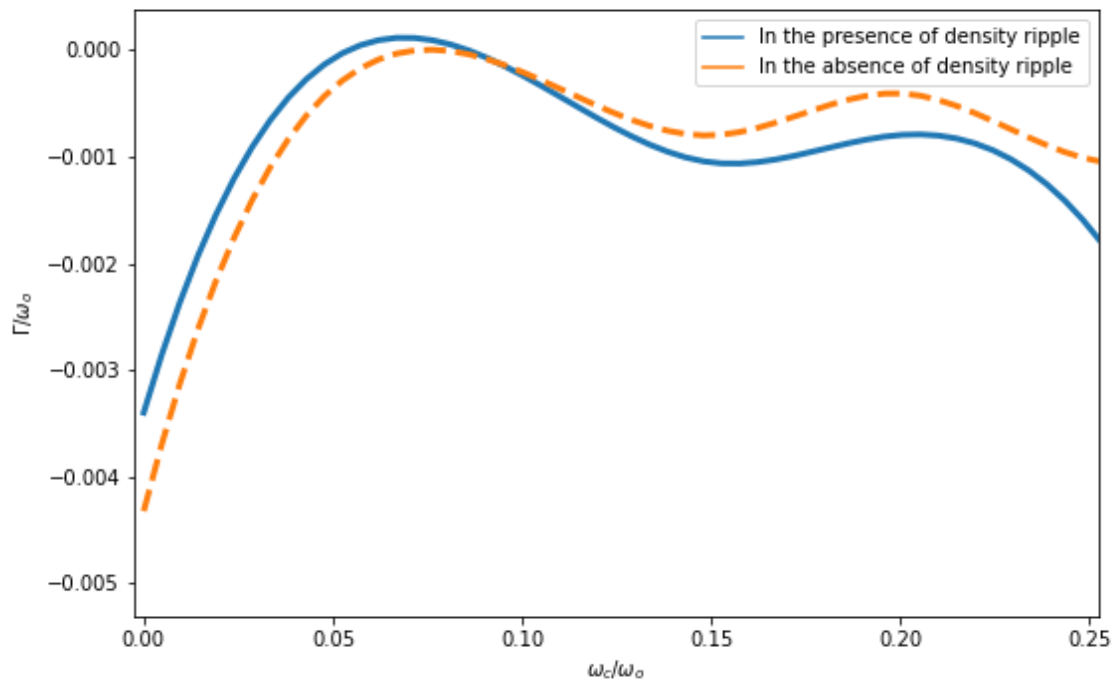


Figure 4.2: Variation of growth rate with magnetic field in the presence and absence of density ripple

In Fig.(4.2), effect of density rippled plasma is observed on the variation of normalized growth rate of SFRS with cyclotron frequency. We compare the growth rate of SFRS in the presence and absence of density ripple. It is observed that significant amount of suppression is observed when density rippled plasma is present as the coupling of magnetic field and density ripple suppresses the amplitude of the wave therefore, reducing it's growth.

Fig.(4.3) shows the variation normalized growth rate with normalized spot size ( $r_o\omega_o/c$ ) at  $p= 1,2$  and  $3$ . The overall combined effect of density rippled plasma and azimuthal magnetic field clearly suppressed the growth of SFRS.

## 4.4 Conclusion

In conclusion, the localization of the LHW in the presence of density rippled plasma and magnetic field, the SFRS growth rate is significantly reduced which could therefore reduce the preheating of fuel in ICF.

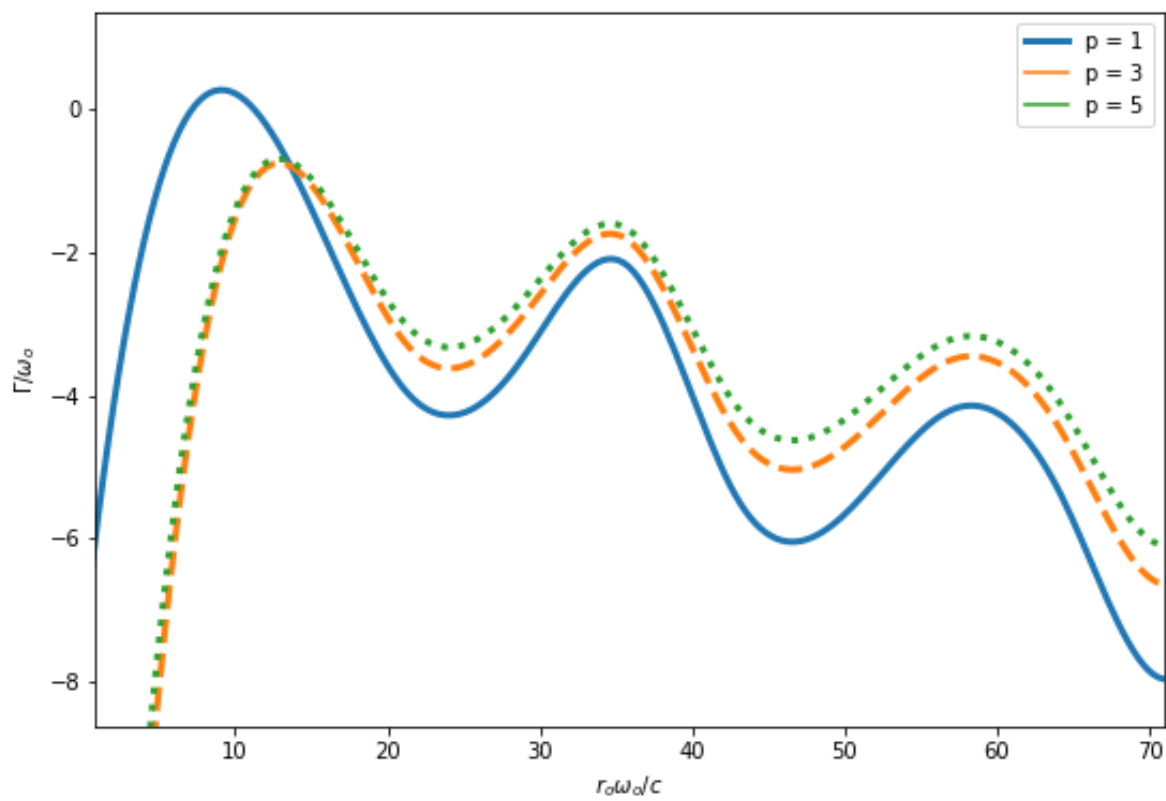


Figure 4.3: Variation of growth rate with the spot size of laser beam at various Eigen values

## Bibliography

- [1] J. Nuckolls, L. Wood, A. Thiessen and G. Zimmerman, *Nature* **239**, 139–142 (1972).
- [2] J. Lindl, *Physics of plasmas* **2**, 3933–4024 (1995).
- [3] R. L. McCrory, J. M. Soures, C. P. Verdon, F. J. Marshall, S. A. Letzring, S. Skupsky, T. J. Kessler, R. L. Kremens, J. P. Knauer, H. Kim, and J. Delettrez, *Nature* **335**, 225–229 (1988).
- [4] William. L. Kruer, *The physics of laser plasma interaction*, Addison-Wesley, New York (1988).
- [5] R. P. Drake, R. E. Turner, B.F. Lasinski, K. G. Estabrook, E. M. Campbell, C. L. Wang, D. W. Phillion, E. A. Williams and W. L. Kruer, *Physical review letters* **53**, 1739 (1984).
- [6] W. Seka, E. A Williams, R. S. Craxton, L. M. Goldman, R. W. Short and K. Tanaka, *The Physics of fluids* **27**, 2181–2186 (1984).
- [7] S. Depierreux, C. Neuville, C. Baccou, V. Tassin, M. Casanova, P. E. Masson-Laborde, N. Borisenko, A. Orekhov, A. Colaitis, A. Debayle and G. Duchateau, *Physical review letters* **177**, 235002 (2016).
- [8] A. Simon, R. W. Short, E. A. Williams, T. Dewandre, *The Physics of fluids* **26**, 3107–3118 (1983).
- [9] W. Seka, D. H. Edgell, J. F. Myatt, A. V. Maximov, R. W. Short, V. N. Goncharov, H. A. Baldis, *Physics of Plasmas* **16**, 052701 (2009).
- [10] W. Seka, J. F. Myatt, R. W. Short, D. H. Froula, J. Katz, V. N. Goncharov, I. V. Igumenshchev, *Physical review letters* **112**, 145001 (2014).
- [11] M. J. Rosenberg, A. A. Solodov, W. Seka, R. K. Follett, J. F. Myatt, A. V. Maximov, C. Ren, S. Cao, S., P. Michel, M. Hohenberger and J. P. Palastro, *Physics of Plasmas* **27**, 042705 (2020).
- [12] P. Michel, M. J. Rosenberg, W. Seka, A. A. Solodov, R. W. Short, T. Chapman, C. Goyon, N. Lemos, M. Hohenberger, J. D. Moody and S. P. Regan, *Physical Review E* **99**, 033203 (2019).
- [13] D. N. Gupta, P. Yadav, D. G. Jang, M. S. Hur, H. Suk and K. Avinash, *Physics of Plasmas* **22**, 052101 (2015).



- [14] Z. J. Liu, C. Y. Zheng, L. H. Cao, B. Li, J. Xiang and L. Hao, *Physics of Plasmas* **24**, 032701 (2017).
- [15] T. Gong, J. Zheng, Z. Li, Y. Ding, D. Yang, G. Hu and B. Zhao, *Physics of Plasmas* **22**, 092706 (2015).
- [16] L. J. Perkins, DD-MM. Ho, B. G. Logan, BG G. B. Zimmerman, M. A. Rhodes, D. J. Strozzi, D. T. Blackfield and S. A. Hawkins, *Physics of Plasmas* **6**, 062708 (2017).
- [17] J. P. Knauer, O. V. Gotchev, P. Y. Chang, D. D. Meyerhofer, O. Polomarov, R. Betti, J. A. Frenje, C. K. Li, MJ-E Manuel, R. D. Petrasso and J. R. Rygg, *Physics of Plasmas* **17**, 056318 (2010).
- [18] P. Y. Chang, G. Fiksel, M. Hohenberger, J. P. Knauer, R. Betti, F. J. Marshall, D. D. Meyerhofer, F. H. Séguin and R. D. Petrasso, *Physics of Plasmas* **107**, 035006 (2011).
- [19] V. Sajal, D. Dahiya and V. K. Tripathi, *Physics of Plasmas* **14**, 032109 (2007).
- [20] C. A. Walsh, K. McGlinchey, J. K. Tong, B. D. Appelbe, A. Crilly, M. F. Zhang and J. P. Chittenden, *Physics of Plasmas* **26**, 022701 (2019).
- [21] N. K. Jaiman, V. K. Tripathi and M. P. Srivastava, *Physics Letters A* **232**, 252–256 (2007).
- [22] V. Sajal, N. Sharma, K. Navneet, R. Kumar and V. K. Tripathi, *Optics Communications* **285**, 3563–3566 (2012).
- [23] V. B. Pathak and V. K. Tripathi, *Physics of Plasmas* **15**, 022301 (2008).
- [24] H. C. Barr and F. F. Chen, *The Physics of Fluids* **30**, 1180–1188 (1987).
- [25] M. J. Rosenberg, A. A. A. Solodov, W. Seka, R. K. Follett, J. F. Myatt, A. V. Maximov, C. Ren, S. Cao, P. Michel, M. Hohenberger and J. P. Palastro, *Physics of Plasmas* **27**, 042705 (2020).
- [26] Z. J. Liu, Y. H. Chen, C. Y. Zheng, L. H. Cao, B. Li, J. Xiang, L. Hao and K. Lan, *Physics of Plasmas* **24**, 082704 (2017).
- [27] P. Michel, L. Divol, E. L. Dewald, J. L. Milovich, M. Hohenberger, O. S. Jones, L. B. Hopkins, R. L. Berger, W. L. Kruer and J. D. Moody, *Physical review letters* **115**, 055003 (2015).
- [28] S. H. Cao, R. Yan, H. Wen, J. Li and C. Ren, *Physical Review E* **111**, 053205 (2020).
- [29] C. Rousseaux, M. Rabec le Gloahec, S. D. Baton, F. Amiranoff, J. Fuchs, L. Gremillet, J. C. Adam, A. Heron and P. Mora, *Physics of Plasmas* **2**, 4261–4269 (2002).

## Chapter 5

# Ignition and Burn calculations for advanced fuels in ICF

### 5.1 Introduction

The generation of vast volumes of energy at competitive rates with minimal environmental impact is a complex and unsolved challenge. The debate over population development, growing inequalities in access to natural resources, education, and decent living standards across the world, as well as the increasing stress of human activities on the atmosphere and climate, can only be overcome by concerted actions from all developing countries to improve energy production and delivery. Renewable energy development and more productive energy use are critical components of the overall energy plan. Still, without long-term nuclear energy supply, these interventions are incompatible with rising ecological, fiscal, and political demands. Nuclear fusion, as compared to all other options, has apparent benefits in all of these areas: it does not generate highly radioactive long-lived elements.

A high-energy-density environment can now be routinely created in the laboratory thanks to the current generation of high-power lasers [1, 2]. The notion of compressing a compact target using high-power lasers to get thermonuclear fuel to ignition conditions was initially published by Nuckolls [3] in 1972. A powerful shock is discharged into the shell when the core pressure surpasses the pressure in the collapsing shell. The deceleration phase is termed after it. The ultimate fuel assembly at stagnation consists of a low-density (30–100 g/cm<sup>3</sup>), high-temperature (5–10 keV) core—the hot spot—surrounded by a dense (300–1000 g/cm<sup>3</sup>), cold (200–500 eV) fuel layer—the compressed shell. When a deuterium and tritium combine to create a 14.1 MeV neutron and a 3.56 MeV alpha particle, such plasma conditions are adequate to initiate DT thermonuclear fusion. Alpha heating is the name for this positive feedback loop.

The highest fusion cross-section is for the deuterium-tritium reaction;  $D+T \rightarrow n(14.1\text{MeV})+He^4(3.5\text{MeV})$  for several keV temperature. A DT target could be ignited because it only needs a low ignition temperature of 5 to 10 keV and produces the necessary energy output with a limited  $\rho R$  of 2-5 g/cm<sup>2</sup>. Ignition conditions are achieved with a driver energy of 5-10 MJ and with a fuel mass of a few mg. The tritium inventory and neutron output must be kept to a minimum in an ICF reactor for environmental and safety reasons. There have been proposals [8] for ICF reactors that can be regulated by imploding deuterium targets with a limited volume of DT at the core. The thermonuclear energy emitted in the ignitor can ignite D + D reactions in the deuterium after the DT has ignited. The energy released

in a D + T reaction is around five times greater than that produced in a D + D reaction. Tahir *et al.* [9] gave a theory to reduce the amount of tritium in an inertial fusion target while maintaining a large increase in production energy. They have also shown analytically that a 50:50 mixture of deuterium and tritium is not required; however, a 70:30 ratio of the two isotopes should be used. This combination would result in a 40% reduction in the use of tritium in the aim while only a 16% reduction in production radiation. As a result, the amount of tritium utilised in a reactor each day may be decreased. This might result in a decrease in overall tritium inventory, which is essential for both safety and the environment. The feasibility of using various forms of fuels in possible inertial fusion power reactors, such as DT, pure deuterium,  $DH^3$ , and  $B^{11}$ , has previously been investigated [11]. They showed that by designing targets with a significantly reduced tritium content, it is possible to eliminate tritium inventory, thus improving the power plant's protection. Low-level tritium targets can also provide enough electricity to keep the power plant running. In this research we study DT fuels of different concentration levels and a proposed target design with low tritium inventory. In section 2, we present the analytical study on burning up of non-equimolar DT under ICF conditions for various DT ratios. In section 3, 1-D hydrodynamic simulation results are described. In Section 4, target design is described and finally in section 5 conclusions are made.

The fusion reaction rate is given by,

$$N_D N_T < \sigma v > \quad (5.1)$$

The rate of ICF is very high, so we need to account for fuel depletion,

$$\frac{dn(t)}{dt} = N_D(t) N_T(t) < \sigma v > \quad (5.2)$$

where, n is the number of fusion reactions per unit volume. Therefore, the obtained fraction of deuterium and tritium fuel burned (i e., burn fraction) is:

$$f_{bD} = \frac{10n}{9N_o} \quad (5.3)$$

$$f_{bT} = \frac{10n}{N_o} \quad (5.4)$$

Here,  $f_{bD}$  is burn fraction of deuterium and  $f_{bT}$  is burn fraction of tritium,  $N_o$  is the initial ion number density. Now, after differentiating the burn fraction we write

$$\frac{df_b}{0.1f_{bT}^2 - f_{bT} + 0.9} = N_o < \sigma v > dt \quad (5.5)$$

On solving Eq. (5) further, we substituting  $N_o = \rho/m_{DT}$  and confinement time  $< \tau > = r/4c_s$  into the solved equation. Finally, for 30% of burn fraction of tritium ( $f_{bT}$ ),  $\rho R$  is

Fuel concentration of Deuterium(D) and Tritium(T)	Density-Radius product ( $\rho r$ ) for 30% tritium burn fraction ( $\text{kg/m}^2$ )	Overall burn fraction ( $f_b$ ) equivalent to $f_{bT} = 0.3$
10% T and 90% D	11.2	0.06
20% T and 80% D	12.9	0.12
30% T and 70% D	15.2	0.18
40% T and 60% D	18.5	0.24

Table 5.1: Overall burn fraction equivalent to  $f_{bt} = 0.3$ 

Radius of the sphere ( $r$ ) (cm)	Density-Radius product ( $\rho r$ ) ( $\text{g/cm}^2$ )	Mass of fuel ( $m$ ) (kg)
0.001	1	$4.189 \times 10^{-9}$
0.002	2	$3.351 \times 10^{-8}$
0.003	3	$1.131 \times 10^{-7}$
0.004	4	$2.681 \times 10^{-7}$
0.005	5	$5.236 \times 10^{-7}$

Table 5.2: Density-Radius product and mass of fuel for different radius of sphere

obtained. Now, we consider the case of taking four different ratios of DT, i.e., 90 : 10, 80 : 20, 70 : 30 and 60 : 40 keeping 50 : 50 as benchmark. For each case we calculate 30% of burn fraction of tritium, as shown in Table 5.1.

## 5.2 Hydrodynamic simulation results

This section presents the numerical simulation of burn analysis for different ratios of DT fuel using 1-D hydrodynamic simulations. For each ratio of fuel initial temperature is 30 keV, density of fuel ( $\rho$ ) is  $1000 \text{ g/cm}^3$ . Table 5.2 show the values of  $\rho r$  and mass of fuel taken for different radius of spheres.

From the 1-D Hydrodynamic simulation performed, figure 5.1 show the maximum energy

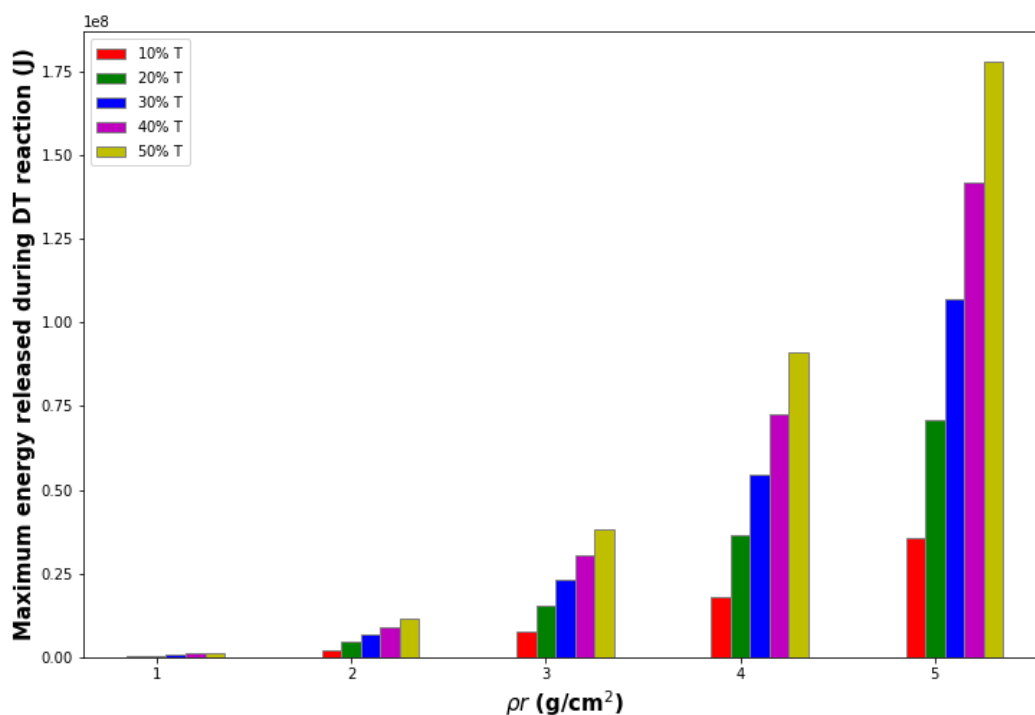


Figure 5.1: Maximum energy released in DT fusion reactions

released in DT fusion reactions for different ratios of DT fuel.

It can be clearly observed that maximum energy released for a DT reaction is more in higher tritium concentration DT fuel. The energy difference between 50:50 DT and 60:40 DT for each  $\rho r$  ranges between 19% to 22%, the energy difference between 50:50 DT and 70:30 DT is from 38% to 40%, the energy difference between 50:50 DT and 80:20 DT is between 59% to 60% and 79% to 80% is the energy difference between 50:50 DT and 90:10 DT. Some of the previous studies done showed that even if the tritium level of the fuel is reduced by 30% to 40%, it will still create enough energy to run a power plant efficiently.[13, 12]. Instead, a combination with a considerably greater proportion of deuterium may be used without sacrificing much output energy [9].

Figures 5.2, 5.3, 5.4 and 5.5 show the comparison of simulation and analytical results for variation of  $\rho r$  with tritium burn fraction. From these graphs we can see that in tritium-poor fuel, greater tritium utilization is achieved at lower  $\rho r$ . The values of simulation and analytical results vary because we have not considered DD reactions in our analytical study. By producing low-level tritium targets, the entire tritium inventory might be lowered. Therefore, various problems related to tritium inventory can be reduced.

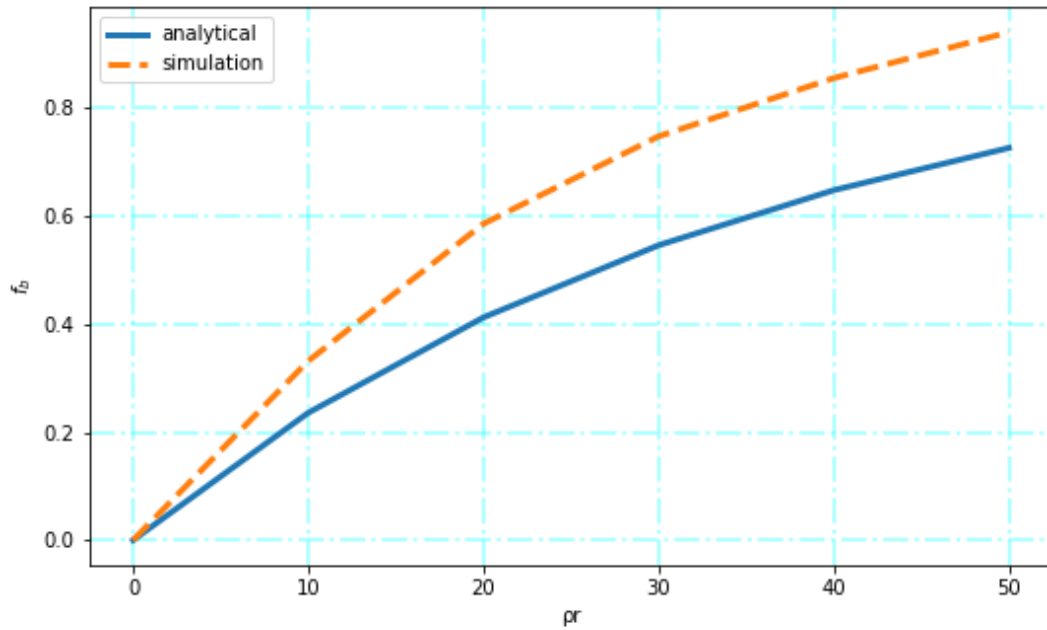


Figure 5.2: Variation of tritium burn fraction ( $f_b$ ) with density-radius product ( $\rho r$ ) for 10%T

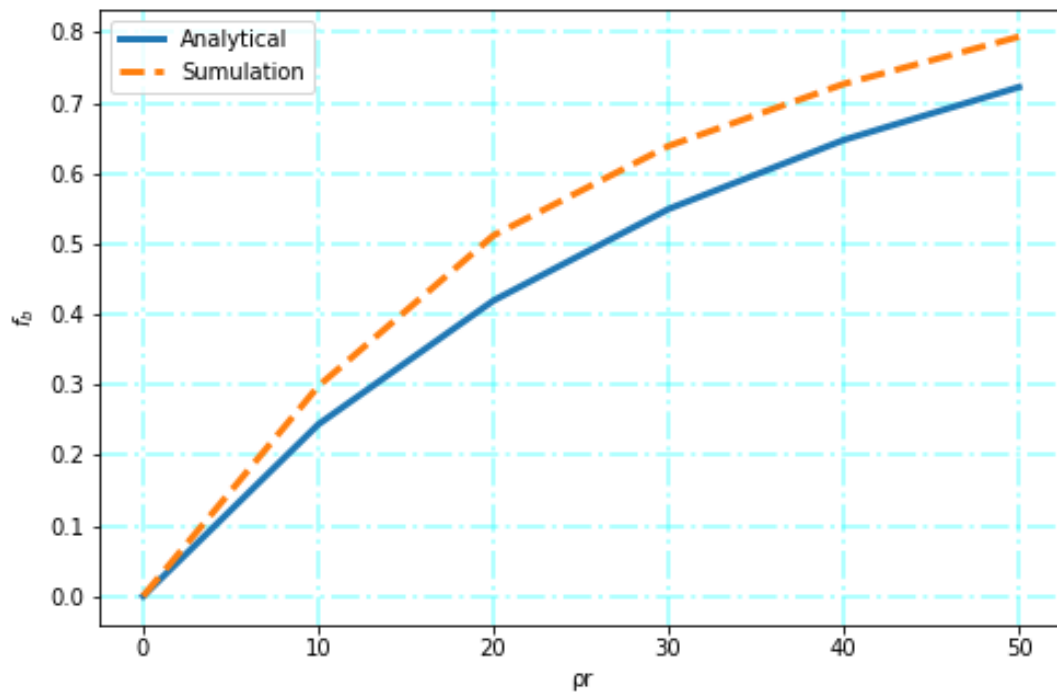


Figure 5.3: Variation of tritium burn fraction ( $f_b$ ) with density-radius product ( $\rho r$ ) for 20%T

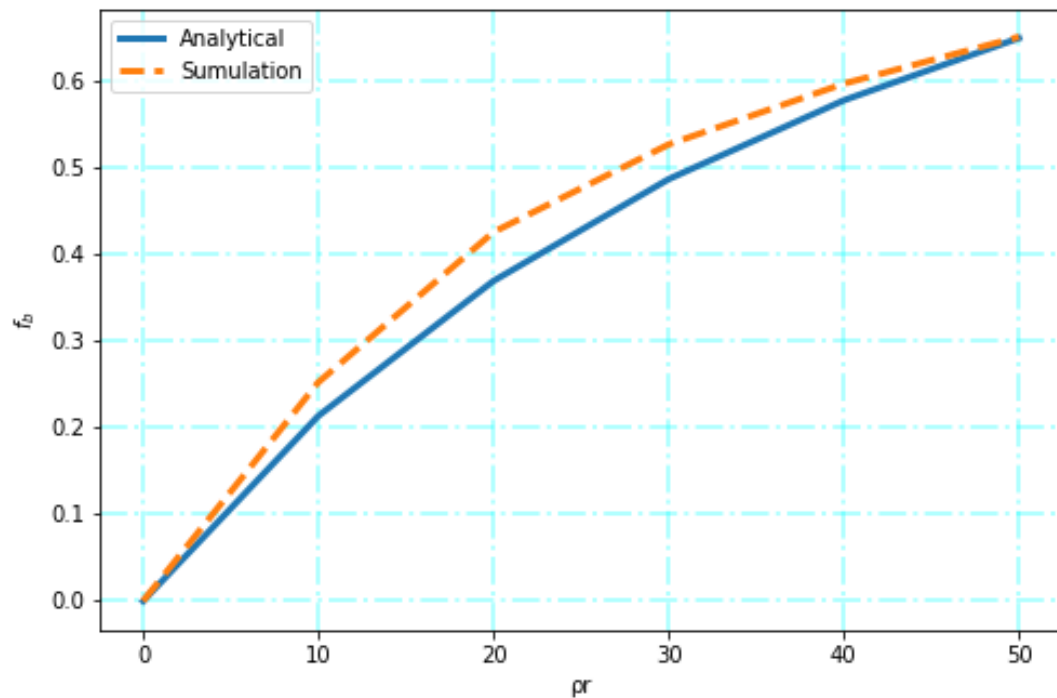


Figure 5.4: Variation of tritium burn fraction ( $f_b$ ) with density-radius product ( $\rho r$ ) for 30%T

### 5.3 Target Design

From the results obtained and analysed, we propose a layered target design for DT spherical shell as shown in figure 5.6. The center most layer comprises of 50:50 DT. Then every next layer has reduced tritium concentration, i e., 60:40 DT, then 70:30 DT, then 80:20 DT and finally the outermost layer has only 10% tritium . This model reduces the amount of tritium required for ICF (although the maximum and easiest way of obtaining ignition is by 50:50 DT only) without effecting much on the overall energy production, as discussed before (from figure 5.1). From this model the expensive tritium is not on the outer layers and is present mostly at the centre and hence more tritium breeding is possible. Also, this scheme leads to minimization of tritium in the system, therefore keeping the environment comparatively safer.

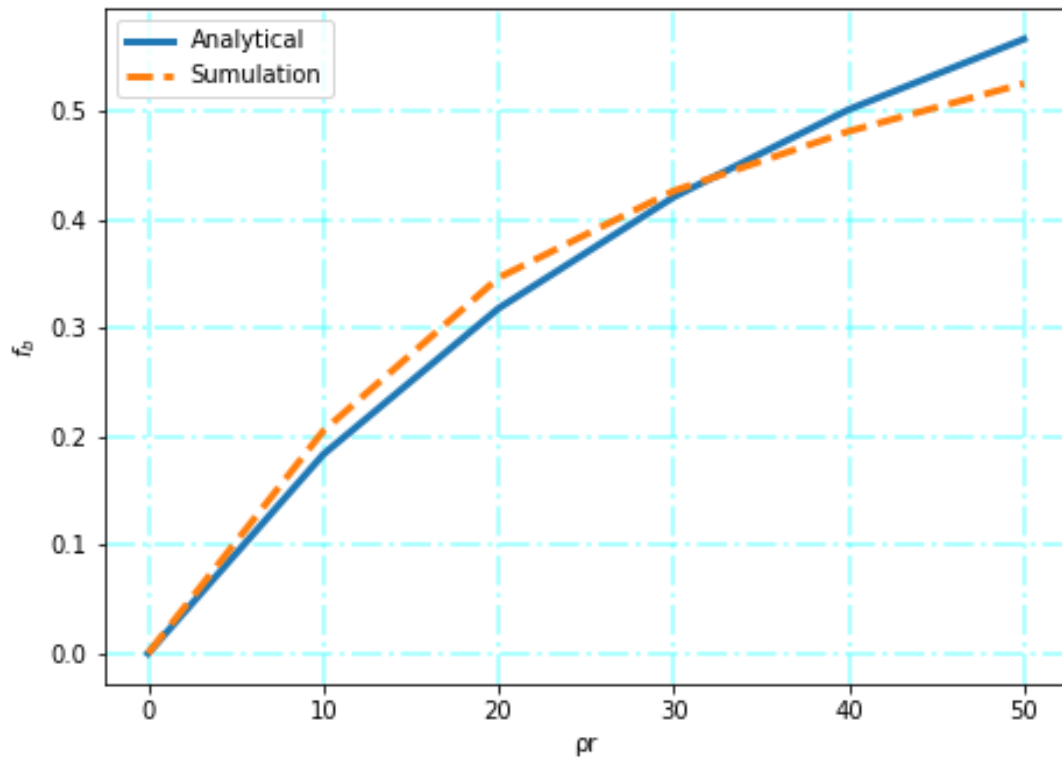


Figure 5.5: Variation of tritium burn fraction ( $f_b$ ) with density-radius product ( $\rho r$ ) for 40%T

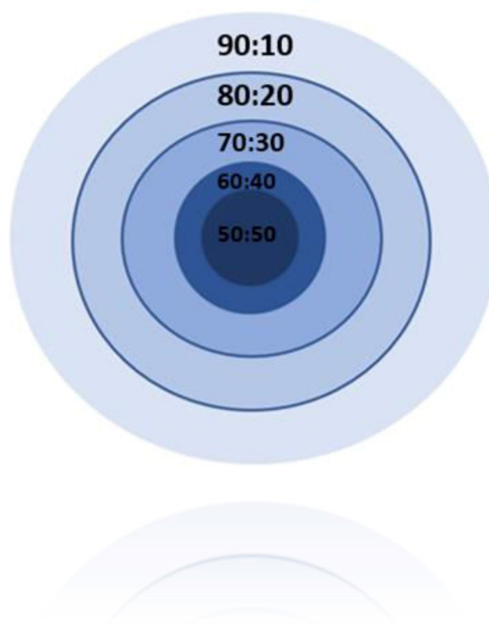


Figure 5.6: Layered schematic diagram



## 5.4 Conclusion

This study suggests that in a ICF target, we can utilize a combination of different concentration of fuels instead of only using a 50:50 combination of deuterium and tritium. A combination with a considerably greater proportion of deuterium may be used without sacrificing much output energy. This impact might result in a large reduction in tritium inventory, which is crucial from an environmental and safety standpoint. This concept can also be used in inertial fusion.

## Bibliography

- [1] R. Betti and O. A. Hurricane, *Nature* **12**, 435–448 (2016).
- [2] S. Nakai and K. Mima, *Reports on Progress in Physics* **67**, 321 (2004).
- [3] J. Nuckolls, L. Wood, A. Thiessen and G. Zimmerman, *Nature* **239**, 139–142 (1972).
- [4] S. Atzeni and J. Meyer-ter-Vehn, *The physics of inertial fusion: beam plasma interaction, hydrodynamics, hot dense matter*, **125**, (2004).
- [5] J. D. Lindl, R. L. McCrory and E. M. Campbell, *Physics Today* **45**, 32 (1992).
- [6] M. Tamba, N. Nagata, S. Kawata and K. Niu, *Radiation and environmental biophysics* **22**, 215–223 (1983).
- [7] M. Tamba, N. Nagata, S. Kawata and K. Niu, *Journal of the Physical Society of Japan* **53**, 3416–3426 (1984).
- [8] N. A. Tahir, and D. H. H. Hoffmann, *Fusion technology* **33**, 164–170 (1998).
- [9] N. A. Tahir, and D. H. H. Hoffmann, *Fusion engineering and design* **24**, 413–418 (1994).
- [10] M. Tamba, N. Nagata, S. Kawata and K. Niu, *Physics of Plasmas* **22**, 110501 (2015).
- [11] N. A. Tahir, and D. H. H. Hoffmann, *Laser and Particle Beams* **15**, 575–587 (1997).
- [12] S. Skupsky, *Nuclear Fusion* **18**, 843 (1978).
- [13] S. Skupsky, *Laser and Particle Beams* **10**, 479–484 (1992).

## Chapter 6

# SRS coupling with decay instability in a magnetized plasma.

### 6.1 Introduction

For successful ICF designs, it is critical to understand LPI's. Preheating from hot electrons generated by SRS and TPD reduces implosion efficiency and is a critical issue for direct-drive ICF [1, 2]. Ignition-scale direct-drive targets will have a corona plasma with extended density scale lengths, potentially lowering SRS and TPD thresholds and boosting preheating. As a result, studies at the NIF [3] have shown that SRS is becoming more critical than TPD [4]. SRS is a well-known nonlinear phenomenon in high-power laser-plasma interaction, with applications in ICF, laser-based charged particle acceleration and other fields. When the plasma density is less than the quarter-critical density, a large amplitude laser pump  $(\omega_o, k_o)$  decays into a plasma wave  $(\omega, k)$  and a dispersed electromagnetic wave  $(\omega_1, k_1)$ .  $k = k_o + k_1$  and  $\omega = \omega_o + \omega_1$  are required by the momentum and energy conservation requirements. The highest growth occurs when the scattered electromagnetic wave propagates in the opposite direction of the pump wave in long pulse tests, although stimulated Raman forward scattering is critical in short pulse investigations. Under a variety of circumstances, extensive study on both the backward and forward SRS has been done.

SRS scattering in various parametric circumstances has been described both theoretically and experimentally[5, 6, 7, 8, 9]. The impact of SRS rescattering on the nonlinear scattering spectrum and the saturation mechanism of instabilities in the region where backward SRS is strongly damped has been explored in several prior works[6, 7]. Recent research has looked into abnormally hot electrons caused by SRS rescattering[5]. Many investigations [10, 11] have demonstrated that the daughter EPW is subjected to LDI, resulting in a secondary plasma wave and an IAW. The nonlinear saturation of SRS is influenced by the decay instability of the daughter plasma wave. [12, 13]. LDI previously has been used to explain how SRS reflectivity is affected by IAW dampening[14]. Other sources, however, can also be used to explain this. The presence of LDI connected to SRS was confirmed by Eplierreux et al. [15] who discovered secondary IAW and plasma waves resonantly produced by LDI. The energy from the daughter Langmuir wave is transferred into the secondary plasma wave, which is not in resonance with SRS, in the LDI cascade. As a result, LDI coupling can function as an energy sink for the SRS process and as a nonlinear saturation mechanism for SRS. [16].

Hot electrons influence on the SRS combined with decay instability in the presence of magnetized plasma is investigated in this work. The laser's intense electrons increase the plasma wave's Landau damping and impact the parametric process, which goes like this: The electron plasma wave ( $EPW_1$ ) and an electromagnetic sideband wave (SBW) are both excited by the laser. This electron plasma wave breaks down into an IAW and a secondary electron plasma wave ( $EPW_2$ ). The IAW's density perturbation combines with the  $EPW_1$ 's oscillating plasma electron velocity to generate a non-linear current that drives the  $EPW_2$ . The  $EPW_1$  and  $EPW_2$  drive the IAW by exerting a ponderomotive force on electrons. The non-linear current suppresses the amplifying  $EPW_1$  by coupling the density disturbance caused by  $EPW_1$  which leads to decay instability with the electrons' oscillatory velocity. The  $EPW_1$  is driven by the ponderomotive force generated by the pump and the electromagnetic SBW. The accompanying density perturbation interacts with the pump to create a non-linear current, which drives the SBW. In section 2 we consider the background theory for carrying out this work. In section 3 and 4 we do the instability analysis and instability coupling of the SRS and decay instability respectively. In section 5 we present the results and finally make the required conclusions in section 6.

## 6.2 Theoretical Considerations

Consider two electron populations with  $n_e^o$  as the density of electron at temperature  $T_e$  and  $n_h^o$  as density of hot electrons at temperature  $T_h$ , with a drifting Maxwellian distribution. The Maxwellian distribution function is represented as;

$$f_o(v_z) = n_h^o \left( \frac{m}{2\pi k T_h} \right)^{\frac{3}{2}} \exp \left[ \frac{-(v_z - v_h)^2}{(v_{th}^h)^2} \right] \quad (6.1)$$

From this we can obtain susceptibility of hot electron frequency  $\omega$  as;

$$\chi_h = \frac{2\omega_{pd}^2}{k_w^2 (v_{th}^h)^2} Z \left( 1 + \frac{\omega - k_w v_h}{k_w v_{th}^h} \right)^2 \quad (6.2)$$

where,  $\omega_{pd}$ ,  $v_h$ , and  $v_{th}^h$  is the plasma frequency, drifting velocity of hot electrons and thermal velocity, respectively in direction z. Similarly, plasma electron susceptibility is given by;

$$\chi_e = \frac{2\omega_p^2}{k_w^2 v_{th}^2} Z \left( 1 + \frac{\omega}{k_w v_{th}^h} \right)^2 \quad (6.3)$$

Here,  $v_{th}$  is electron thermal velocity given by  $(2T_e/m)^{1/2}$  and  $\omega_p = n_e^o e^2 / m \epsilon_o$  is the plasma frequency with e as electron charge, m as mass of the electron,  $T_e$  is the thermal energy of plasma electrons and  $\epsilon_o$  as free space permittivity. Plasma wave's dispersion relation with hot electrons is  $\epsilon = 1 + \chi_e + \chi_h = 0$ . The ion density of plasma with hot electrons is

$n_o^o + n_h^o$ . Therefore we neglect hot electron concentration to non-linear coupling. Depending on whether the wave's phase velocity is larger or lower than  $v_{oh}^h$ , they play a key role in creating linear damping or growth in the Langmuir wave.

### 6.3 Instability Analysis

Consider a high power laser with frequency  $\omega_o$ ,

$$\vec{E}_o = \hat{x}A \exp[-i(\omega_o t - k_o z)] \quad (6.4)$$

propagating through plasma with static magnetic field  $B_s \hat{z}$

$$\vec{B}_o = \frac{c(\vec{k}_o \times \vec{E}_o)}{\omega_o} \quad (6.5)$$

The pump imparts oscillatory velocity  $\vec{v}_o = v_o(\hat{x} + i\hat{y})$  to electrons where,

$$v_o = \frac{eE_o}{im(\omega_o - \omega_c)} \quad (6.6)$$

where  $\omega_c$  is the cyclotron frequency given by  $\omega_c = eB_s/mc$ . Here the electron charge is  $e$ , mass of electrons is  $m$  and  $c$  is the speed of light. The laser couples to a backscattered SBW of field,  $\vec{E}_1 = \hat{x}A \exp[-i(\omega_1 - k_1 z)]$ , and a daughter plasma wave ( $EPW_1$ ) of potential  $\Phi_w = \phi_w \exp[-i(-k_w z)]$  where  $\omega_1 = \omega - \omega_o$  and  $k_1 = k - k_o$ . The parametric procedures are depicted schematically in Figure 6.1

The electron plasma wave  $EPW_1$  decays into IAW of potential  $\Phi_s = \phi_s \exp[-i(\omega_s t - k_s z)]$  and a back scattered  $EPW_2$  of potential  $\Phi_d = \phi_d \exp[-i(\omega_d t - k_d z)]$  where  $\omega_d = \omega_s - \omega$  and  $k_d = k_s - k_w$ .

The electrons acquire oscillatory velocity,  $v_1 = \frac{eE_1}{im(\omega_1 - \omega_c)}$ , from the scattered wave. At  $(\omega, \vec{k}_w)$ , where  $\Phi_p = \phi_s \exp[-i(\omega_d t - k_d z)]$ . Here,  $\omega_c$  is the cyclotron frequency. The pump (initial) and the dispersed-wave exert a ponderomotive force,  $\vec{F}_p$ , on the electrons. The electron density perturbation becomes at  $(\omega, \vec{k}_w)$  is,

$$n_w^o = \frac{k_w^2 \epsilon_o}{e} (\chi_e + \chi_h) (\Phi_w + \Phi_p) \quad (6.7)$$

Here,  $\chi_e = -(\omega_p^2 + k_w^2 + v_{th}^2/\omega^2)$ . This density perturbation has a non-linear part ( $n_{wd}^{nl}$ ) because of the presence of decay instability. Hence, at  $(\omega, \vec{k}_w)$ , the total density perturbation is,

$$n_w^T = \frac{k_w^2 \epsilon_o}{e} \chi_e (\Phi_w + \Phi_p) + n_{wd}^{nl} \quad (6.8)$$

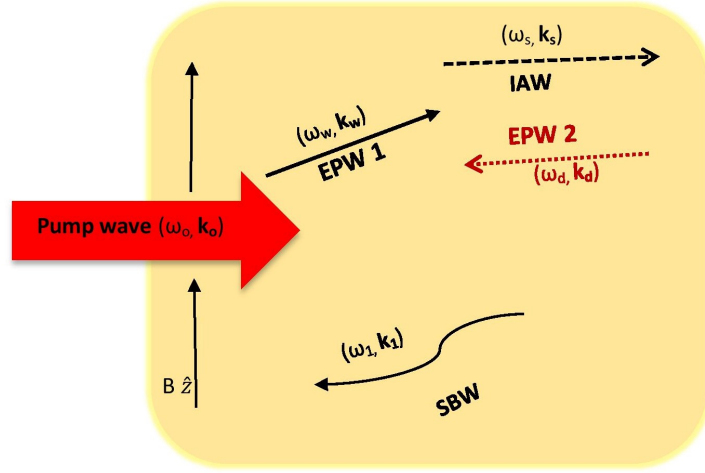


Figure 6.1: Schematic diagram representing the SRS coupled to decay instability

Similar process is carried by  $EPW_2$ . It imparts oscillatory velocity ( $\vec{v}_d$ ) to electrons,

$$v_d = \frac{e\vec{k}_d\Phi_d}{m(\omega_d - \omega_c)} \quad (6.9)$$

The electrons are additionally subjected to,  $F_{pd} = \vec{e}\nabla\Phi_{pd}$  (ponderomotive force), by the  $EPW_1$  and  $EPW_2$ , where  $\Phi_{pd} = -m(\vec{v}_w\vec{v}_d/2e)$ . The oscillatory velocity of  $EPW_1$  is denoted by  $\vec{v}_w = -e\vec{k}_d\Phi_d/m(\omega_w - \omega_c)$ . The density perturbations of electron-ion are given by the equations below at  $(\omega_s, \vec{k}_s)$  due to  $\Phi_s$  and  $\Phi_{pd}$ .

$$n_s = \frac{k_s^2\varepsilon_o}{e}\chi_{es}(\Phi_s + \Phi_{pd}) \quad (6.10)$$

$$n_s^i = \frac{k_s^2\varepsilon_o}{e}\chi_{is}(\Phi_s + \Phi_{pd}) \quad (6.11)$$

Here,  $\chi_{es} = \omega_{pi}^2/(k_s c_s)^2$ ,  $\chi_{is} = -\omega_{pi}^2/\omega_s^2$ ,  $\omega_{pi} = (n_o^o e^2/m_i \varepsilon_o)^{1/2}$  is the frequency of ions in plasma, ion mass is  $m_i$  and  $c_s = (T_e/m_i)^{1/2}$ .

Because of the coupling of  $EPW_2$  and IAW, the density perturbation becomes,

$$n_{wd}^{nl} = -\frac{k_w k_d k_s^2 \varepsilon_o}{2m\omega\omega_d}\chi_{es}(\Phi_s + \Phi_{pd})\Phi_d^* \quad (6.12)$$

Now, in order to obtain the value of total density perturbation, we substitute Eq. (6.12) in Eq. (6.8). We get,

$$n_w^T = \frac{k_w^2 \varepsilon_o}{e}\chi_e + (\Phi_w + \Phi_p) - \frac{k_w k_d k_s^2 \varepsilon_o}{2m\omega\omega_d}\chi_{es}(\Phi_s + \Phi_{pd})\Phi_d^* \quad (6.13)$$

Now, substituting Eq.(6.18) in Poisson's equation,  $\nabla^2\Phi_w = n_w/\varepsilon_o$  for  $EPW_1$ , we get

$$\varepsilon_p\Phi + \chi_e\Phi_p = \frac{k_w k_d k_s^2 \varepsilon_o}{2m\omega\omega_d} \chi_{es}(\Phi_s\Phi_d^*) \quad (6.14)$$

Here,  $\varepsilon_p = 1 + chi_e + chi_h$ . In this case,  $\chi_h$  is relatively small in compared to  $\chi_e$ .  $EPW_1$ 's Landau damping is only aided by these wandering electrons. We've also examined x1. This is true when the IAW's linear damping is less than  $\omega_s$ .  $EPW_1$ 's behaviour is governed by this equation. On the RHS of the equation presents the coupled term, explaining decay instability that affects SRS.

## 6.4 Instability Coupling

Consider a non-linear coupling, i e.  $\chi_e \approx 1$ . In order to produce a non-linear density perturbation at  $\omega_o$ ,  $n_w$  couples with  $v_1$ .

$$\vec{J}_o^{nl} = -\frac{1}{2}e\vec{v}_1^* \frac{k_w^2 \varepsilon_o}{e} \Phi_w \quad (6.15)$$

The linear part of current density is,

$$\vec{j}_o^l = -\frac{n_o^o e^2 \vec{E}_o}{mi\omega_o} \quad (6.16)$$

Using Maxwell's 3<sup>rd</sup> and 4<sup>th</sup> equation in pump wave at  $(\omega_o, k_o)$  we obtain,

$$x_o \vec{E}_o = -i \frac{\omega_o}{2} k_w^2 v_1^* \Phi_w \quad (6.17)$$

Eq. (6.17) describes the behaviour of pump wave. Here  $x_o = \omega_o^2 - \omega_p^2 - k_o^2 c^2$ . Similarly, at  $\omega_1$ , the density perturbations  $n_w$  couples with  $v_o$  to give,

$$\vec{J}_1^{nl} = -\frac{1}{2}e\vec{v}_1^* \frac{k_w^2 \varepsilon_o}{e} \Phi_w \quad (6.18)$$

which is the non-linear current density. Repeating the same procedure to obtain the behaviour of SBW we get,

$$x_1 \vec{E}_1 = -i \frac{\omega_1}{2} k_w^2 v_o^* \Phi_w \quad (6.19)$$

Here,  $x_1 = \omega_1^2 - \omega_p^2 - k_1^2 c^2$ .

At  $\omega_d = \omega_s - \omega$ ,  $J'_{wd} = -e(n_o^o \vec{v}_d + 1/2 n_s \vec{v}_w)$  is the current density with a linear and nonlinear component. Consider  $n'_{wd}$  as electron charge density perturbation. Using these values to

solve the equation of continuity, we get

$$\frac{\partial n'_{wd}}{\partial t} = \frac{1}{e} \nabla \cdot J'_{wd} \quad (6.20)$$

$$n_{wd} - n'_o \frac{k_d v_d}{\omega_d} - \frac{n_s k_d v_w^*}{2\omega_d} = 0 \quad (6.21)$$

In order to obtain the equation governing ion-acoustic wave, we solve for by substituting Eq. (6.11) and (6.12) in Poisson's equation  $\nabla^2 \Phi_s = e(n_s - n'_s)/\varepsilon_o$  and obtain,

$$\varepsilon_s \Phi_s + \chi_{es} \frac{k_d v_w \Phi_d}{2\omega_d} \quad (6.22)$$

Here,  $\varepsilon_s = 1 + \chi'_e$ . Now, we solve for  $EPW_2$  by substituting Eq. (6.21) in Poisson's equation  $\nabla^2 \Phi_d = en_{wd}/\varepsilon_o$ . With back-scattering of electrons, effect of hot electrons can be neglected.

$$\varepsilon_d \Phi_d + \frac{k_s^2 k_d v_w \Phi_d}{k_d^2 2\omega_d} \quad (6.23)$$

Finally, from Eq.'s (6.14), (6.17), (6.19), (6.22) and (6.23), we obtain the coupled mode equations.

$$\frac{\partial a_o}{\partial \tau} + i \frac{l_w^2 p q^2 f_o}{4} a_w(\tau) a_1^*(\tau) \quad (6.24)$$

$$\frac{\partial a_1}{\partial \tau} + C a_1(\tau) + i \frac{l_w^2 p q^2 f_1}{4} a_w(\tau) a_o^*(\tau) \quad (6.25)$$

$$\frac{\partial a_w}{\partial \tau} + \gamma_w a_w(\tau) - i \frac{\chi_e W}{4p} a_o(\tau) a_1(\tau) + i \frac{l_d l_s^2 \chi_{es} p q^2 f_o^2}{4 l_d f_d} a_s(\tau) a_w^*(\tau) \quad (6.26)$$

$$\frac{\partial a_d}{\partial \tau} + \gamma_d a_d(\tau) - i \frac{l_w l_s^2 \chi_{es} p q^2 f_o^2}{4 l_d f} a_s(\tau) a_w^*(\tau) \quad (6.27)$$

$$\frac{\partial a_s}{\partial \tau} - i \frac{f_s^3 \chi_{es} l_d l_w p q^2 f_o^2}{4 l_d f} a_s(\tau) a_d(\tau) \quad (6.28)$$

The above five equations represent the coupled equations of SRS with decay instability. The right-hand side of equation (26) has a second component that couples decay instability to SRS'  $EPW_1$ . All these equations are represented in dimensionless form with conventional loss of SBW  $C = c/(8\pi\omega_{pi})$ ,  $\chi_e = -f_p^2/f^2 - l_w^2 q^2 f_o^2/f^2$ ,  $\chi_{es} = (2.5 \times 10^3)/(f_o l_s q)^2$ ,  $a_o = eE_o/m\omega_o v_{th}$ ,  $a_1 = eE_1/m\omega_1 v_{th}$ ,  $a_w = e\Phi_w/T_e$ ,  $a_d = e\Phi_d/T_e$ ,  $a_s = e\Phi_s/T_e$ ,  $l_w = k_w/k_o$ ,  $l_s = k_s/k_o$ ,  $l_d = k_d/k_o$ ,  $l_1 = k_1/k_o$ ,  $f_o = \omega_o/\omega_{pi}$ ,  $f_1 = \omega_1/\omega_{pi}$ ,  $f = \omega/\omega_{pi}$ ,  $f_s = \omega_s/\omega_{pi}$ ,  $q = k_o v_{th}/\omega_o$ ,  $p = T_e/mv_{th}$ ,  $T_w = \gamma_w/\omega_{pi}$ ,  $T_d = \gamma_d/\omega_{pi}$  and  $tw_{pi} = \tau$ .



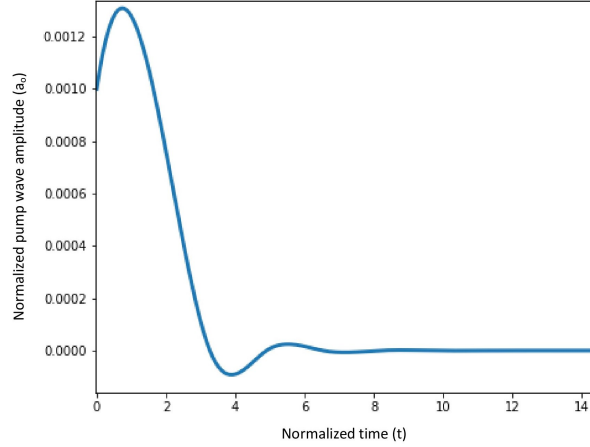


Figure 6.2: Normalized amplitudes of pump wave ( $a_o$ ) with normalized time ( $t$ ) in hot electron plasma. The parameters used are as follows;  $\lambda = 0.035\mu m$ ,  $r_o = 10\mu m$ ,  $\omega_p/\omega_o = 0.022$ ,  $T_e = 400eV$ .

## 6.5 Results and Discussions

The final coupled equations (6.24) to (6.28) are solved numerically. A laser of wavelength  $\lambda = 0.35\mu m$ , electron density considered is  $10^{21} cm^{-3}$ , initial spot-size  $r_o = 10\mu m$  is considered. The SRS condition  $n_o^o \leq n_{cr}/4$  is satisfied since the critical density obtained is  $9 \times 10^{21} cm^{-3}$ . The initial conditions of amplitude considered are;  $a_o=0.01$ ,  $a_1 = 0.001$ ,  $a_w = 1.00$ ,  $a_d = 0.01$ ,  $a_s=0.001$ .

Figure (6.2) and (6.3) show the change of amplitude of pump wave and and back-scattered wave with time keeping  $\omega_p/\omega_o = 0.022$  constant. The amplitudes reduced significantly after achieving resonance at different periods. In the beginning, the pump wave amplitude increases due to plasma effects. As the instability sets up, the sideband wave amplitude starts to increase. The plasma wave grows due to the SRS and attains a large amplitude. The large amplitude plasma wave them susceptible to evolve the decay instability.

In figure (6.4), the evolution of plasma wave is shown with hot electrons ( $v_h/c = 0.1$ ) keeping  $\omega_p/\omega_o = 0.022$ .  $E_{pw1}$  grows plasma-like, and from hot electrons, the wave takes in energy.  $E_{pw2}$ 's Landau damping is unaffected by energetic electrons because  $E_{pw2}$ 's drift is in the other direction.  $E_{pw1}$ 's amplitude grows with time because of Landau's growth, but this expansion may be halted due to the hot electrons confined in the wave's lowest potential energy. When  $e\Phi_w \approx 1/2mv_h^2$  is present, this happens.  $E_{pw1}$  is supposed to grow like Landau due to hot electrons for  $e\Phi_w \leq 1/2mv_h^2$ , but for  $e\Phi_w > 1/2mv_h^2$ , the hot electrons distribution function reaches a minimum point, and  $E_{pw1}$  growth ceases. After this point only because of parametric coupling does the wave the  $E_{pw1}$  gain energy.

Figure (6.5) shows the effect of the presence of magnetic field in plasma. It is observed that, when the magnetic field was zero, ( $\omega_c/\omega_o = 0$ ), the amplitude of the wave was much higher than the amplitude of wave in the presence of magnetic field. It can be concluded

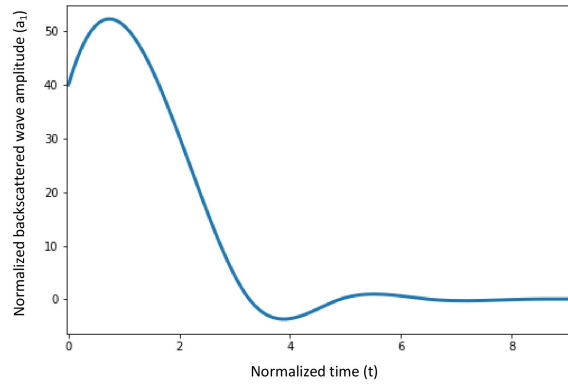


Figure 6.3: Normalized amplitudes of back-scattered electromagnetic wave ( $a_1$ ) with normalized time ( $t$ ) in hot electron plasma. The parameters used are as follows;  $\lambda = 0.035\mu m$ ,  $r_o = 10\mu m$ ,  $\omega_p/\omega_o = 0.022$ ,  $T_e = 400eV$

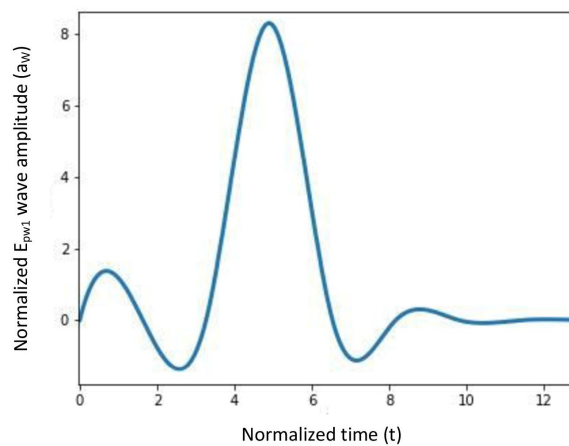


Figure 6.4: Normalized amplitudes of  $E_{pw1}$  ( $a_w$ ) with normalized time ( $t$ ) in hot electron plasma. The parameters used are as follows;  $\lambda = 0.035\mu m$ ,  $r_o = 10\mu m$ ,  $\omega_p/\omega_o = 0.022$ ,  $T_e = 400eV$

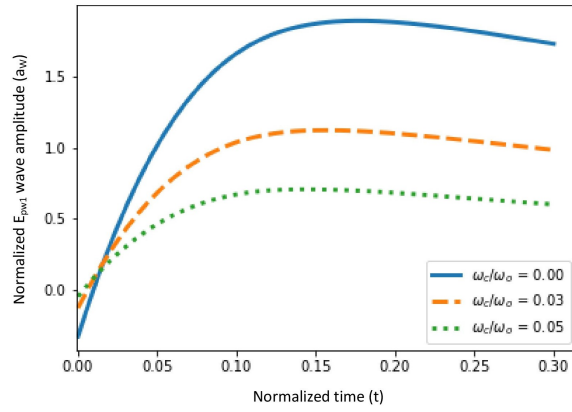


Figure 6.5: Normalized amplitudes of  $E_{pw1}$  ( $a_W$ ) with normalized time ( $t$ ) in hot electron plasma with varying in magnetic field. The parameters used are as follows;  $\lambda = 0.035\mu m$ ,  $r_o = 10\mu m$ ,  $\omega_p/\omega_o = 0.022$ ,  $T_e = 400eV$

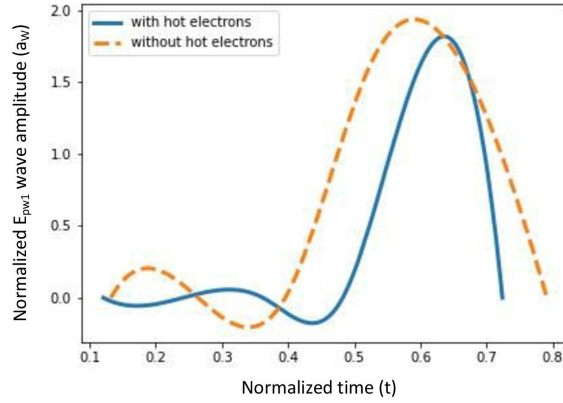


Figure 6.6: Normalized amplitudes of  $E_{pw1}$  ( $a_W$ ) with normalized time ( $t$ ) in the presence and absence of hot electron plasma with constant magnetic field ( $\omega_c/\omega_o = 0.03$ ). The parameters used are as follows;  $\lambda = 0.035\mu m$ ,  $r_o = 10\mu m$ ,  $\omega_p/\omega_o = 0.022$ ,  $T_e = 400eV$

from here that, the suppression of instability may be observed if magnetic field is present.

Figure (6.6) presents the effect of presence and absence of hot electrons in plasma on the  $E_{pw1}$ . We observed reduction in the amplitude of the wave and occurrence of resonance was also delayed in comparison with the absence of hot electrons.

Figure (6.7) shows variation in the temporal growth with the variation in the amplitude of  $E_{pw2}$ . Amplitude is observed to be suppressed after attaining resonance, keeping  $\omega_p/\omega_o = 0.022$ . The effect of variation in magnetic field on  $E_{pw2}$  is observed from figure (6.8). As the magnetic field is increased, the amplitude of the wave is suppressed significantly. When no magnetic field was present, ( $\omega_c/\omega_o = 0$ ), the wave amplitude was very high in comparison to the amplitude in the presence of magnetic field.

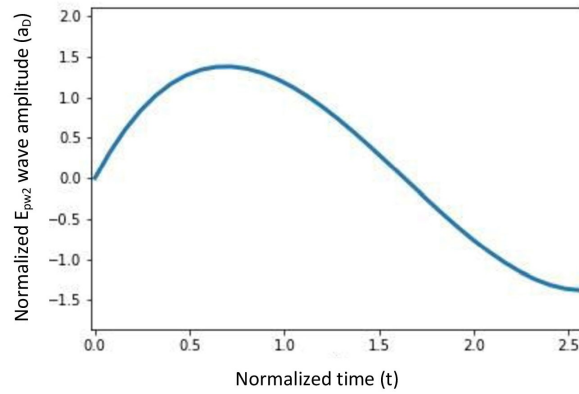


Figure 6.7: Normalized amplitudes of  $E_{pw2}$  ( $a_D$ ) with normalized time( $t$ ) in hot electron plasma. The parameters used are as follows;  $\lambda = 0.035\mu m$ ,  $r_o = 10\mu m$ ,  $\omega_p/\omega_o = 0.022$ ,  $T_e = 400eV$

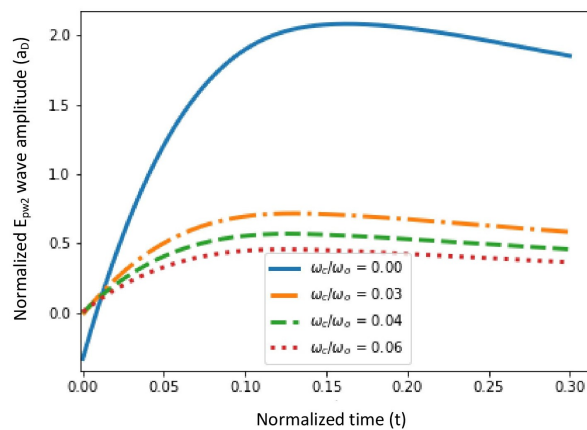


Figure 6.8: Normalized amplitudes of  $E_{pw2}$  ( $a_D$ ) with normalized time ( $t$ ) in hot electron plasma with varying in magnetic field. The parameters used are as follows;  $\lambda = 0.035\mu m$ ,  $r_o = 10\mu m$ ,  $\omega_p/\omega_o = 0.022$ ,  $T_e = 400eV$

## 6.6 Conclusion

Based on the fluid analysis, we have presented a simple analytical model for the stimulated Raman scattering coupled with decay instability in a magnetized plasma incorporating the effects of hot drifting electrons. The pump laser wave is susceptible to excite stimulated Raman instability. The large amplitude plasma wave generated via SRS is again susceptible to evolve decay instability. In this cascade process, the secondary  $E_{PW1}$  and ion acoustic wave are non resonant for the SRS. The fluid theory of SRS combined with decay instability reveals that nonlocal influences diminish SRS significantly, and the latter has a considerable effect on SRS saturation. The primary  $E_{PW1}$  dampens quickly and becomes saturated. The primary  $E_{PW1}$  uses LDI as an energy sink. The amplitude of main  $E_{PW1}$  increases over time as the SRS grows, but it ultimately decreases when energy is diverted to the LDI in the presence of hot drifting electrons and magnetic field. The overall energy transfer from the wave to the plasma electrons via Landau damping causes the wave's amplitude peaks to gradually diminish. This reduction in amplitude of the SRS instability might help in reducing the preheating of plasma in ICF.

## Bibliography

- [1] V. A. Smalyuk, D. Shvarts, R. Betti, J. A. Delettrez, D. H. Edgell, V. Y. Glebov, V. N. Goncharov, R. L. McCrory, D. D. Meyerhofer, P. B. Radha and S. P. Regan, Physical review letters, **18**, (2008) 185005
- [2] V. N. Goncharov, T. C. Sangster, P. B. Radha, R. Betti, T. R. Boehly, T. J. B. Collins, R. S. Craxton, J. A. Delettrez, R. Epstein, V. Y. Glebov and S. X. Hu, Physics of Plasmas, **5**, (2008) 056310.
- [3] Moses, E.I., Bonanno, R.E., Haynam, C.A., Kauffman, R.L., MacGowan, B.J., Patterson, R.W., Sawicki, R.H. and Van Wonterghem, B.M., 2007. The national ignition facility: path to ignition in the laboratory. The European Physical Journal D, 44(2), 215-218.
- [4] M. J. Rosenberg, A. A. Solodov, J. F. Myatt, W. Seka, P. Michel, M. Hohenberger, R. W. Short, R. Epstein, S. P. Regan, E. M. Campbell and T. Chapman, Physical review letters, **5**, (2018) 055001.
- [5] B. J. Winjum, J. E. Fahlen, F. S. Tsung and W. B. Mori, Physical review letters, **16**, (2013) 165001.
- [6] W. L. Kruer, K. Estabrook, B. F. Lasinski and A. B. Langdon, The Physics of Fluids, **7**, (1980) 1326-1329.
- [7] D. E. Hinkel, S. W. Haan, A. B. Langdon, T. R. Dittrich, C. H. Still and M. M. Marinak, Physics of Plasmas, **3**, (2004) 1128-1144.
- [8] K. Mima, M. S. Jovanović, Y. Sentoku, Z. M. Sheng, M. M. Škorić, T. Sato, Physics of Plasmas, **5**, (2001) 2349-2356.
- [9] O. Klimo, S. Weber, V. T. Tikhonchuk and J. Limpouch, Plasma Physics and Controlled Fusion, **5**, (2010) 055013.
- [10] K. L. Baker, R. P. Drake, B. S. Bauer, K. G. Estabrook, A. M. Rubenchik, C. Labaune, H. A. Baldis, N. Renard, S. D. Baton, E. Schifano and A. Michard, Physical review letters, **1**, (1996) 67.
- [11] C. Labaune, H. A. Baldis, B. S. Bauer, V. T. Tikhonchuk and G. Laval, Physics of Plasmas, **1**, (1998) 234-242.
- [12] R. L. Berger, C. H. Still, E. A. Williams and A. B. Langdon, Physics of Plasmas, **12**, (1998) 4337-4356.

- 
- [13] D. A. Russell, D. F. DuBois and H. A. Rose, *Physics of Plasmas*, **4**, 1999 1294-1317.
- [14] D. S. Montgomery, J. A. Cobble, J. C. Fernandez, R. J. ocia, R. P. Johnson, N. Renard-LeGalloudec, H. A. Rose and D. A. Russell, *Physics of Plasmas*, **5**, (2002) 2311-2320.
- [15] S. Depierreux, J. Fuchs, C. Labaune, A. Michard, H. A. Baldis, D. Pesme, S. Hüller and G. Laval, *Physical review letters*, **13**, (2000) 2869.
- [16] A. K. Ram, C. C. Chow and A. Bera, *Plasma Physics and Controlled Fusion*, **3**, (1994) 1460.
- [17] H. P. Freund, R. A. Smith, K. Papadopoulos and P. Palmadesso, *The Physics of Fluids*, **3**, (1981) 442-446.
- [18] M. Tanaka and K. Papadopoulos, *The Physics of fluids*, **7**, (1983) 1697-1699.

# Chapter 7

## Summary and Conclusion

This thesis has presented analytical and numerical research focusing on laser plasma interaction and burn in ICF.

The research looks at strong self-focusing of a Gaussian laser beam in the presence of an upward plasma density ramp in a plasma-loaded cone, which might be useful in cone-guided fast ignition or other applications where smaller focal spots and/or higher laser intensity are desirable. The beam-width parameter is used to describe the field distribution of the laser beam. The defocusing of the laser beam is reduced with this arrangement. As a result, the laser beam remains concentrated to a tiny spot size over multiple Rayleigh lengths, which is critical for consistent performance in an extended plasma produced by a laser prepulse interaction. The simulation findings demonstrate that in this scenario, the plasma frequency rises and self-focusing happens faster than in a uniform density plasma. Clearly, these are the results of a simplified model of laser-plasma interaction, and further research is needed to fully understand the significance and value of this behaviour in cone-guided rapid ignition. Fast ignition necessitates a lengthy heating beam,  $\approx 10$  ps, and on such a timescale, a model that accurately accounts for the development and hydrodynamic motion of the plasma within the cone is required. Furthermore, the reader is reminded that the existence of preplasma has been demonstrated in experimental investigations at decreased size to have a detrimental impact on coupling, and that we are just looking at one element of the laser-plasma interaction here. The effect of SRS on ICF has also been studied in this thesis. The study of using magnetized density rippled plasma describes that, the SFRS growth rate is considerably decreases owing to the localization of the lower hybrid wave in the presence of density rippling plasma and azimuthal magnetic field, which might minimise fuel preheating in ICF. The coupling of decay instability with SRS is also studied. It is observed that the instability amplitude reduces significantly which might be helpful in reducing the preheating of fuel in ICF. Lastly, the research on burn analysis for advanced fuels was done. It proposes that instead of utilising a 50:50 mix of deuterium and tritium in an ICF target, we might use a mixture of various fuel concentrations. Without compromising much output energy, a combination with a significantly higher proportion of deuterium may be utilised. This influence might lead to a significant reduction in tritium inventory, which is important for environmental and safety reasons. Inertial fusion can also benefit from this notion.

Finally, the challenges like, fuel preheating in ICF, defocusing of a laser in ICF and requirement of tritium inventory reduction in ICF, have been analysed in this thesis. The author has done analytical study and numerical simulations of this work, however, further simulation modeling, like PIC simulation or Monte Carlo simulations can be done in this work



to support the analytical and numerical results obtained. In future the author wishes to extend this work for different ICF schemes and laser-plasma profiles in simulation modeling like PIC.

## LIST OF PAPERS BASED ON THESIS

- 1 **Kamboj, O.**, Ghotra, H. S., Thakur, V., Pasley, J. R., Kant, N. (2021). *Optimizing laser focal spot size using self-focusing in a cone-guided fast-ignition ICF target.* , European Physical Journal Plus, 136, [484].
- 2 **Kamboj, O.**, Thakur, V., Ghotra, H. S., Kant, N. (2019, August). Strong self-focusing for laser interaction with DT fusion target. In AIP Conference Proceedings (Vol. 2136, No. 1, p. 060011). AIP Publishing LLC.
- 3 **Kamboj, O.**, Yadav, A., Gupta, DN., Pasley, J. R., Kant, N., *Suppression of stimulated forward Raman scattering by static density fluctuations in the presence of a magnetic field, with application to Inertial Confinement Fusion*, Submitting to Physics of Plasmas.
- 4 **Kamboj, O.**, Kant, N., and Pasley, J. R., *Analysis of burn-up in inertially confined non-equimolar DT*, Submitting to Physics of Plasma and Controlled Fusion.
- 5 **Kamboj, O.** and Gupta, DN., *Study of stimulated Raman scattering in presence of two hot drifting electrons in plasma*, Submitting to Contributions in Plasma Physics.
- 6 **Kamboj, O.**, Yadav, A. Kant, N., *Stimulated forward Raman scattering in density rippled magnetized plasma*, Accepted-RAFAS-21.
- 7 **Kamboj, O.**, Pasley, J. R. and Kant, N., *Theory of stimulated Raman scattering with decay instability in the presence of static magnetic field in inertial confinement fusion*, submitting to Communications in Theoretical Physics.
- 8 Ali, H., **Kamboj, o.** and Kant, N., *Combined effects of magnetized plasma and density ripple on the suppression of stimulated Raman scattering* , Under review in Brazilian Journal of Physics.
- 9 Ali, H., **Kamboj, o.** and Kant, N., *Study of Stimulated Backward Raman scattering in a Density Rippled Magnetized Plasma*, Accepted RAFAS 21.
- 10 Ali, H., **Kamboj, o.** and Kant, N., *Stimulated Backward Raman scattering in a Magnetized Density Rippled Plasma*, Submitted to ECPD 2021.

## CONFERENCES

1. **Invited talk** at 5<sup>th</sup> Asia-Pacific Conference on Plasma Physics, 2021 on *Optimizing laser focal spot size using self-focusing in a cone-guided fast-ignition ICF target*, Japan.
2. **Oral Presentation** at 5<sup>th</sup> Asia-Pacific Conference on Plasma Physics, 2021 on *Suppression of stimulated forward Raman scattering by static density fluctuations in the presence of magnetic field in ICF scheme*, Japan

3. **Oral Presentation** at Recent Advances in Fundamental and Applied Science, 2021 on *Study of stimulated Raman forward scattering in presence of azimuthal magnetic field in a density rippled plasma in inertial confinement fusion*, Punjab.
4. **Oral Presentation** at Thirteenth International Conference on Plasma Science and Applications, 2020 on *Analysis of burn-up in inertially confined non-equimolar DT.*, Odisha.
5. **Poster Presentation** at 12<sup>th</sup> International Conference on Plasma Science and Applications, 2019 on *Strong self-focusing of a chirped Gaussian laser beam for inertial confinement fusion in presence of upward plasma density ramp*
6. **Poster Presentation** at International Conference on Photonics, Metamaterials and Plasmonics, 2019 on *Strong Self-Focusing For Laser Interaction with DT Fusion Target*
7. **Poster Presentation** at Indian Science Congress, 2019 on *Strong Self-Focusing For Laser Interaction with DT Fusion Target*

### SUMMER SCHOOLS

1. **Culham Plasma Physics Summer School, 2021**, UK.
2. **ELI Summer School, 2021**- Poster on *Suppression of stimulated forward Raman scattering by static density fluctuations in the presence of magnetic field in ICF scheme*, Czech Republic.
3. **5<sup>th</sup> International Summer School on the Physics of Plasma-Surface interactions, 2021**- Oral presentation in *Study of stimulated Raman forward scattering in presence of azimuthal magnetic field in a density rippled plasma in inertial confinement fusion*, Moscow. Got awarded with "outstanding talk".
4. **15<sup>th</sup> Kudowa Summer School "Towards Fusion Energy"- Virtual Edition, 2020**- Oral Presentation on *Optimizing laser focal spot-size using self-focusing in a cone-guided fast ignition ICF target*, Poland.
5. **4<sup>th</sup> Online International Summer School on the Physics of Plasma-Surface interactions, 2020**- Attended, Moscow.

### WORKSHOPS

1. **The European Fusion Education Network (FuseNet), 2021**-Mini workshop on Fusion Engineering, Germany.
2. **41th International Hirschegg Online Workshop on Physics of High Energy Density in Matter, 2021**- Poster presentation on *Analysis of Burn-Up in Inertially Confined Non-Equimolar DT.*, Germany.
3. **European Fusion Teacher's Day, 2020**, FuseNet.